BERTIL BRÄNNBACKA

Technical improvements of Windside wind turbine systems

Julkaisun nimike

Teknisiä parannuksia Windside-tuulivoimaloihin

Tiivistelmä

Tuulivoiman käyttö on kasvanut tasaisesti, koska ympäristötietoisuus on lisääntynyt ja vastuullinen energiantuotanto vaikuttaa kaikkiin ihmisiin. Kierteisiä pystyakselisia tuulivoimaloita käytetään usein ladattaessa akkuja automaattisilla sääasemilla, vapaa-ajan rakennuksissa jne. On erittäin toivottavaa, että tuulivoimala toimii suurella hyötysuhteella mahdollisimman paljon.

Akkujen lataus tuulivoimaloissa on sekä alhaisilla että suurilla tuulennopeuksilla haastavaa. Näin ollen tämän tutkimuksen päätavoitteena on löytää keinoja kehittää akunlatausta alhaisilla ja suurilla tuulennopeuksilla käyttämällä apulaitteina kaupallisesti saatavilla olevia sähköisiä komponentteja.

Lähestymistapana oli tutkia tuulivoimaloita todellisissa tuuliolosuhteissa. Tutkittiin kahta erikokoista Windside-tuulivoimalaa. Todellista dataa kerättiin ja analysoitiin. Myös analyyttistä mallia käytettiin onton akselin kehittämisessä. Prototyyppiakselia tutkittiin iskutesteillä ja modaalianalyysillä. Lisäksi simuloitiin jännitettä nostavaa hakkuriteholähdettä ja tähti-kolmio-kytkimen toimintaa.

Tämän työn keskeisiä teknillisiä saavutuksia ovat automaattisesti palautuva tähti-kolmio-kytkin ja ontto akseli. Niiden edut ovat moninaisia. Niitä voidaan käyttää sovelluksissa, joissa tarvitaan pieniä pystyakselisia tuuliturbiineita. Automaattisesti palautuvan tähti-kolmio-kytkimen käyttö pienissä tuulivoimaloissa lisää vuotuista energiantuottoa 9 % ja 24 V:n akkujen käyttö 12 V:n sijasta 7 %. Onton akselin käyttäminen kasvattaa tutkitun isomman voimalatyypin käytettävyyttä. Kehitetty ontto akseli vähentää kokonaispainoa ja käytettyjen raaka-aineiden määrää.

Asiasanat

Pystyakselinen tuulivoimala, akun lataus, energiantuotto, tähti-kolmio kytkin, Windside

Title of publication

Technical improvements of Windside wind turbine systems

Abstract

Motivation for the use of wind power has been increasing steadily because of increased environmental awareness and responsible production of energy affects all human beings. Helical vertical-axis wind turbines are often used to charge batteries in places such as automatic weather stations, recreational buildings etc. It is highly desirable that the turbines operate with high efficiency as much as possible. The problems encountered with battery charging by wind turbines are that the charging is poor in both low and high wind speeds. Thus, the main objective of this study is to find methods of improving the charging of batteries at low and high wind speeds by developing auxiliary devices using original components.

The approach was to study the wind turbines in real wind conditions. Two different sizes of Windside wind turbines were investigated. Field data was collected and analyzed. Also, an analytical model was used in the development of the hollow shaft. The prototype shaft was checked by hammer shock test and modal analysis. Furthermore, simulation studies were used to develop the step-up converter and to show the operation of the star delta switch.

Two novel techniques developed in this work are an automatic reversible star-delta switch, and a hollow shaft. The benefits of the developed items are manyfold. They can be utilized in applications where small vertical-axis wind turbines are used. The use of automatic reversible star-delta switch increases the annual energy yield of the small turbines by 9 % and the use of 24 V battery bank instead of 12 V by 7 %. The hollow shaft increases the usability of the type wind turbines examined. The developed hollow shaft reduces the overall weight and raw materials used.

PREFACE

This thesis derives from a wind power activity at the University of Vaasa from the beginning of year 2002 to the end of 2013. The participants in the project were Department of Electrical Engineering in University of Vaasa and the manufacturer of studied wind turbine devices, i.e. Oy Windside Production Ltd. Two small wind turbines each of 300 W rated powers and a larger wind turbine of 2 kW rated power from the manufacturer were used. All studied wind turbines were in real use, mounted on roofs of university buildings at the University of Vaasa in Vaasa in west coast region in middle of Finland. The studied smaller wind turbines were mounted on the roof of the six-floor height library building Tritonia and the bigger wind turbine on the roof the five-floor height Fabriikki building.

The research work related to this thesis has been carried out in the Technobothnia Laboratory in Vaasa and at several real wind turbine devices at the University of Vaasa during years 2001–2011 as a separate wind power project. A part of the measurements have been done at the manufacture's factory in Pihtipudas.

Professor Timo Vekara at the University of Vaasa has supervised the work. I want to warmly thank him for foresee, inspiration and guidance at the vertical-axis wind turbine project.

Professor Kimmo Kauhaniemi at the University of Vaasa has evaluated some of the work. I want to thank him for it.

The researchers Timo Rinne and Heikki Salminen have been of great help and both mentally and with practical and theoretical things throughout the period.

Oy Windside Production Ltd arranged a part of the equipment for the tests and I thank their CEO Risto Joutsiniemi for that.

This research work has been performed during the years when I acted as a laboratory engineer of electrical engineering at the University of Vaasa.

Vaasa, Finland, May 21st, 2015

Bertil Brännbacka

Contents

Figures

Tables

Nomenclature

Greek letters

α	Angular acceleration (rad/s^2)
γ	Wind shear exponent
δ	Load angle
η_c	Efficiency of converter
η_g	Efficiency of generator
η_r	Efficiency of rectifier
η_t	Efficiency of transmission
λ	Tip speed ratio
μ	Viscosity of the fluid (N s/m^2)
ρ	Air density (kg/m^3)
ρ_s	Shaft density (kg/dm^3)
σ	Wind speed standard deviation (m/s)
τ	Cycle period (s)
Φ_{fa}	Flux in the air gap
φ	Phase angle
Ω	Angular velocity of turbine rotor (rad/s)
ω	Angular frequency (rad/s)
ω_s	Synchronous speed (rad/s)

Roman letters

A	Cross-sectional area (m^2)
a	Induction factor
A_x	A scale factor
c	A cycle
C_{act}	Available battery capacity (Ah)
C_d	Drag coefficient
C_l	Lift coefficient
C_{max}	Maximal battery storage capacity (Ah)
C_p	Power coefficient
$C_{p,\,max}$	Maximum value of power coefficient
C_{pe}	Coefficient of Electric Power
C_{pm}	Coefficient of Mechanical Power
C_{tot}	Overall efficiency
e	Overlap distance (m)
dt	Differential operator in relation to time
d	Inner diameter of the shaft (mm)
D	Outer diameter of the shaft (mm)
E	Young's modulus (N/mm^2)
e_a	EMF induced in phase a (V)
E_a	Excitation voltage in phase a, rms value (V)
E_f	Induced EMF/phase (V)
E_k	Kinetic energy (J)

f	Frequency (Hz)
F_d	Drag force (N)
H	Height of the turbine (m)
H_{act}	Actual hour rating (h)
θ	Helical angle (deg)
I	Current (A)
I_a	Phase current (A)
I_{am}	Area moment of Inertia (m^4)
I_{AC}	Alternating current (A)
I_{DC}	Direct current (A)
I_{in}	Input current (A)
I_L	Line current (A)
I_m	Moment of Inertia (kgm^2)
I_{out}	Output current (A)
I_t	Turbulence intensity
k	Shape factor
K	Mode factor
l	Length of the shaft (m)
L	Characteristic length (m)
m	Mass (kg)
m_l	Mass per length (kg/m)
m_b	Mass of the blades (kg)
n	Rotational speed (r/min)
N_s	Equivalent number of turns
p	Pressure (N/m^2)
p_p	Number of pole pairs
P_D	Electrical power in delta connection (W)
P_e	The electric output power (W)
P_g	The electric output power of the generator (W)
P_m	Mechanical output power of the turbine (W)
$P_{m,ideal}$	Ideal mechanical power (W)
$P_{m,max}$	Maximum mechanical power (W)
P_r	Power at the reference height z_r (W)
P_w	Power in the wind (W)
P_Y	Electrical power in star connection (W)
P_z	Power at the height z (W)
r	Radius (m)
r_{max}	Maximum radius (m)
R	Resistance (Ω)
R_{max}	Maximum roughness height of profile (mm)
R_a	Stator resistance in phase a (Ω)
R_e	Reynolds number
R_f	Relative frequency of wind velocities
t	Time (s)
T	Thrust (N)
T_h	Time (h)
T_α	Torque due to angular acceleration (Nm)

T_m	Turbine torque (Nm)
T_L	Load torque (Nm)
U	Wind speed (m/s)
U_{ave}	Average velocity of air flow (m/s)
U_{rel}	Wind velocity relative to the power-producing surfaces (m/s)
U_r	Wind speed at the reference height z_r (m/s)
U_z	Wind speed at height z (m/s)
V_a	Terminal voltage in phase a (V)
V_B	Voltage of battery (V)
V_L	Line voltage (V)
$V_{L\text{-}L}$	Line to line voltage (V)
V_{in}	Input voltage (V)
V_{out}	Output voltage (V)
W	Energy (kWh)
x	Thickness of the parcel (m)
X_a	Total reactance in phase a (Ω)
z	Height above sea level (m)
z_r	Reference height above sea level (m)

Abbreviations

AC	Alternating current
AGM	Absorbed glass mat
CCA	Cold cranking amps
CFD	Computational fluid dynamics
D	Duty ratio
DC	Direct current
DSP	Digital signal processing
ESR	Equivalent series resistance
GEL	Gel form
HAWT	Horizontal-axis wind turbine
IEEE	Institute of electrical and electronics engineers
IEC	International electrotechnical commission
NC	Normally closed
NO	Normally open
MOSFET	Metal oxide semiconductor field effect transistor
MBC	Model-based control
MPPT	Maximum peak power tracker
P&O	Perturbation and observation
PWM	Pulse width modulation
rpm	Revolutions per minute
R	Multiple R
USA-1	Ultrasonic anemometer
WAsP	Wind application and analysis program
VAWT	Vertical-axis wind turbine
VRLA	Valve-regulated lead-acid

1 INTRODUCTION

This chapter starts with the background and motivation of this study, followed by the research scope and objectives of the study. It is followed by the research implications of the study and literature review of similar studies. Finally, the organization of the thesis is described.

1.1 Background and motivation

Among other things because of the accidents in some nuclear power plants at the end of 20th century and due to wind power does not leave waste, it is nowadays a popular way of producing electrical energy. Wind turbines are used for the production of electrical energy to the grid, in many European countries, so also in Finland and all over the world. Nowadays, most of the wind power plants for large scale production are of horizontal-axis wind turbine (HAWT) type. The vertical-axis wind turbines (VAWT) considered in the research is very rare and often used for charging of batteries in inaccessible surroundings. Figure 1 shows the type of vertical-axis wind turbine that has been studied.
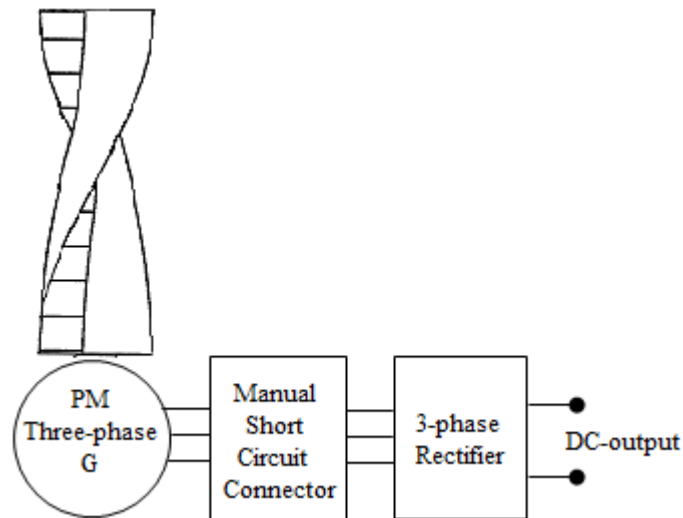
Figure 1.   Typical vertical-axis wind turbine that has been studied.

Because a wind turbine in long time use is expected to produce electrical energy in varying wind conditions, the reliable functioning of the device and its energy efficiency are very important. In vehicles and motorboats the battery charging systems are not in full efficiency at low speed of rotation, and at full speed overload is not recommendable. In sailing, light winds are a challenge, gusty winds often intractable, hard winds an enjoyment whereas stormy winds can be hazard-

ous. New building requirements in the urban areas are tightened, so that low-noise wind turbine types are preferred.

This thesis discusses battery charging and low voltage power production by two sizes of vertical-axis wind turbines of Windside types. It all started from a wind power project at the University of Vaasa, in which I became interested to find out the turbines characteristics and usage. Since 1982 Windside turbines and systems have been commercially manufactured in Finland and now they are used over the world in a variety of battery charging applications. Whereas withstanding extreme cold temperatures and huge wind velocities, the rugged and reliable turbine is capable of survive and even continue the production in severe atmospheric conditions. However, compared to modern, large wind turbine types used for generating electricity, the low maximum power coefficient and the high-solidity rotor design of Windside turbine are probably not economically viable in large-scale energy production.

Wind turbines used for battery charging have poor energy efficiency in low and high wind speeds. In light winds the output voltage of generator is too low in comparison to the battery voltage. In strong winds, use of only either one of star- or delta-connected generator leads to a poor overall output power characteristic. In the long time use in strong wind, the batteries must be prevented from overcharging and a control unit is therefore included in basic battery charging systems. In stormy winds the generator must be prevented from overload.

1.2   Research scope, arguments and objectives

The objective of this study is to explore of the possibilities of increasing the overall energy yield with Windside vertical-axis turbines in long term use, mainly by using the appropriate peripheral devices and controllers. The question is whether this is possible.

The aims of this work are to find proper methods to increase the charging in the range of low and high rotational speed, improve long time charging in varying wind speeds, if possible increase the energy yield in gusty wind speed and simultaneously prevent battery from overcharging and the generator from overloading.

The arguments of the thesis are:

i. If using only either star connected or delta connected generator in the whole operating range it is not possible to receive as high energy yield as by combining these in a way as shown. The studied wind turbines have poor energy yield in either low or high wind speeds because it uses only star or delta connected generator. The wind turbines will give better charging characteristics in whole operating range i.e. both low and high wind speeds.

ii. The studied wind turbines can provide better charging characteristics using a voltage booster unit for low wind speeds and an automatic reversible star-delta switch for high wind speeds. Why? This is because then charging voltage exceeds the battery voltage, the battery can be recharged. A three-phase generator shows three times lower internal resistance and impedance when it is delta connected instead of star connected and therefore it is much better to use delta connection than star connection in high wind speed. They studied wind turbines have previously been used with only star connected generators.

iii. How this is done? This thesis shows that the voltage booster unit and the automatic reversible star-delta switch can be built using electrical and electronic components. The energy yield of the studied wind turbines could be increased by more than 9 %, using the units developed in this study. The developed new units will be additional and supplementary products for wind power plants.

The objective of this research is to find ways of improving the production of electric energy by small Windside vertical-axis wind turbines. The aim was to do that with automatic electric control systems, without designing of new wind turbine, wind turbine rotor or electric generator to the device to be developed. This has reduced the questions to be addressed in the study to five.

The first research question *RQ 1* is important as the voltage level is easily changed by the number of cells or batteries that are connected in series. The components are generator, rectifier system, converter and batteries.

> *RQ 1:* *What is the effect of the voltage level used on the production of electricity?*

The second research question *RQ 2* has been probed and solved by several manufacturers around the world. No such solutions existed in the basic wind turbine

systems, which now would be more effective. It was important to develop such additional equipment and to investigate its impact on the output power and energy yield.

> *RQ 2:*   *How to increase the produced electric energy in low wind speeds?*

The third research question *RQ 3* was important, because of the impact of climate change that would cause high winds and heavy storms.

> *RQ 3:*   *How the studied wind turbines would give excellent charge characteristics in the entire operating range, especially at high wind speeds?*

The fourth issue *RQ 4* arose during the work and must be solved, because vibration limited the use and thus output energy in hard winds.

> *RQ 4:*   *How to overcome the problems of natural frequencies?*

Although the intention was not to consider mechanical design characteristics such as the effect of natural frequency in the turbine shafts, it became very important to first solve these problems. In startup tests on the site, it appeared that the critical speed occurred in both sizes of wind turbines used in the first instance before the rated output power was reached. This led to the development of a hollow shaft for the larger wind turbine.

The fifth question *RQ 5* aims to find solutions for fully automatic control of the turbines in the current wind conditions, from weak to stormy winds. The idea was that the developed automatic control devices should work at the field also far away from the national grids without a personal computer (PC) and with a power supply only from the battery bank, belonging to the wind turbine. Another aim was that developed devices, may also be available as commercial products, which may be found in parts lists of manufacturers in the future.

> *RQ 5:*   *How to do these things, so that their function is automatic and can be applicable to real wind power systems?*

1.3   State of the art

Literature survey on improvements for better performance on the production of electrical energy of vertical-axis wind turbines with permanent magnet generator similar to the ones studied in this work implies that methods like to those pro-

posed here, have not been reported. *It was found in this study that by using the developed star-delta switch with rotational speed as control parameter, the output power can significantly be increased due to much higher output current in high wind speeds.*

However it is now known that in horizontal-axis wind turbines with doubly-fed induction generator from Vestas® (2014), star-delta switch with active power as control parameter is used. The stator of the generator can be switched to the grid both in star and in delta mode. *It keeps the current in the stator relatively low also at high yield.* The system operates in star mode up to approximately 800 kW and in delta mode above and up to 2 MW.

A series of experiments have been carried out by Saha & Rajkumar (2005:1780) with semicircular and twisted types of Savonius wind turbine rotor in a three-bladed system. It was reported that the performance studies of the rotor system in both the cases have been made on the basis of starting characteristics, no load speeds, static torque, torque coefficient, coefficient of performance and efficiency. Wind tunnel studies show the potential of the Savonius rotor with twisted blades in terms of smooth running, higher efficiency and self-starting capability as compared to that of the semicircular bladed rotor. All the tests were conducted at a room temperature of 25 °C.

Tests on helical Savonius rotors were conducted by Kamoji, Kedare & Prabhu (2009:521) in an open jet wind tunnel to measure the coefficient of static torque, coefficient of torque and power coefficient for each helical Savonius rotor. The performance of helical rotor with shaft between the end plates and helical rotor without shaft between the end plates at different overlap ratios of 0.0, 0.1 and 0.16 were compared. It was found that the static torque coefficients at all the rotor angles for all helical Savonius rotors tested in this study were positive and that the rotor was sensitive to the Reynolds number. Increase in the Reynolds number increases the maximum power coefficient of the rotor.

It has been reported by Deb, Gupta & Misra (2013:132) that helical Savonius rotor without rotor shaft at rotor angles of 45° and 90° could improve the rotor performance as a whole during its power stroke by increasing the aerodynamic torque production of the rotor.

A comparative study of torque and speed control for pulse width modulated (PWM) converter fed generator in small wind energy system made by Mirecki, Roboam & Richardeau (2004:998) shows that the efficiency is quite the same for both algorithms even if the torque controlled MPPT is a little bit better than the speed controlled system. A structure including a diode converter with a DC-DC

chopper is a cheaper and simpler solution for which the results are quite satisfactory. No mechanical sensors are needed. Even if the tuning of the generator torque is indirect and highly slower, the high inertia of the turbine operates as a wind filter offering a globally powerful solution. Furthermore, an optimal curve giving the output battery current versus the DC voltage at the output of the diode bridge can be determined by simulation and/or by experiment. Another advantage is that this curve directly includes the system losses for any operating points.

Since the basic system for a Windside wind turbine contained a rectifier bridge and no mechanical sensors were needed, it was natural to test a system with a DC-DC converter without knowledge of the optimal output power curve for the studied wind turbine.

A novel wind turbine is designed by Clague & Oi (2008:262) to provide heating for hot water storage systems in residential houses. It was found that the efficiency of studied vertical-axis Savonius rotor can be optimized for various wind conditions by switching between different load resistances.

The design of a hybrid turbine based on a straight bladed Darrieus turbine along with a double step Savonius turbine was studied by Alam & Iqbal (2009:1178). The hybrid turbine is built and tested in variable speed water flows. This design idea can also be implemented for wind applications. Four bladed Darrieus rotor is placed on top of a Savonius rotor. The hybrid vertical-axis turbine has much better self-starting characteristics and better conversion efficiency at higher flow speeds. It was found that the cut-in speed of the hybrid turbine with the Savonius rotor is about 0.3 m/s. This shows the quick self-starting behaviour of the hybrid turbine compared to the Darrieus type used alone. During the design of a hybrid turbine, it is recommended to choose a proper radius ratio of the turbines as well as proper positioning of the two turbines.

The following three sources of study deal with the maximization of energy production from small wind turbines, which is also the aim of this study. Control system that maximizes wind energy production has been tested by several groups of researchers.

Maximization of energy production from small wind turbines for battery charging was investigated by Corbus et al. (1999:1). It was found that the main technical challenge in the design of a wind-electric battery charging station is to come up with a system configuration and control algorithm that maximizes wind energy production from the turbine and also provided favorable charging conditions for batteries. This task is complex because of the variability of the wind, which results in varying wind turbine output power. Ideally, the system configuration and

its controller should optimize the match between the wind rotor and load, thereby allowing the maximum available power from the wind to be used, while at the same time charging the batteries with an optimum charge profile for a given type of battery. This maximizes the number of batteries charged by a station within a certain time period.

The modeling and simulation of a vertical-axis direct drive topology wind turbine are implemented by Eid, Abdel-Salam & Abdel-Rahman (2006:166). They modeled and simulated a small wind power system using a vertical-axis wind turbine coupled with axial-flux permanent magnet synchronous generator in transient conditions. They found that the control algorithm was effective over a wide range of wind speeds. The wind turbine is controlled to operate at optimal generator speed, thus operating at maximum efficiency and extracting maximum electrical power from the wind. The output voltage of the buck-boost converter is controlled to be constant at any wind speed for battery charging purpose, and the simulation results demonstrate the effectiveness of the proposed control.

A design of a static converter for a vertical-axis wind energy conversion system (WECS) based on permanent magnet generators were introduced by De Almeida & Oliveira Jr. (2011:825). They concluded that the principal advantages of using the semi-controlled rectifier are: simplicity, since all active switches are connected to a common point, robustness, as short circuit through a leg is impossible to happen, and high efficiency due to reduced number of elements.

The last four considerations is all about skipping a natural frequency in a wind turbine, the energy yield of small wind turbines, maximum average power coefficient of a vertical-axis wind turbine and a definite opinion on drag-based wind turbines.

Skipping of natural frequency in a horizontal-axis wind turbine was described by Tempel & Molenaar (2002:220–221). They state that the variable speed turbines are equipped with comprehensive controls to keep the system running at optimum speed for the particular wind speed. Such variability of the rotation speed narrows the intervals of safe frequencies for the structure and, moreover, the controller can be used to create new intervals. It is found that even though the natural frequency lies in the range of the rotation frequency band, the controller can be programmed to skip the region around the natural frequency. This will prevent the rotor from exciting the tower frequency. The tuning of the controller is better to be done after installation and measurements of the actual first natural frequency. This is because uncertainties in the soil conditions of the foundation and in the installation works can make the actual frequency deviate appreciably from the design.

This frequency skipping has been applied successfully at the Utgrunden Wind Farm in Sweden.

In investigating the energy yield of small wind turbines in low wind speed areas, Ani, Polinder & Ferreira (2011:93) have compared several commercially available small wind turbines systems such as vertical-axis type with three helical blades without power limiting control above rated wind speed, multi-bladed furling controlled horizontal axis type, stall controlled horizontal axis type and blade pitch controlled horizontal axis type. The comparison is based on the annual energy yield per swept area (kWh/m^2) and cost per generated electricity (€/kWh) in a low wind speed climate. It was found from the results that most systems did not meet the performance stated by the manufacturers. Calculated annual energy yield of some turbines were higher than measured values from field tests by up to a factor of two. Results also show that in large diameter turbines the €/kWh is lower than in small diameter turbines while many small diameter turbines had higher kWh/m^2 than large diameter turbines. However, above 3 m in diameter, large diameter turbines performed better, having both low €/kWh and high kWh/m^2.

Maximum averaged power coefficient of the Savonius type turbine was investigated by Akwa, Vielmob & Petryb (2012:3054). They found that Savonius type of turbine is not very common and its application for obtaining useful energy from air stream is an alternative to the use of conventional wind turbines. It was also found that the performance of a Savonius wind rotor can be affected by geometric and air flow parameters. It was found that the following parameters have influence on the function of a Savonius wind turbine: end plates, aspect ratio, buckets spacing, buckets overlap, buckets number, rotor stages, buckets and rotor shapes, shaft and other accessories, Reynolds number and turbulence intensity.

About purely drag-based wind turbines

A drag machine was deemed to be useless by Kragten (2009). He reported that the Cup anemometers are normally not used to generate power. They run unloaded and the rotational speed is a measure of the wind speed. However, to generate power, very large cup anemometers have been built, but the power which can be generated by such a windmill is very low. The maximum power coefficient which can be realized for a drag machine is not higher than about 0.05 and much more material is needed to realize a certain swept area than for a horizontal-axis windmill. He concludes that development of windmills using the drag force as the propelling force is a waste of time and money.

1.4   Organisation of this thesis

The structure of the content of this thesis is shown in Figure 1. This thesis is organized in five chapters. In Chapter 1 an introduction, including the research questions to the thesis was presented.

```
┌─────────────────────────────────────┐
│  Research scope and objectives        │
└─────────────────────────────────────┘
                  │
                  ▼
┌─────────────────────────────────────┐
│  The character of wind                │
│  Wind power                           │
│  Battery charging systems             │
│  Batteries                            │
│                                       │
└─────────────────────────────────────┘
                  │
                  ▼
┌─────────────────────────────────────┐
│  Environmental aspects                │
│  Mechanical aspects                   │
│                                       │
└─────────────────────────────────────┘
                  │
                  ▼
┌─────────────────────────────────────┐
│  Wind turbine                         │
│  Vertical-axis wind turbine           │
│  Hollow shaft                         │
│                                       │
└─────────────────────────────────────┘
                  │
                  ▼
┌─────────────────────────────────────┐
│  Electrical systems                   │
│  Measurement instruments and          │
│  systems                              │
│  Control systems                      │
│                                       │
└─────────────────────────────────────┘
                  │
                  ▼
┌─────────────────────────────────────┐
│  Component test results               │
│  System test results                  │
│                                       │
└─────────────────────────────────────┘
                  │
                  ▼
┌─────────────────────────────────────┐
│  Discussion of results                │
│  Conclusions and outlook              │
│                                       │
└─────────────────────────────────────┘
```

Figure 2.   The structure of this thesis.

In Chapter 2 natural phenomena, theory and technology related to wind power are presented. Chapter 3 discusses studied systems and developed devices. Chapter 4 gives the results of the study and Chapter 5 concludes the research and gives answers to the research questions.

1.5   Limitations of this thesis

In this thesis the following restrictions are used:

  (i)   This work is limited to advantageous and realistic solutions.
  (ii)   Only one wind turbine type is studied because this type was inadequately investigated and not at all reported in scientific literature.
  (iii)   The main focus is on small wind turbines. The focus is not in the development of inverter based solutions, even though such belong to the larger wind turbine.
  (iv)   No series capacitor is used in conjunction with the generator because it has been done by many others.
  (v)   Problems of low battery voltage due to long periods of weak winds are not investigated because of the scope of this study.
  (vi)   The torque of the turbines or generators and efficiency of studied generators were not measured because of the common shaft for the turbine and generator.
  (vii)   MPPT logic is used only in low wind speeds because this solution was not found by the others. They have investigated various wind turbines with MPPT logic of their full wind speed range.
  (viii) In this thesis the aim was to increase the output energy by use of existing main components type generators and rotors, not to build new ones.

2   WIND TURBINES

This chapter presents physics of wind turbines including the power in the wind, different types of wind turbines and efficiency rates of drive trains of wind turbines. The chapter starts with the natural winds followed by aerodynamics and fluid mechanics for wind turbines. Then, it describes the output power of ideal wind turbines, followed by a description of permanent magnet generator. After that, the generators under study are described, followed by a description of the output power of real wind turbines and equations for rotational motion. Finally, the chapter describes the principles for determination of performance of studied wind turbines and calculation of annual energy yield. Described things form an important basis for utilization of the energy that exists in natural winds.

Wind energy is kinetic energy that is present in moving air. The amount of its energy content depends mainly on wind speed, but is also lightly affected by the air density, which depends on the air temperature, barometric pressure, and altitude. Wind energy is clean and doesn't leave much waste in power production.

Wind energy has been used by humans thousands of years for sailing in boats and for grinding in wind mills. Modern wind turbines are improvements of prehistoric windmills and wind pumping systems. However, modern wings in horizontal-axis turbines diverge from wings in ancient wind mills. Modern blades are designed so that they remind of an airplane wing and because of composite materials used it is possible to give them the elongated form they have today.

The Savonius-type wind turbine with two overlapped blades was patented in Finland in 1924 and the studied Windside-type wind turbine with helical rotor in 1985. Savonius turbine has been investigated and still is under research by numerous researchers but Windside turbine has not been studied to any significant extent.

In this research, the intention is to investigate properties of a Windside vertical-axis turbine and look at ways to improve turbine characteristics to charge batteries, mainly by using electrical auxiliary equipment.

At the beginning of this research, there were a number of unanswered questions. Windside vertical-axis turbine rotates fast enough in light winds. Can it then be loaded? Is the generator voltage, in general, and especially after the rectifier high enough for charging a battery? What characteristic has the turbine in high wind speeds? Can these properties be improved? These are some of the questions that have been answered in this study.

2.1   Natural winds

Wind is a very versatile and complex natural phenomenon. Here it is described from the wind power production perspective only. Global and local winds are first discussed, followed by wind turbulence and gusts.

2.1.1   Global winds

Solar energy warms the surface of the Earth in different ways at different latitudes. The bilateral location between the Earth and the sun means that the area round the equator receives much more solar radiation than pole areas. The atmosphere around Earth loses energy due to wave radiation (Tammelin 1991). Since the Earth is rotating, any movement on the Northern hemisphere is diverted to the right, if we look at it from our own position on the ground, but on the Southern hemisphere to the left. This apparent bending force is known as the Coriolis force. Note that rising warm and moist air results in a low pressure zone and descending cold, dry air results in a high pressure zone.

These zones of high and low pressure create the major wind belts which are shown in Figure 3. Note that the Hadley cell extends from the equator to about 30 degrees N and S latitude, the Ferrel cell extends from about 30 to 60 degrees N and S latitude and the Polar cell extends from 60 degrees latitude to the poles (90 degrees N and S latitude). (Global wind systems 2007.)

Prevailing winds are winds that blow predominantly from a single general direction over a particular point on the surface of the Earth.

The Earth therefore pumps energy from the tropics to the poles. The circulation of the Earth's atmosphere and oceans is the dominant pumping mechanism. The ocean streams are created by the global wind systems on the earth. This global wind system keeps the ocean streams going. Ocean streams can be seen as very large rivers in the sea. They are divided in surface currents and deep water currents. The surface currents are warm water streams and the deep water currents are cold water streams. Deeper currents travel slowly and move in different direction than the surface currents.

The short wave solar radiation and outgoing long wave terrestrial radiation varies with latitude as shown in Figure 4. The tropics are net absorbers of radiation and the poles are net emitters.
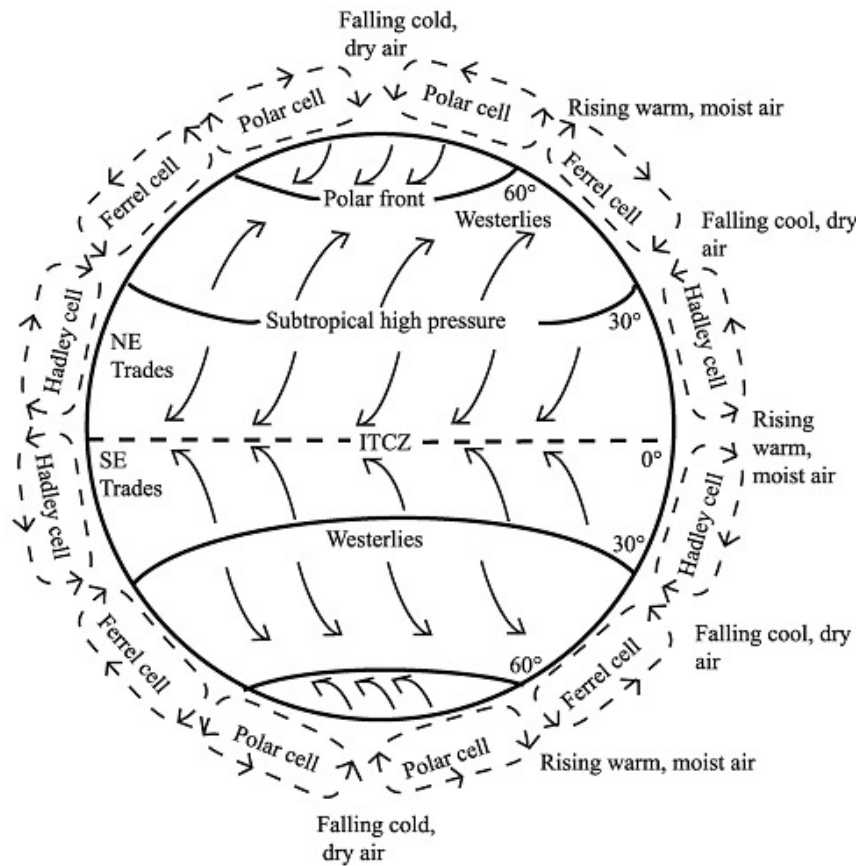
Figure 3.   The complete diagram summarizing atmospheric circulation (Global wind systems 2007).
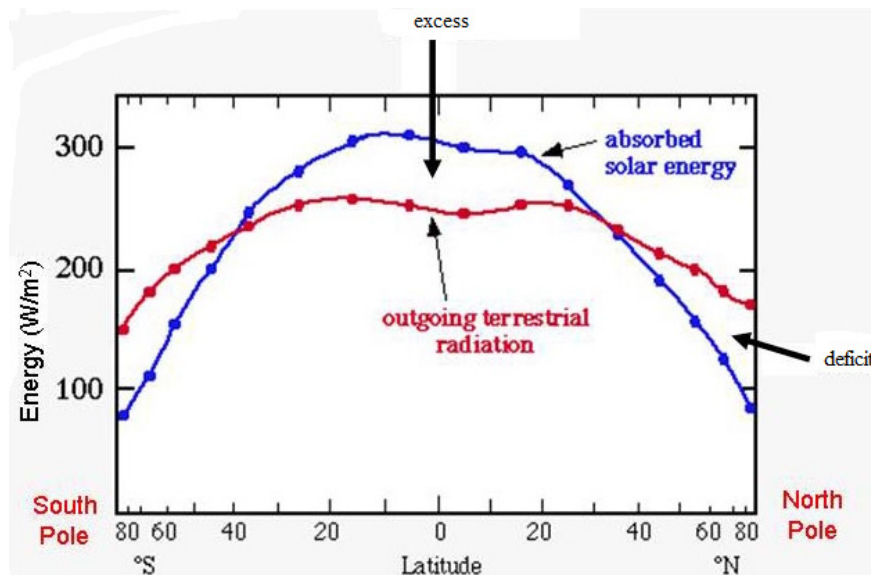
Figure 4.   Shortwave solar radiation and outgoing terrestrial long wave radiation vary with latitude (Climate Prediction.net 2007).

2.1.2   *Local winds*

The relative movement of air in relation to the rotary movement of the Earth is called wind. The following forces affect in the atmosphere:

(i)   Gravitation force
(ii)   Pressure gradient force
(iii) Friction force
(iv)   Centrifugal force
(v)   Coriolis force.

Local winds are always superimposed upon large scale wind systems. Wind direction is influenced by the sum of global and local effects. When larger scale winds are light, local winds may dominate. Offshore winds are more laminar than land based winds, because the friction caused from the ground is smaller at offshore.

In coast regions the temperature difference between land and sea results in breezes. The sea breeze blows landward at daytime and at nighttime the land breeze blows in the opposite direction. The land breeze has generally lower wind velocities, because the temperature difference between land and sea is smaller at night.

Diurnal valley winds are thermally driven winds that blow along the axis of *valley*, up valley flows during daytime and down valley flows at nighttime. Valley winds are the lower branch of a closed circulation that arises when air in a valley is colder or warmer than is farther down valley or over adjacent plain at the same altitude. Unlike slope winds, valley winds are not preliminary a function of the slope of the underlying valley floor. (Chow, De Wekker & Snyder 2012.)

Wind speeds depend on altitude

The wind speed increases with height most rapidly near the ground. Two common functions are presented to describe the change in mean wind speed with height up to 200 m and both are based on experiments.

Power exponent function is

(1) $$U_z = U_r \left(\frac{z}{z_r}\right)^{\gamma},$$

where z is the height above sea level, U_r is the wind speed at the reference height z_r above sea level, U_z is the speed at height z, and γ is the wind shear exponent which depends on the roughness of the terrain. In terrain with cut grass the value of wind shear exponent is 0.14 which is near to the 1/7 power law, 0.143, used in

North America. In our terrain with trees, hedges and few buildings the value of wind shear exponent is 0.29 (Gipe 2004:41).

Logarithmic function how the wind speed depends on altitude is

$$(2) \qquad U_z = U_r \frac{\ln(z/z_0)}{\ln(z_r/z_0)},$$

where U_r is the wind speed at the height z_r above the sea level and z_0 is the roughness length (height). (Walker & Jenkins 1997:7.)

The power available in the wind increases with increased height above sea. The relationship is

$$(3) \qquad \frac{P_z}{P_r} = \left(\frac{z}{z_r}\right)^{3\gamma},$$

where P_z is the power at the height z and P_r is the power at the reference height z_r.

Classes of wind power density

Wind conditions at site are described using wind power classes. Wind power classes 1 to 7 shown in Table 1 are widely used. In general, sites with a wind power class rating of 4 or higher are preferred for large scale wind plants. (American Wind Energy Association 2012).

Table 1.   Classes of wind power density at the heights of 10 m and 50 m[a].

	10 m		50 m	
Wind power class	**Wind power density (W/m^2)**	**Wind speed[b] (m/s)**	**Wind power density (W/m^2)**	**Wind speed[b] (m/s)**
1	less than 100	less than 4.4	less than 200	less than 5.6
2	100–150	4.4–5.1	200–300	5.6–6.4
3	150–200	5.1–5.6	300–400	6.4–7.0
4	200–250	5.6–6.0	400–500	7.0–7.5
5	250–300	6.0–6.4	500–600	7.5–8.0
6	300–400	6.4–7.0	600–800	8.0–8.8
7	more than 400	more than 7.0	more than 800	more than 8.8

(a)   Vertical extrapolation of wind is speed based on the 1/7 power law.

(b)   Mean wind speed is based on the Rayleigh speed distribution of equivalent wind power density. Wind speed is for standard sea-level conditions. To maintain the same power density, speed increases 3 %/1,000 m (5 %/5,000 ft) of elevation.

The Weibull function

The Weibull distribution is a mathematical probability which describes wind speed distribution on site.

Weibull function R_f the relative frequency of wind velocities is

(4) $$R_f = \frac{k}{A_x}\left(\frac{U}{A_x}\right)^{k-1} e^{-\left(\frac{U}{A_x}\right)^{k_x}},$$

where A_x is the scale factor and k the shape factor. The special case of Weibull distribution, with $k = 2$, is called Rayleigh distribution.

Wind speed distribution at University of Vaasa

The weather stations at University of Vaasa are called Fabriikki and Tritonia after the buildings on the roofs of which stations were fitted. Each of the measurement stations can be found in Internet. Figure 5 shows the annual wind speed distribution measured in 2006 at Tritonia weather stations at University of Vaasa. Low wind speeds were frequent (Weather stations at University of Vaasa). If using Weibull function for annual wind speed distribution in our area, the factor k is greater than 1 but less than 2. (Wilson 2014).
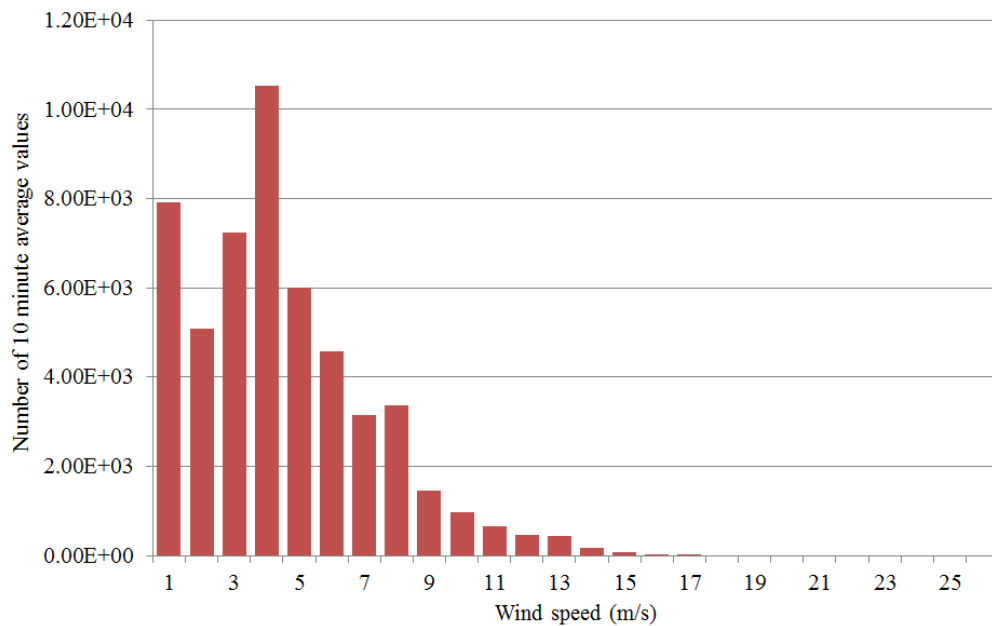
Figure 5.   Annual wind speed distribution at Tritonia weather station in Vaasa, in 2006, at the height of 43 m altitude. Numbers of 10 min average values are shown.

The measured results from the two stations Fabriikki and Tritonia correlated well during several past years. Very similar results were obtained for several years during this work. Mostly low 10 min averages were recorded. The average value of 10 min average values became 4 m/s for year 2006. About 2–5 storms per year with winds up to 25 m/s were detected during years 2005–2009.

In many open or high places around the world, the most abundant wind speed during a calendar year is significantly higher than in Vaasa, but in urban locations lower. In most locations wind speed varies with the seasons and time of the day.

The Finnish Wind Atlas

The new Finnish Wind Atlas is an important tool for estimation of the regional and local wind energy potential in Finland. The Wind Atlas contains average monthly and annual values of wind speed (m/s), potential power production (MWh) calculated for 400 m above sea or ground level. Wind direction is distributed into sectors of 30 degrees. The detailed results are presented on interactive maps which also allow data for selected areas to be downloaded. (Finnish Wind Atlas 2012.)

The Wind Atlas is produced by the European state-of-the-art numerical weather forecasting model AROME using (2.5 x 2.5 km^2 grid resolution) and by the Danish Wind Application and Analysis Program WAsP (downscaling to 250 x 250 m^2 grid at selected areas). The WAsP data is produced as monthly means without distribution into wind direction sectors for heights from 50 m to 150 m or 200 m. The WAsP Lib-files are given for each 2.5 x 2.5 km^2 grid. (Finnish Wind Atlas 2012.)

The Wind Atlas was produced by simulating the weather of 72 selected months in the past (about 5040 days á 24 h). The months for simulation were selected on the basis of statistical analyses of the ERA40 and ERA-Interim data sets. (Finnish Wind Atlas 2012.)

The impact of climate change on average wind speed and wind power potential has been studied on the basis of data from numerical climate change modelling. It is estimated that annual average wind speed could increase by a few per cent during the coming decades, especially as a result of the lessening of sea ice in the Bothnian Bay.

However, the impact of climate change has not been taken into account in the wind speed or power production values given in the Wind Atlas. (Finnish Wind Atlas 2012.)

The Wind Atlas project was ordered in 2008 by the Ministry of Employment and Economy after an international tender had been held. The Wind Atlas was produced by the Finnish Meteorological Institute, with Risoe DTU as a subcontractor (WAsP Lib-file runs). Additional wind data taken at masts and towers were provided for verification of the model results by Vaisala Oyj, WPD Finland and Ålands Vindenergi Andelslag. The project was coordinated by Motiva. The Wind Atlas internet pages were made public on 25 November 2009. (Finnish Wind Atlas 2012.)

Let us now compare measurements of wind speed in this thesis with data in Wind atlas. The wind data of average yearly wind speeds in Vaasa area at 50 m altitude, presented by the Finnish Wind Atlas conforms not exactly to own measured results. One interpretation of the color map in the Finnish wind atlas for the University of Vaasa gives an average annual wind speed of 7–7.5 m/s at a height of 50 meters, while real measurements at the University of Vaasa gives an average value of 4 m/s, which is the calculated average of measured 10 min averages in the year 2006. However, it should be said that weather station Tritonia is at 7 m lower altitude and only 3 m above roof of buildings! From the Finnish Wind Atlas one can find out that at 50 m above sea offshore in the Gulf of Bothnia average

wind speeds are significantly higher than on the coast with protective archipelago and urban environment where our stations are situated.

2.1.3   Wind turbulence and gusts

Wind turbulence refers to wind speed fluctuations on a short timescale. However, there is no established time period over which such wind speed variations are officially classed as turbulent. Power spectral analysis shows the wind speed variation timescales containing the most energy. (Tavner 2012:244.)

Horizontal wind speed spectrum measured at a height of 100 m shows two major peaks. The first major peak at the low frequency end of the spectrum occurs at a period of about 4 days. It seems reasonable, that this peak is the result of fluctuations in wind speed due to the passage of large synoptic-scale pressure systems. The other occurs at a period of 1 min. A spectral gap occurs at a period of 1 hr. (von der Hoven 1957:161–162.)

The IEC standard uses a measure called the turbulence intensity, I_t, which is the ratio of the wind speed standard deviation, σ, to the mean wind speed, u, for each 10 min reporting period: (IEC 61400; Tavner 2012:245.)

(5) $\qquad I_t = \dfrac{\sigma}{u}.$

A wind gust is a sudden, brief increase in speed of the wind. According to U.S. weather observing practice, gusts are reported when the peak wind speed reaches at least 8.23 m/s and the variation in wind speed between the peaks and lulls is at least 4.63 m/s. The duration of a gust is usually less than 20 seconds.

An extreme operating gust (EOG) is a rapid wind speed increase of 24–36 m/s over 5 seconds (IEC 61400-1:27). For the purpose of this section gusts will be assumed to be special cases within wind velocity spectrum, which may be considered to be short-term extreme event forms of turbulence (Tavner 2012:245–246).

2.2   Aerodynamics and fluid mechanics

Forces on a wind turbine blade depend on airflow, attack angle and shape of the blade. In this section, lift and drag forces are first discussed and then Reynolds theory is presented. Forms and roughness height of the blade are also discussed.

Let us assume that the incoming air flow to a stationary airfoil is laminar. Air flow over a stationary airfoil produces two forces, a *lift* force perpendicular to the air flow and a *drag* force in the direction of air flow. The existence of the lift force depends upon *laminar* flow over the airfoil, which means that the air flows smoothly over both sides of the airfoil. If turbulent flow exists rather than laminar flow, there will be little or no lift force. The air flowing over the top of the airfoil has to speed up because of a greater distance to travel and this increase in speed causes a slight decrease in pressure. This pressure difference across the airfoil yields the lift force, which is perpendicular to the direction of air flow. (Johnson 2001:4–4.)

These forces and the overall performance of a wind turbine depend on the construction and orientation of the blades. One important parameter of a blade is the *pitch angle*, which is the angle between the chord line of the blade and the plane of rotation, as shown in Figure 6. The *chord line* is the straight line connecting the leading and trailing edges of an airfoil. The plane of rotation is the plane in which the blade tips lie as they rotate. The blade tips actually trace out a circle which lies on the plane of rotation. Full output power would normally be obtained when the wind direction is perpendicular to the plane of rotation. (Johnson 2001:4–6.)

Because of the helical rotor of Windside wind turbine angle of attack becomes perpendicular, i.e. best, only for limited areas of the blades. Therefore, it can be expected, that the turbine will produce low lift forces. However, the helical turbine should deliver a stable torque compared to a Savonius turbine with two wings.

The pitch angle depending only on the orientation of the blade. Another important blade parameter is the *angle of attack*, which is the angle between the chord line of the blade and the relative wind or the effective direction of air flow. It is a dynamic angle, depending on both the speed of the blade and the speed of the wind. The blade speed at a distance r from the hub and with an angular velocity Ω is $r\Omega$. (Johnson 2001:4–6.)
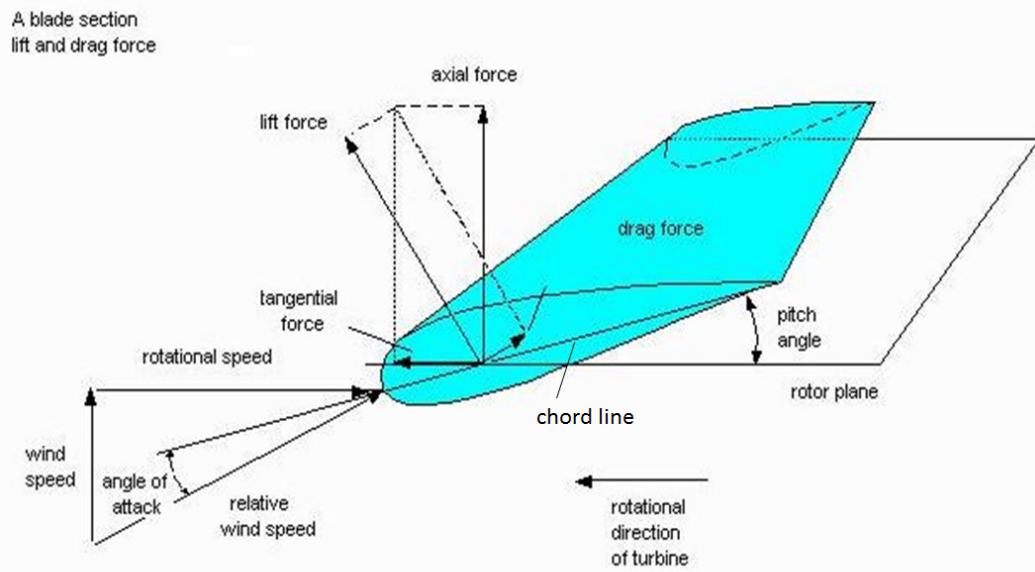
Figure 6.   Force vectors for a blade profile (Wind Power; an interactive presentation 2010).

A wind turbine can be classified in three types: either lift based design, drag based design or combined type designs. A three-cup anemometer commonly used for measuring wind speed is a drag-based vertical-axis machine. A good way of determining whether the design a vertical-axis wind turbine (VAWT) is based on drag or lift is to see if the value of tip speeds can be more than the value of wind speed or the tip speed ratio better than 1. If the speed of the wings is exactly the same as the wind speed, it is operating with a tip speed ratio 1. Above 1 means some amount of lift, while below 1 means mostly drag. Lift based designs can usually output much more power, more efficiently (Eggleston & AWEA Staff 1998). The studied Windside turbine is a combined type of wind turbine.

The drag increases in proportion to the frontal area of the wind turbine and depends on the shape of it. Different shapes have very different drags and the size of the drag for a given shape is usually indicated by the drag coefficient, C_d, which is defined as the drag force per square meter frontal area of the turbine. A hemisphere, like the cup of a cup anemometer, open towards the wind has a very high C_d of 1.42, whereas its C_d is only 0.38 if you turn it 180º around a vertical-axis. A modern automobile typically has a C_d in the range 0.27–0.35. A runner has a C_d about 0.5 and an airfoil shape used on aircraft wings, typically has an extremely small C_d about 0.04. (Danish Wind Industry Association 2002.)

In real situations, the air flow is more or less turbulent. In cases of offshore and in the coast line the air flow is more laminar than in land based sites. High quality

winds have laminar flow. Wind turbine will work well, if the airflow around the blades is laminar. High buildings or obstructions give turbulent air flows.

2.2.1   Drag force

The drag force F_d, for a given fixed object can be calculated by

$$(6) \qquad F_\mathrm{d} = \frac{1}{2} C_\mathrm{d} \rho A U^2,$$

where F_d is the drag force measured in N (Newton), C_d the drag coefficient, ρ is the air density kg/m^3, A is the frontal area of the object in m^2, and U is the wind speed in m/s.

The reason why the square of U is used in Eq. (6) is that we are dealing with a force. If we had looked at the power loss from drag instead, we should have multiplied by the cube of U.

A flat plate facing the wind has much higher drag coefficient than a typical airfoil and the flat plate has its maximum drag coefficient, when the surface of the plate is perpendicular to the air flow. Also, a typical airfoil or profile has its maximum drag coefficient when the angle of attack is near 90 degrees.

2.2.2   Reynolds number

In reality, there is not just one, but two kinds of drag: pressure drag, and friction drag. At very low velocities, and for small objects, say dust particles, the friction drag dominates. At high velocities and with large object sizes pressure differences dominate. The drag coefficient for an object will therefore depend on which type of flow is dominating. A microscopic parachute will not work like a large parachute. Fortunately, we are able to predict which type of flow we are dealing with if we know the so-called Reynolds number; which is named after the British engineer Sir Osborne Reynolds, 1842–1912, for the experiment. The Reynolds number R_e is dimensionless, i.e. it is a ratio of two quantities with the same unit and it is defined by

$$(7) \qquad R_e = \frac{\rho U L}{\mu},$$

where U the relative speed of the fluid in m/s, L the characteristic length, in this case the largest cross section of the frontal area in m, and μ the viscosity of the fluid in Ns/m^2. The viscosity of air, also called the dynamic viscosity of air is

$1.8 \cdot 10^{-5}$ Pa s at 15° C and atmospheric pressure at sea level. ρ is the density of the fluid in kg/m^3. The value in the denominator, μ divided by ρ, is called the kinematic viscosity of air. When the kinematic viscosity is high, the laminar flows dominate. Thus, if the Reynolds number is very small, below 1, one can ignore pressure drag and concentrate on friction drag. If the number is large, above 100, one can ignore the friction drag and look at pressure drag only. Close to the surface of the object friction drag and viscosity are always important. (Danish Wind Industry Association 2002.)

The Reynolds number of wind turbines increases with increased wind speed. The Reynolds number is lower for small vertical-axis Savonius type wind turbines than for big horizontal-axis wind turbines. For a Savonius type wind turbine with height, H, of 30 cm, where each blade is a semicircle to the diameter value 16 cm and with the overlapped distance of 3.2 cm is found that the value of Reynolds number is $1.9 \cdot 10^5$. (Sargolzaei 2007.) For a large horizontal axis wind turbine the Reynolds number is from $5 \cdot 10^6$ to $25 \cdot 10^6$ depending on wind speed and position along the blade span. (Ceyhan 2012.)

At low Reynolds numbers a single thin plate with a suitable circular arc camber can be a good profile. It has been shown in a wind tunnel test that such a curved plate has better lift coefficient than a NACA 0012 (National Advisory Committee for Aeronautics) profile. For all Reynolds numbers below 70,000 the best profile was a thin plate with a 5 % circular arc camber. At all turbulence levels this profile produced the greatest lift to drag ratio, and had the highest lift coefficient at all angles of attack. (Laitone 1997.)

NACA profiles are used for aerofoil wings, turbines and with symmetrical cross-section in sailboats keel and rudder. A suitable profile also for a wind turbine blade with low air speed is NACA 4412. This profile has best lift coefficient with an angle of attack of 14 degrees (Library on Human Powered Flight 2012). Other profiles as having the best lift coefficient at an angle of attack of 6 to 8 degrees can also be found. At an angle of attack of 25 degrees the lift coefficient of the profile NACA 4412 has decreased and the flow is turbulent at upper side of the profile. Other profiles have similar values of angle of attack, when the flow on the upper side of the profile has become turbulent. (Miley 1982.)

To make wind turbine blades with a good lift coefficient requires that the air flow especially around leading edge of the blade is laminar. This can be achieved with a suitable profile for the current air velocities and by that the roughness height, especially at leading edge of the profile, is sufficiently low.

The lift coefficient and the drag coefficient of NACA 63-430 airfoil is affected more obviously by the roughness height less than 0.3 mm than by the roughness height more than 0.3 mm. In other words, the performance of airfoils is more sensitive to small roughness height. As a result, the roughness height of 0.3 mm is proposed to be critical roughness height (Ren & Ou 2009).

Because the lift coefficient of the airfoil is more sensitive to small roughness height it seems that 0.1 to 0.2 mm will be a good roughness height on the leading edge of the wind turbine blade. At low Reynolds numbers, the thin uniform blades, with 5 % circular arc camber, yield the greatest lift coefficient.

2.3   Output power of ideal wind turbines

Theoretical description of output power from ideally rotating wind turbines is here subdivided according to horizontal-axis and vertical-axis drag-type wind turbines. The horizontal-axis wind power plant is described to understand the differences between the types of wind turbines and thus better able to exploit the properties of the studied vertical axis wind turbine. The information is largely taken from sources Johnson 2006 and Manwell 2009.

2.3.1   Horizontal-axis wind turbines

The function of an ideal horizontal axis wind turbine can be described by means of flowing air through the turbine blades. The kinetic energy in a parcel of air of mass m, flowing at speed U in the x direction is

(8) $$E_\mathrm{k} = \frac{1}{2}mU^2 = \frac{1}{2}(\rho A x)U^2,$$

where A is the cross-sectional area in m^2, ρ is the air density in kg/m^3 and x is the thickness of the parcel in m. The kinetic energy is increasing uniformly with x, because the mass is increasing uniformly. The power in the wind P_w is the time derivative of the kinetic energy is

(9) $$P_\mathrm{w} = \frac{\mathrm{d}E_\mathrm{k}}{\mathrm{d}t} = \frac{1}{2}\rho A U^2 \frac{\mathrm{d}x}{\mathrm{d}t} = \frac{1}{2}\rho A U^3.$$

This can be viewed as the power being supplied at the origin to cause the energy of the parcel to increase according to Eq. (8). A wind turbine will extract power from side x, with Eq. (9) representing the total power available at this surface for possible extraction.

Output power of an ideal horizontal-axis wind turbine is obtained on the basis of *actuator disc theory* that was developed for marine propellers by Rankine in 1865, Froude 1885, and was used by Betz 1920.

This actuator disk theory provides a simple, 1-dimensional approach to the problem of rotor modeling. The theory requires making the following assumptions:

    (i)   Homogenous, incompressible, steady state fluid flow
    (ii)   No frictional drag
    (iii)   An infinite number of blades
    (iv)   Uniform trust over the disc or rotor area
    (v)   A non-rotating wake
    (vi)   The static pressure far upstream and far downstream of the rotor is equal to the undisturbed ambient static pressure.

The physical presence of a wind turbine in a large moving air mass and how it modifies the local air speed and pressure as shown in Figure 7 (Johnson 2006:4–2). Applying the conservation of linear momentum to the control volume enclosing the whole system, one can find the net force on the contents of the volume.
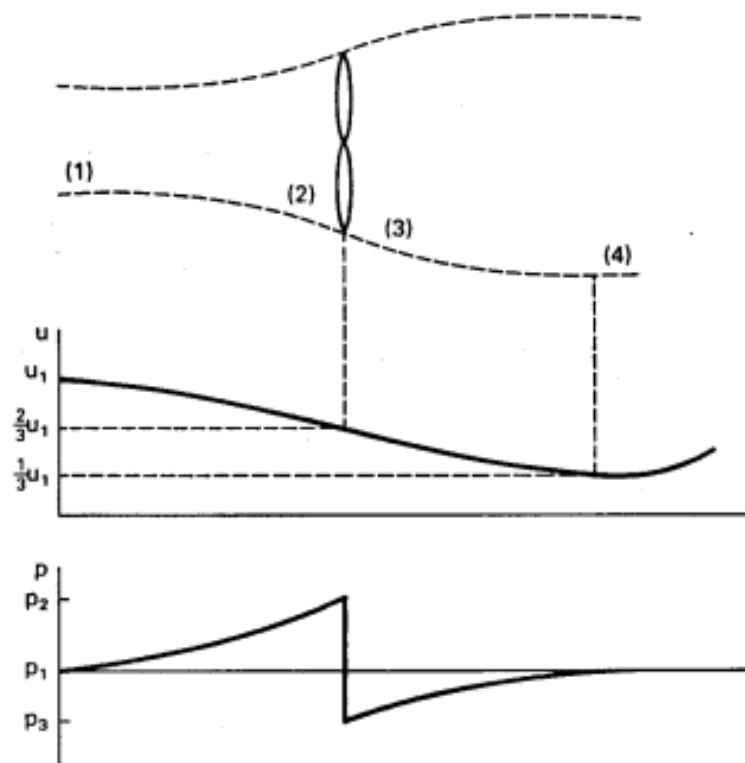
Figure 7.   Circular tube of air mowing through ideal wind turbine. (1), (2), (3) and (4) indicate locations (Johnson 2006:4–4).

That force is equal and opposite to the thrust, T, which is the force of the wind on the wind turbine. From the conservation of linear momentum for a one-dimensional, incompressible, time-invariant flow, the thrust is equal and opposite to the rate of change of momentum of the air stream in Figure 7:

(10) $T = U_1(\rho AU)_1 - U_4(\rho AU)_4.$

For steady state flow in locations 1 and 4, $(\rho AU)_1$ is equal to $(\rho AU)_4$ and to $\dot{m}$, the mass flow rate. Therefore:

(11) $T = \dot{m}(U_1 - U_4).$

The thrust is positive so the velocity behind the rotor, U_4, is less than the free stream velocity, U_1. No work is done on either side of the turbine rotor. Thus the Bernoulli function can be used in the two control volumes on either side of the actuator disc. In the upstream of the disc:

(12) $p_1 + \dfrac{1}{2}\rho U_1^2 = p_2 + \dfrac{1}{2}\rho U_2^2,$

where p_1 and p_2 are pressures in locations (1) and (2) in Figure 7. In the downstream of the disc:

(13) $p_3 + \dfrac{1}{2}\rho U_3^2 = p_4 + \dfrac{1}{2}\rho U_4^2,$

where p_3 and p_4 are pressures in locations (3) and (4) in Figure 7. It is assumed that the far upstream and far downstream pressures are equal ($p_1 = p_4$) and that the velocity across the disc remains the same ($U_2 = U_3$). The thrust can also be expressed as the net sum of the forces on each side of the actuator disc:

(14) $T = A_2(p_2 - p_3),$

Solving for ($p_2 - p_3$) using Equations (12) and (13) and substituting that into Eq. (14), we obtain:

(15) $T = \dfrac{1}{2}\rho A_2(U_1^2 - U_4^2).$

Equating the thrust values from Equation (11) and (15) and recognizing that the mass flow rate is also $\rho A_2 U_2$, the following equation is obtained:

(16) $U_2 = \dfrac{U_1 + U_4}{2}.$

Thus, the wind velocity at the rotor plane, using this simple model, is the average of the upstream and downstream wind speeds. If one defines the axial induction factor, a, as the fractional decrease in wind velocity between the free stream and the rotor plane, then

(17) $$a = \frac{U_1 - U_2}{U_1},$$

gives

(18) $$U_2 = U_1(1 - a),$$

and

(19) $$U_4 = U_1(1 - 2a).$$

The quantity $U_1 a$ is often referred to as the induced velocity at the rotor, in which case the velocity of the wind at the rotor is a combination of the free stream velocity and the induced wind velocity. As the axial induction factor increases from 0, the wind speed behind the rotor slows more and more. If $a = \frac{1}{2}$, the wind slowed to zero velocity behind the rotor and the simple theory is no longer applicable. The output power P is equal to the thrust times the velocity at the disc:

(20) $$P = \frac{1}{2}\rho A_2(U_1^2 - U_4^2)U_2 = \frac{1}{2}\rho A_2 U_2(U_1 + U_4)(U_1 - U_4).$$

Substitution for U_2 and U_4 from Equations (18) and (19) gives:

(21) $$P = \frac{1}{2}\rho A U^3 4a(1 - a)^2,$$

where the control volume area at the rotor, A_2, is replaced by A, the rotor area and the free stream velocity U_1 is replaced by U. (Manwell 2009:92–94.)

Consider a tube of moving air with initial or undisturbed diameter d_1, speed U_1, and pressure p_1 as it approaches the turbine. The speed of the air decreases as the turbine is approached, causing the tube of air to enlarge to the turbine diameter d_2. The air pressure will rise to a maximum just in front of the turbine and will drop below atmospheric pressure behind the turbine. Part of the kinetic energy in the air is converted to potential energy in order to produce this change in pressure. Still more kinetic energy will be converted to potential energy after the turbine, in order to raise the air pressure back to atmospheric.

This causes the wind speed to continue to decrease until the pressure is in equilibrium. Once the low point of wind speed is reached, the speed of the tube of air will increase back to U_1 as it receives kinetic energy from the surrounding air (Eldridge 1980).

It can be shown that under optimum conditions, when maximum power is being transferred from the tube of air to the turbine, the following relationships hold:

(22) $$U_2 = U_3 = \frac{2}{3}U_1,$$

$$U_4 = \frac{1}{3}U_1,$$

$$A_2 = A_3 = \frac{3}{2}A_1 \text{ and}$$

$$A_4 = 3A_1.$$

The mechanical power $P_{\text{m,ideal}}$ extracted is the difference between the input and output power in the wind by substitution of A_4 and U_4 from Eq. (22):

(23) $$P_{\text{m,ideal}} = P_1 - P_4 = \frac{1}{2}\rho\left(A_1 U_1{}^3 - A_4 U_4{}^3\right) = \frac{1}{2}\rho\left(\frac{8}{9}A_1 U_1{}^3\right).$$

The normal method of expressing this extracted power is in terms of the undisturbed wind speed and the turbine area by substitution of A_2 from Eq. (22). For a horizontal wind turbine this yields:

(24) $$P_{\text{m,ideal}} = \frac{1}{2}\rho\left[\frac{8}{9}\left(\frac{2}{3}A_2\right)U_1{}^3\right] = \frac{1}{2}\rho\left(\frac{16}{27}AU^3\right),$$

where the turbine area finally is denoted by A and the undisturbed wind speed by U. The factor $16/27 = 0.593$ is called the *Betz coefficient*. It shows that under the assumptions an actual turbine cannot extract more than 59.3 percent of the power in an undisturbed tube of air of the same area. In practice, the fraction of power extracted will always be less because of mechanical imperfections. In conventional horizontal wind turbines a good fraction is 35–40 percent of the power in the wind under optimum conditions, although fractions of power coefficients as high as 50 percent have been claimed. (Johnson 2006:4–4.) The newest horizontal-axis wind turbines reach power coefficient of 50 percent. (Enercon 2014:9)

2.3.2 Drag-based vertical-axis wind turbines

Vertical-axis wind turbines are created from lift and drag based designs or from combined-type design. Drag based vertical-axis wind turbines work with something similar to the paddles utilized to push a canoe though the water. Assuming that the paddle used to push the canoe does not slip, the maximum speed will be similar to the drag of the paddle. Drag driven wind mills, as shown in Figure 8, were used for over thousand years ago. They included a vertical axes consisting of flat surfaces in which half of the rotor was shielded from the wind. The simplified model on the right in the Figure 8 is used to analyze the performance of this drag machine.

Drag machine   Drag machine model
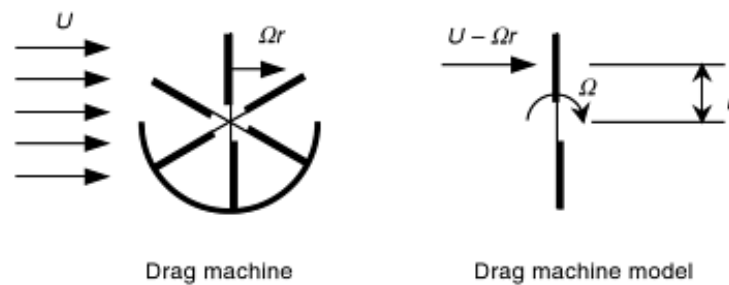
Figure 8. Simple drag machine and model; *U*, velocity of the undisturbed air flow; *Ω*, angular velocity of wind turbine rotor; *r*, radius. (Manwell 2009:114.) The real wind affects, to the right of the figure, only half of the surface of the rotor of the drag machine.

The drag force, F_d, is a function of the relative wind velocity at the moving rotor surface:

$$(25) \qquad F_d = C_d \left[\frac{1}{2} \rho (U - \Omega r)^2 \frac{1}{2} A \right],$$

where *A* is the total machine area and where the three-dimensional drag coefficient, C_d, for the square plate is assumed to be 1.1. (Manwell 2009:114.)

The rotor or turbine power is the product of the torque due to the drag force and rotational speed of the rotor surface:

$$(26) \qquad P_m = C_d \left[\frac{1}{2} \rho (U - \Omega r)^2 \frac{1}{2} A \right] \Omega r = \left(\rho \frac{1}{2} A U^3 \right) \left[\frac{1}{2} C_d \lambda (1 - \lambda)^2 \right].$$

The power coefficient, shown in Figure 9, is a function of λ, the ratio of the surface velocity to the wind speed, and is based on an assumed total machine area of *A* with a C_d value of 1.1:

(27) $$C_{\mathrm{p}} = \left[\frac{1}{2}C_{\mathrm{d}}\lambda(1-\lambda)^2\right].$$
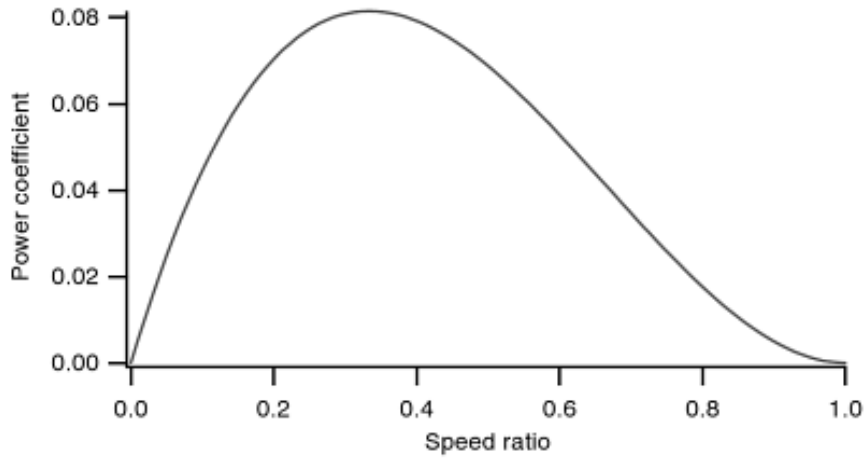
Figure 9.   Power coefficient Eq. (27) for a flat plate drag machine when C_{d} equals to 1.1 (Manwell 2009:114).

The power coefficient is zero at speed ratios of zero (no motion) and 1.0 (the speed at which the surface moves is the wind speeds and it experiences no drag force). The peak power coefficient of 0.08 occurs at the speed ratio of 1/3. The maximum power coefficient is significantly lower than the Betz limit of 0.593. This example also illustrates one of the primary disadvantages of a pure drag machine: the rotor cannot move faster than the wind speed. Thus, the wind velocity relative to the power producing surfaces of the machine, U_{rel}, is limit to the free stream velocity:

(28) $$U_{\mathrm{rel}} = U(1-\lambda),$$

with λ less than 1. (Manwell 2009:115.)

2.4   Permanent magnet generator

The permanent magnet generator can be considered as a cylindrical-rotor synchronous generator.

The equation of the synchronous generator, with the output voltage $\overline{V_a}$ taken as the reference of the phasors:

(29) $$\overline{E_{\mathrm{f}}} = \overline{V_a} + \overline{I_a}R_{\mathrm{a}} + j\overline{I_a}X_{\mathrm{a}},$$

where E_f is the induced EMF/phase, I_a the current/phase, X_a total reactance/phase, R_a stator resistance/phase, V_a terminal voltage/phase, δ load angle and φ the phase angle.
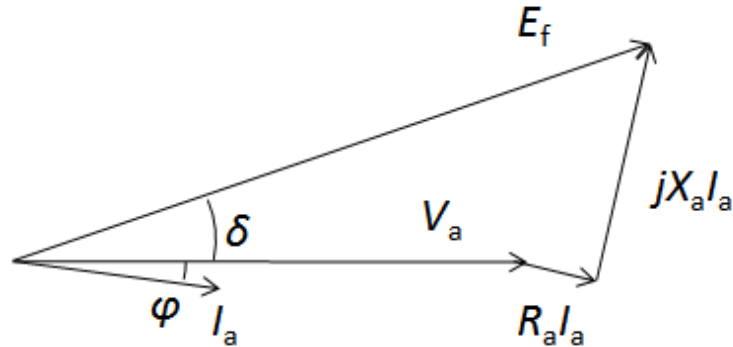
Figure 10.   Phasor diagram of cylindrical-rotor synchronous generator supplying a lagging power factor load.

The phasor diagram of cylindrical-rotor synchronous generator is shown in Figure 10.

When the rotational speed of the generator varies, the induced voltage, terminal voltage and frequency vary also. If the rotational speed of the generator increases, the induced electromotive force (EMF), frequency, and terminal voltage also increase. Output current also increases if the system is connected to any load. Increasing frequency increases internal reactance of the generator. This limits the output current so that it does not increase linearly with increased rotational speed. Finally, the short circuit current at different rotational speeds sets the upper limit for the output current from the generator.

The generator plays a central role in a wind power system. Basic generators from the manufacturer were used (Section 1.5). The used permanent magnet generators were three-phase with common shaft for the generator and the turbine. The generator consists of the stator with the armature windings and the rotor with the permanent magnets. The armature windings are physically separated by 120º, and therefore, each phase is 120º apart from one another. The windings are arranged in three phases. The ends of the phase windings are connected to six terminals. The generator, as is shown in Figure 11 is star connected. It can also be delta connected. Then the connections between W_2, U_2 and V_2 are removed, U_1 is linked to W_2, V_1 to U_2 and W_1 to V_2.
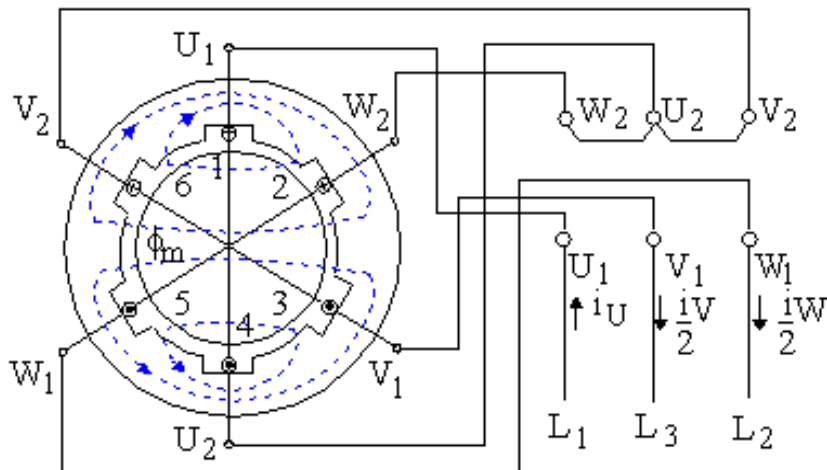
Figure 11. Simplified windings of a three-phase AC-generator. (Aura & Tonteri 1996:119).

When the permanent magnet rotor is rotated by the turbine, voltages are induced in the phase windings. The rotation speed and the frequency of the induced voltage are related by

(30) $$n = \frac{60f}{p_p},$$

or

(31) $$f = \frac{np_p}{60},$$

where f is the frequency, n the rotation speed in rpm and p_p is the number of pole pairs. The induced voltages are directly proportional to the rotational speed. The permanent magnets on the rotor produce a flux ϕ_f in the air gap. This flux rotates at a synchronous speed ω_s rad/s, which is the same as the rotor speed. The flux ϕ_{fa} linking one of the stator phase windings, for example phase a, varies sinusoidally with time:

(32) $$\phi_{fa}(t) = \phi_f sin\omega t,$$

where

(33) $$\omega = 2\pi f = p_p\omega_s.$$

If we assume N_s as an equivalent number of turns in each stator phase winding, the EMF induced in phase a from Eq. (32) is

(34) $e_{fa}(t) = N_s \dfrac{d\phi_{fa}}{dt} = \omega N_s \phi_f cos\omega t.$

This induced voltage in the stator winding is called the excitation voltage, whose rms value is

(35) $E_{fa} = \dfrac{\omega N_s}{\sqrt{2}} \phi_f.$

(Mohan 2003:435.)

An equivalent circuit for one phase of a star connected three-phase PM generator is shown in Figure 12. The resistive load is denoted by R_l and all other values are denoted as in Figure 10. If the value of the resistive load is low, the output current will be high. If the value of the resistive load is 0 Ω, it becomes a short circuit and a short circuit current will flow through the generator.

If the load is a diode and a battery, the peak value of the terminal voltage of the generator must be higher than the sum of the voltage drop of the diode and the terminal voltage of the battery before any battery charging will occur.
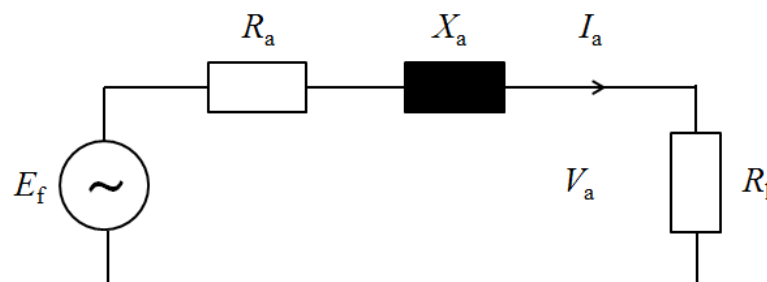
Figure 12.   Equivalent circuit for one phase of a star connected three phase PM generator with a resistive load.

2.5   Star-delta connection

Star-delta connection has been used traditionally to limit the starting current of large (more than 2 kW) three-phase electric motors. In the beginning of its history the connection was manual, but later it was automated by using a timer for controlling the contactors. Thus when the power is cut out, the control signals shut down at once, the contactors and the motor is ready for the following startup.

In this thesis, the aim was to use star-delta switch in the investigated wind tur-
bines and the function the star-delta switch would be made both automatic and
reversible.

2.5.1   *Star-delta and delta-star transformation*

If a three-phase, three-wire supply or a three-phase load is connected in one type
of configuration, it can be easily transformed or changed it into an equivalent con-
figuration of the other type by using either the Star Delta Transformation or Delta
Star Transformation process. Figure 13 shows the three-phase star and delta con-
figurations with resistances. The same calculation rules apply impedances. These
rules are for constant power and frequency.
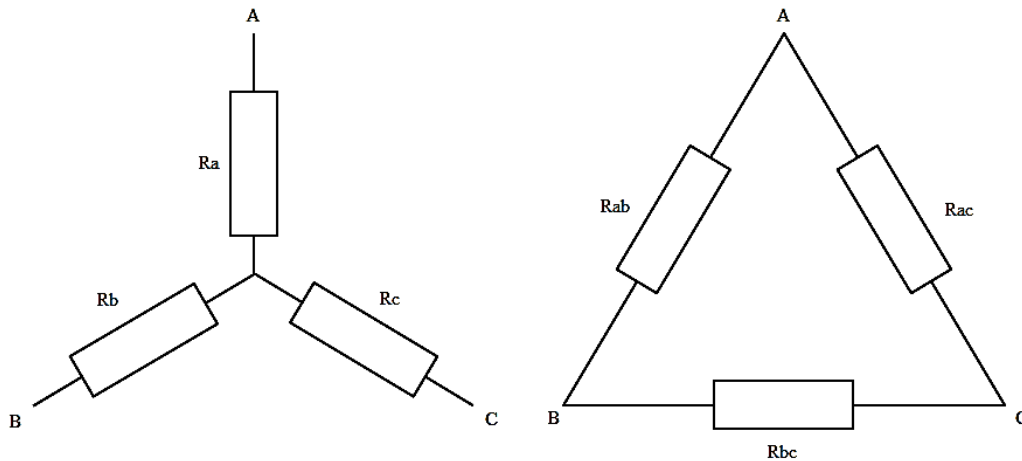
Figure 13.   Star and delta configuration.

In a star-delta transformation the resistance between phases A and B is calculated
by

(36) $$R_{ab} = R_a + R_b + \frac{R_a R_b}{R_c},$$

where R_a, R_b and R_c are phase resistances in star configuration.

Similarly, R_{bc} and R_{ac} are calculated, which means that if the phase resistances in
the star configuration is such 1 Ω, each resistance between two phases of the delta
connection becomes 3 Ω.

In a delta-star transformation is the resistances calculated by

$$(37) \qquad R_a = \frac{R_{ab}R_{ac}}{R_{ab} + R_{bc} + R_{ac}},$$

where R_{ab}, R_{bc} and R_{ac} are resistances between terminals in delta configuration.

Similarly, R_b and R_c are calculated, which means that R_a and R_{ab} are in inverse relationship to the previous star-delta transformation.

2.5.2 Star-delta connection of a three-phase load

As shown in the transformations above, the phase resistance of the star-connection is only 1/3 of the resistance that exists between two phases in delta connection. However, the electrical power is the same in both the configurations. This will not be the case if a three-phase electrical load with symmetrical phase resistances is connected in either star or delta connection. Now, all resistors have the same value and if e.g. R_a is 3 Ω and the line to line voltage V_L is 90 V. Then the line current I_L in star connection is calculated as follows

$$(38) \qquad I_L = \frac{V_L/\sqrt{3}}{R_a} = \frac{90/\sqrt{3}}{3} = \frac{30}{\sqrt{3}} \text{ A}$$

and the electric three-phase power P_Y is

$$(39) \qquad P_Y = \sqrt{3}V_L I_P = \sqrt{3}\,90\,\frac{30}{\sqrt{3}} = 2{,}7 \text{ kW}.$$

If the same electric load as above is connected in delta connection, the phase current I_P is

$$(40) \qquad I_P = \frac{V_L}{R_a} = \frac{90}{3} = 30 \text{ A}.$$

The line current I_L is

$$(41) \qquad I_L = \sqrt{3}I_P = \sqrt{3} \cdot 30 \text{ A}.$$

and the electric three-phase power P_D is

$$(42) \qquad P_D = \sqrt{3}V_L I_L = \sqrt{3} \cdot 90\sqrt{3} \cdot 30 = 3 \cdot 2{,}7 \text{ kW}.$$

2.5.3   The three-phase PM generators under study

Two sizes of tree-phase PM generators were used in this study. The generators are named small and large. Characteristics supplied by the manufacturer of the small generator are given in this section and they are the base for the following simulations. The characteristics of the large generator supplied by the manufacturer are presented in Figures A1.2–5.

The values of small PM generator were:
  (i)   Number of pole pairs 3
  (ii)   Phase resistance 3.6 Ω
  (iii)   Phase inductance 37 mH and
  (iv)   Rated power 300 W.

The values of large PM generator were:
  (i)   Number of pole pairs 8
  (ii)   Phase resistance 1.0 Ω
  (iii)   Phase inductance 19 mH and
  (iv)   Rated power 2 kW.

The phase resistance of the large generator was measured and the phase inductance was calculated with open circuit voltage and short circuit characteristics.

The open circuit voltages of the small PM generator used is shown in Figure 14. The open voltage with star connection is √3 times higher than with delta.
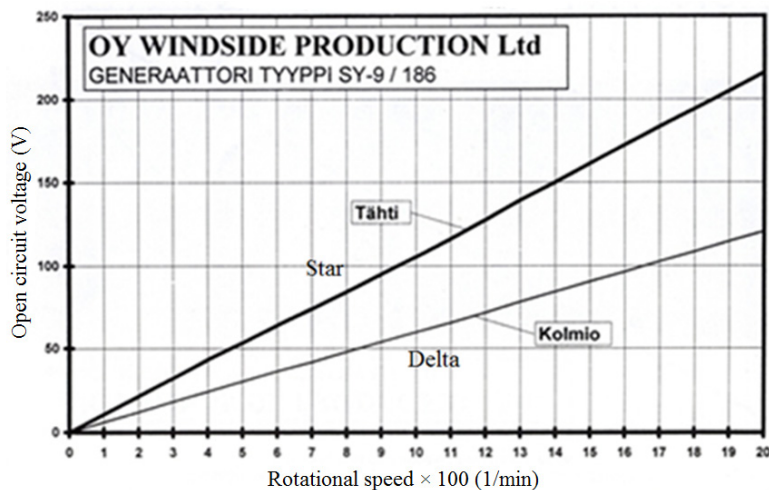
Figure 14.   Open circuit voltages of the studied small PM generator measured after rectifier (Oy Windside Production Ltd 2012).

These open circuit voltages have been measured after the uncontrolled six pulse rectifier and should therefore be divided by 3 divided by π and the square root of 2 to get the open circuit phase to phase voltage. To get the phase voltage the phase to phase voltage should be divided by the square root of 3. It is assumed that the DC power is continuous. This theory is found from Section Uncontrolled and Controlled Rectifiers in The Power Electronics Handbook as is edited by Skvarenina (Swamy 2002:4.2).

The short circuit current characteristics shown in Figure 15 have also been measured after the six-pulse rectifier bridge. When resistive load and assumed that the DC power is continuous the alternating current is calculated also by

(43) $$I_{AC} = \frac{\pi I_{DC}}{3\sqrt{2}},$$

where I_{DC} is a short circuit current of Figure 15 or a charging current of Figure 16.

It is not possible to obtain a current higher than the short circuit current Eq. (41), reason being that it will be difficult to get high output power with star connected generator compared with delta connected. The short circuit current with delta connection is √3 times higher than with star.
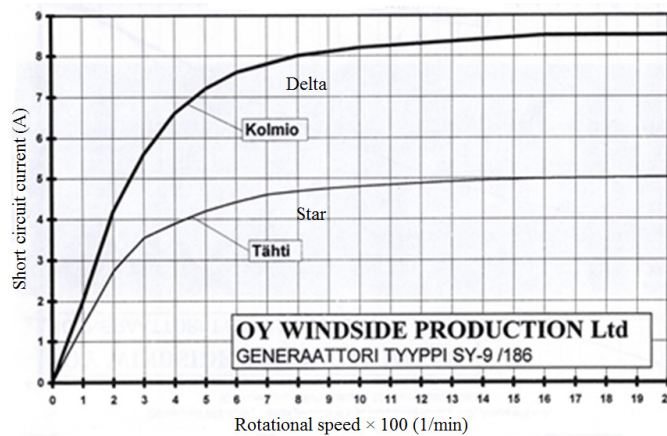
Figure 15. The short circuit characteristics of the studied small PM generator measured after rectifier (Oy Windside Production Ltd 2012).

The charging characteristics of the small PM generator used have been measured on the test bench by the manufacturer. The characteristics are shown in Figure 16. The output current by delta connection is higher than by star connection at rotational speed values greater than 700 rpm. At high rotational speed the output current is about 60 % higher by delta connected generator than by star connection.

Intersection of battery charging graphs in Figure 16 is due to differences in open circuit voltage and internal impedance when using star or delta connected three-phase generator.
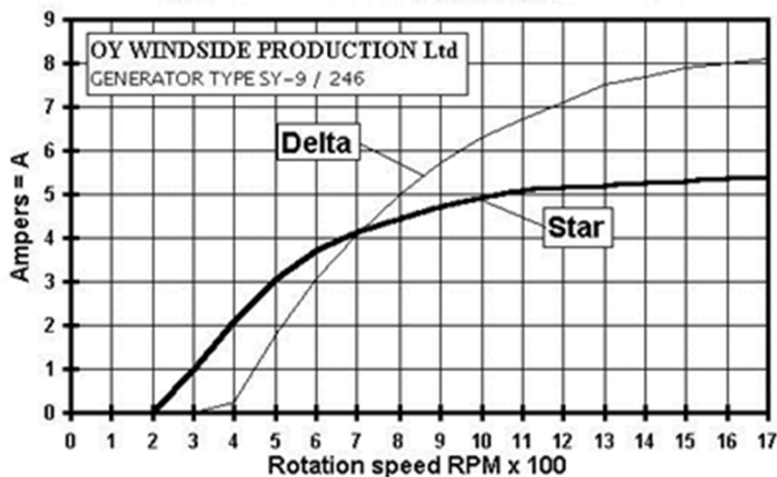
Figure 16.   The charging characteristics of the generator in star or in delta when battery is 24 V (Oy Windside Production Ltd 2012).

The open circuit voltage of star connected generator compared with of delta connected becomes high enough to begin charging a battery with a certain battery voltage at lower rotational speeds. Increase in rotational speed increases the open voltage (Fig. 14) but also the frequency so that the inductive reactance increases. Therefore, the internal impedance of the generator also increases with increasing rotational speed. The internal impedance of star connected generator compared to delta connected is three times higher. Therefore, the delta connection is better than star connection at high rotational speed. When open circuit voltage of delta connected generator is increased sufficiently an efficient battery charging begins.

The increased internal impedance of star connected generator compared to delta connected affects more the charging current at higher rotational speed and therefore delta connection is better than star connection.

Simulations were done by using Simplorer® simulation software (Ansys Simplorer 2014). Simulations were done both with 24 V and 12 V battery banks. The simulation software had a limited number of components which prevented reading the alternating current (AC), which is therefore calculated. The simulated circuit is shown in Figure 17. The simulated system changed from star connection to delta connection at time 100 ms. The AC voltage sources E1, E2 and E3 were parameterized according to the phase voltage by star connection and used frequency values are calculated from the corresponding rotational speed values, all

from Figure 14. The phase resistance and phase inductance were parameterized with the values of the studied small PM generator.
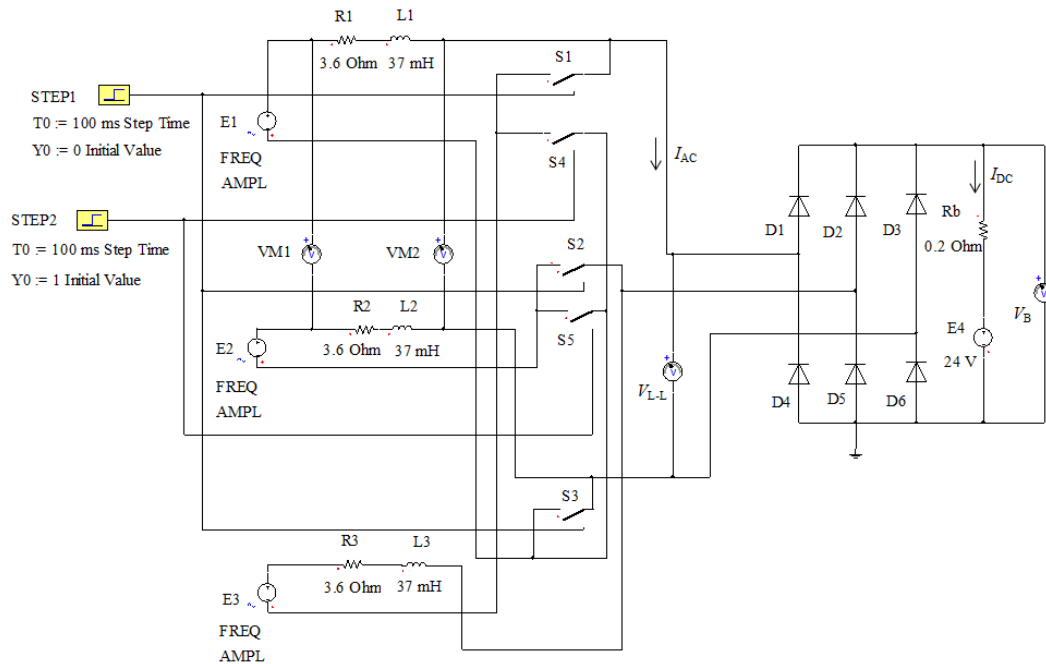
Figure 17.   Main circuit of PM generator system used in a wind turbine WS-0.30B, which was simulated. The generator is equipped with a star-delta switch. The battery bank is 24 V.

Battery voltage was parameterized to 24 V, the battery bank internal resistance to 0.2 Ω and the voltage drop of one diode to 0.7 V.

The phase to phase voltage V_{L-L}, battery voltage V_B and battery charging current I_{DC} were observed.   The alternating current I_{AC} values were calculated by Eq. (43). The results from simulations are tabulated and are presented with XY graphs.

The situation when the rotational speed is 400 rpm is shown in Figure 18. The EMF voltage per phase, $E_{f\ phase\ rms}$, is 18.75 V and the frequency f is 27.5 Hz. Then the output charging direct current $I_{DC\ star}$ is 1.98 A with star connection, and the with delta connection output charging direct current $I_{DC\ delta}$ is only 0.06 A. The alternating currents I_{AC} values are calculated by Eq. (43) and they are 1.47 A and 0.04 A respectively. Output currents are now lower with delta connection than by star connection. The top value of V_{L-L} is the battery voltage added by two times the diode drop voltage. $V_{L-L\ delta}$ is low and near sinusoidal. Figure 19 shows a situation at a rotational speed of 800 rpm. The $E_{f\ phase\ rms}$ value is 37.51 V and the frequency value is 40 Hz. The output current $I_{DC\ star}$ value is 4.29 A, and the

output current $I_{DC\,delta}$ value is 5.51 A. The alternating currents I_{AC} values are then calculated to 3.13 A and 4.08 A respectively. Output currents are now higher by delta connection than by star connection!
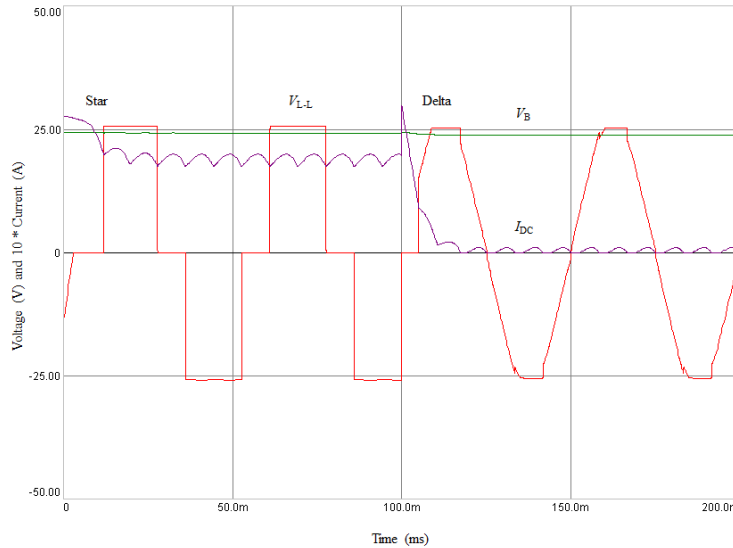
Figure 18. Voltages V_{L-L} and V_B and current I_{DC} as functions of time. Transition from star to delta occurs at time instant 100 ms. A small PM generator of WS-0.30 wind turbine with star-delta switch was simulated. The rotational speed value is 400 rpm.
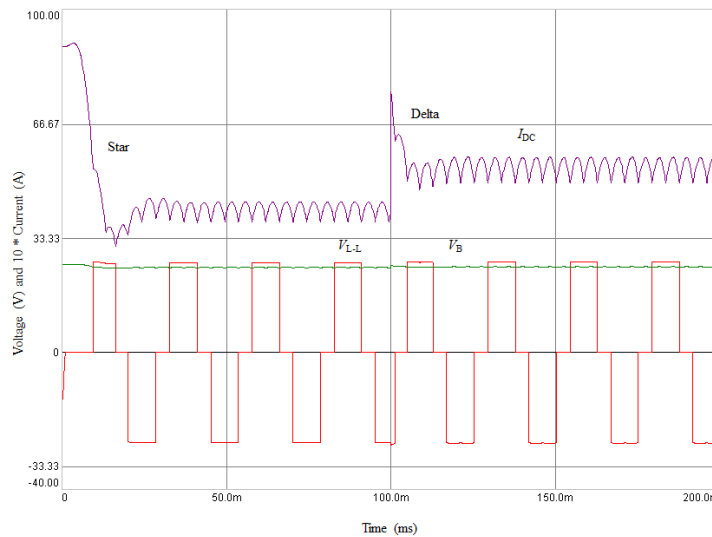
Figure 19. Voltages V_{L-L} and V_B and current I_{DC} as functions of time. Transition from star to delta occurs at time 100 ms. The small PM generator of a WS-0.30B wind turbine was simulated with star-delta switch by an open circuit voltage value of 37.51 V and a frequency value of 40 Hz.

Figure 20 shows a situation at a rotational speed value of 1400 rpm. The $E_{f\,phase\,rms}$ value is 65.64 V and the frequency value is 70 Hz. Then the output current $I_{DC\,star}$ value is 5.02 A, and the output current $I_{DC\,delta}$ value is increased to 8.12 A. The alternating currents I_{AC} values are then calculated to 3.72 A and 6.01 A respective. Output currents are now much higher by delta connection than by star connection.
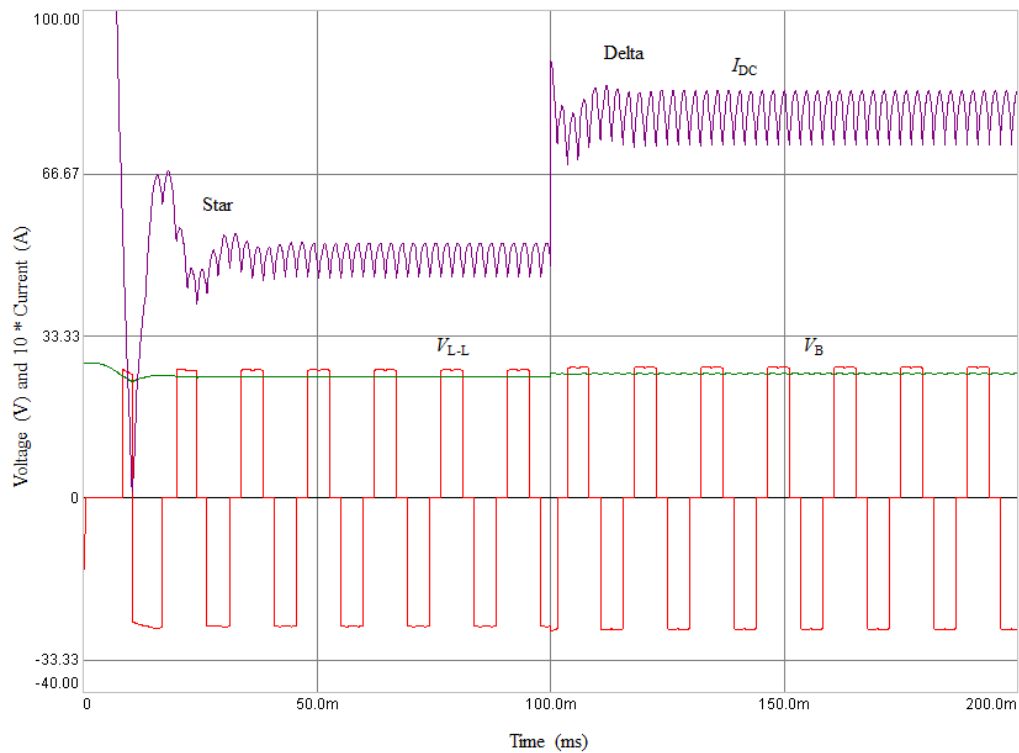
Figure 20.   Voltages V_{L-L} and V_B and current I_{DC} as functions of time. Transition from star to delta occurs at time 100 ms. A small PM generator of WS-0.30B wind turbine is simulated with star-delta switch by increased open circuit voltage and frequency values. The output current value is here higher with delta connected than with star connected generator.

The simulated results are processed by using Excel® software. $I_{AC\,star}$ and $I_{AC\,delta}$ are calculated by Eq. (43). After this an XY chart is plotted. The so obtained XY graph can then be compared with the XY chart obtained from real measurement. It is seen from Table 2 and Figure 23 that it does not help even if the rotational speed is increased drastically to 4000 rpm with star connection.

Table 2.   Results from simulation of the circuit in Figure 17. A battery bank voltage value of 24 V and an internal battery bank resistance value of 0.2 Ω were used.

rpm	f (Hz)	E (V)	$I_{DC\,star}$	$I_{AC\,star}$	$I_{DC\,delta}$	$I_{AC\,delta}$
0.00	0.00	0.00	0.00	0.00	0.00	0.00
200.00	10.00	9.38	0.00	0.00	0.00	0.00
300.00	15.00	14.07	0.78	0.58	0.00	0.00
400.00	20.00	18.75	1.98	1.47	0.06	0.04
500.00	25.00	23.44	2.85	2.11	1.57	1.16
600.00	30.00	28.13	3.48	2.58	3.13	2.32
800.00	40.00	37.51	4.23	3.13	5.51	4.08
1000.00	50.00	46.89	4.64	3.44	6.88	5.09
1200.00	60.00	56.26	4.91	3.64	7.57	5.61
1400.00	70.00	65.64	5.02	3.72	8.12	6.01
1600.00	80.00	75.02	5.16	3.82	8.43	6.24
1800.00	90.00	84.39	5.19	3.84	8.67	6.42
2000.00	100.00	93.77	5.23	3.87	8.85	6.55
4000.00	200.00	187.54	5.40	4.00	9.36	6.93

DC currents presented in Table 2 are shown in XY chart form in Figure 21. When this chart is compared with Figure 16 supplied by the manufacturer it is found to be very similar graphs of the charging currents.
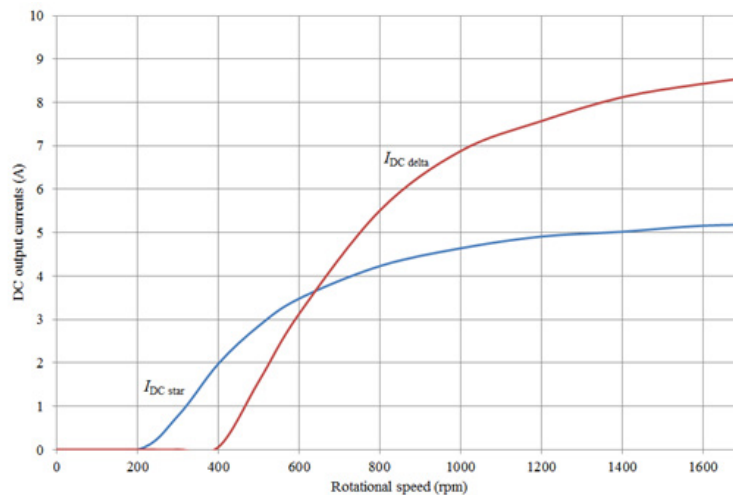
Figure 21.   The DC charging currents as functions of rotational speed by the small PM generator of WS-0.30B simulated with a 24 V battery bank.

The alternating output currents as functions of rotational speed of the small PM generator when it is simulated connected in star or delta is shown in Figure 22.
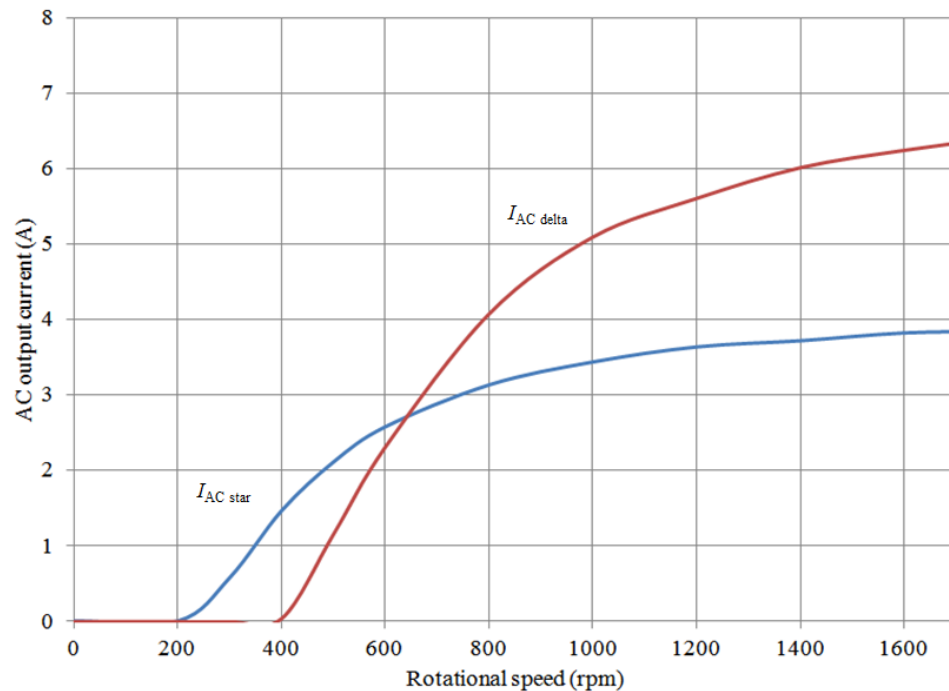
Figure 22.   The alternating currents as functions of rotational speed by the small PM generator of WS-0.30B simulated with a 24 V battery bank.

A six pulse rectifier is used between the generator and the batteries. In high rotational speed the AC charging current is significantly higher when the delta configuration is used, instead of star configuration, because the impedance is only 1/3 of the impedance in star configuration and when the open circuit voltage by star connection is only √3 times higher! The value of internal impedance per phase increases to more than 16 Ω by star connection at high rotational speed.

The simulation results have shown a clear difference of output current between star and delta connected small variable speed PM generator when it is used for battery charging.

Two additional important consequences were observed during simulations for small generator. First, if the pole pairs of the generator were reduced then the frequency was proportionally reduced. Therefore, the values of internal impedances became lower and the values of short circuit currents increased. Second, if the battery voltage is lower than the voltage of a fully charged battery, then the intersection of star and delta graphs shown in Figure 21 occurred at lower rotational speed. If the battery voltage is higher than the rated voltage, the intersection of the graphs occurred at higher rotational speed.

A simulation was also done by a 12 V battery bank. The results are shown in Table 3. The simulated results are also here processed by using Excel® software. $I_{AC\ star}$ and $I_{AC\ delta}$ are calculated. After this a XY chart is plotted in Figure 23.

Table 3.   Results from simulation of the circuit in Figure 17 but with two 12 V batteries connected in parallel. The internal resistance value of each battery is 0.1 Ω.

rpm	f(Hz)	E(V)	$I_{DC\ star}$	$I_{AC\ star}$	$I_{DC\ delta}$	$I_{AC\ delta}$
0.00	0.00	0.00	0.00	0.00	0.00	0.00
100.00	5.00	4.69	0.00	0.00	0.00	0.00
200.00	10.00	9.38	1.09	0.81	0.00	0.00
300.00	15.00	14.07	2.37	1.75	1.85	1.37
400.00	20.00	18.75	3.26	2.41	3.86	2.86
600.00	30.00	28.13	4.26	3.15	6.31	4.67
800.00	40.00	37.51	4.73	3.50	7.51	5.56
1000.00	50.00	46.89	4.99	3.69	8.19	6.06
1200.00	60.00	56.26	5.11	3.78	8.48	6.28
1400.00	70.00	65.64	5.22	3.87	8.75	6.48
1600.00	80.00	75.02	5.29	3.92	8.88	6.57
1800.00	90.00	84.39	5.33	3.95	9.01	6.67
2000.00	100.00	93.77	5.38	3.98	9.06	6.71
4000.00	200.00	187.54	5.46	4.04	9.54	7.06

The output alternating current is low with star connected generator even if the rotational speed is drastically increased to 4000 rpm.

The obtained XY graph of simulation with a 12 V battery bank is shown in Figure 23 and can then be compared with the XY chart of the simulated curves with a 24 V battery bank.
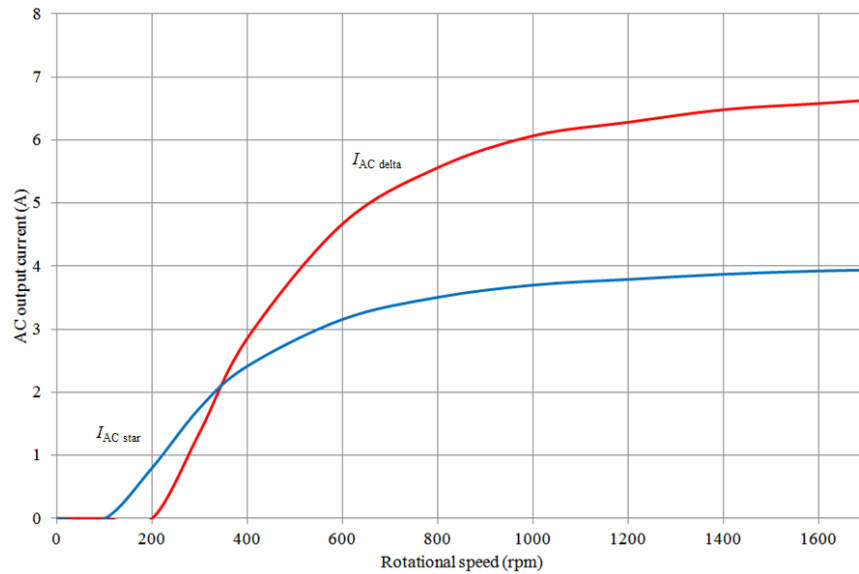
Figure 23. The alternating currents as functions of rotational speed by the small PM generator of WS-0.30B simulated with a 12 V battery bank.

However, the simulated 12 V configuration starts charging at lower rotational speed than a 24 V configuration but because the battery voltage of 12 V configurations is only half of 24 V configuration, the output power is also half.

2.5.4 Star-delta connection of a three-phase wind generator

When a three-phase wind generator is used for battery charging, the three-phase AC voltage of generator is often rectified using a three-phase full-wave bridge rectifier circuit. As we saw in the previous paragraph the three-phase electric power is three times greater when a balanced load is connected in delta compared to the Y connection. This is because the phase voltage in the star connection is the line voltage divided $\sqrt{3}$ and the line current in the delta connection is phase current multiplied by $\sqrt{3}$.

When using a small variable speed wind turbine directly driving a three-phase PM generator with suitable short circuit current value, for battery charging via rectifier, the system can be regulated by overvoltage protection at the battery bank.

The total torque produced by the wind rotor due to the wind speed, determines the mechanical power that rotates the generator shaft. Different types of wind turbines use the overall power of the wind better or worse depending on the power coefficient, C_p, value of the turbine.

The difference between star and delta connections is that star connection generates high voltage at low current, and delta connection generates low voltage at high current. When the generator is used to recharge batteries by star-connected instead of delta connected system, the output voltage rises faster with increasing rotational speed. However, the output current becomes not as high because of the higher value of the winding impedance. Increasing rotational speed increases the frequency of the alternating voltage. With increasing frequency the inductive reactance of the windings increases, which means that the internal impedance of the generator increases and prevents a rapid increase of the output current. The increase in output current is less with star connected generator than with delta connected due to high impedance values at increased rotational speed.

When the generator is used to recharge batteries with delta connection instead of star connection, it produces more power at high wind speeds. At high wind speed, the delta connected generator produces high output current as opposed to star connection. However, the rotational speed is higher, when the generator is delta connected compared to star connected, since the generator has fewer winding turns between phase to phase terminals. A clear difference between the output currents at high rotational speeds i.e. high wind speeds by different generator connections is shown in Tables 2 and 3.

The concept that the current wind speed determines the type of generator connection that should be used, gave rise to the idea of having an automatic reversible star-delta switch. Because the wind speed is often gusty, it was chosen to let the signal of the rotational speed controlling the reversible star-delta switch. An automatic reversible star-delta switch should increase the total energy production. The studied wind turbine gives more electrical energy with the use of a star-delta switch, compared to using only star connected generator. A completely autonomous automatic reversible star-delta switch, for the small wind turbine, was designed and tested. Switch data was selected from the manufacture's specification of generator, own tests of the generator and appropriate hysteresis values from practical tests. The practical tests of Windside wind turbines showed that it is advantageous to use an automatic reversible star-delta switch.

2.6   Output power of real wind turbines

The electrical output power from real wind turbines is the power in the wind and that acquired by the turbine minus the losses in the turbine, transmission, generator and power electronic devices. The rotors of real wind turbines have mass and therefore also moment of inertia.

The rated power is a quantity of power assigned, generally by a manufacturer, for a specified operating condition of a component, device or equipment. For wind turbines the rated power is maximum continuous electrical power output which a wind turbine generator system (WTGS) is designed to achieve under normal operating conditions. (IEC 61400-12-1.3.20:2014). Therefore, all electrical components in a WTGS and especially generator itself must be sized for the rated output power.

In this thesis, the generator output power is denoted by P_g and it was measured as close to the generator as possible. The electrical output power could then be monitored so that the rated power is not exceeded and true comparisons between different configurations could be made. However in real wind turbine performance testing electric power output that is delivered to the electrical power network is measured. (IEC 61400-12-3.1:2014.)

If the wind turbine is directly driven losses of the gearbox fall off, and system efficiency is improved. Many wind turbines are nowadays without gearbox. Large horizontal axis wind turbines are often equipped with a high power inverter. Small horizontal or vertical-axis turbines are equipped with a rectifier bridge, a step up converter or an inverter. Large horizontal axis wind turbines are connected to the grid while small horizontal and vertical-axis is made for charging batteries, or through an inverter feed directly consumption apparatus in a small network.

Wind turbine classes

Those planning wind turbines in Finland and elsewhere have to be acquainted with wind turbine classes according to IEC standard. Wind turbine classes are just one of the factors which need to be considered during the complex process of planning a wind power plant. Wind turbine classes determine which turbine is suitable for the existing wind conditions of a particular site. They are mainly defined by the average annual wind speed measured at the turbine's hub height.

For small wind turbines, defined with swept area less than 200 m^2 are in five classes, i.e. I, II, III, IV and a class S covers offshore conditions. The annual average wind speed in the classes are 10 m/s, 8.5 m/s, 7.5 m/s, 6 m/s and for class S varying from case to case. (IEC 61400-2:2006.)

2.6.1   Horizontal-axis wind turbines

The drive train efficiency of a horizontal axis wind turbine with gearbox and PM generator with full power converter can be illustrated as in Figure 24.
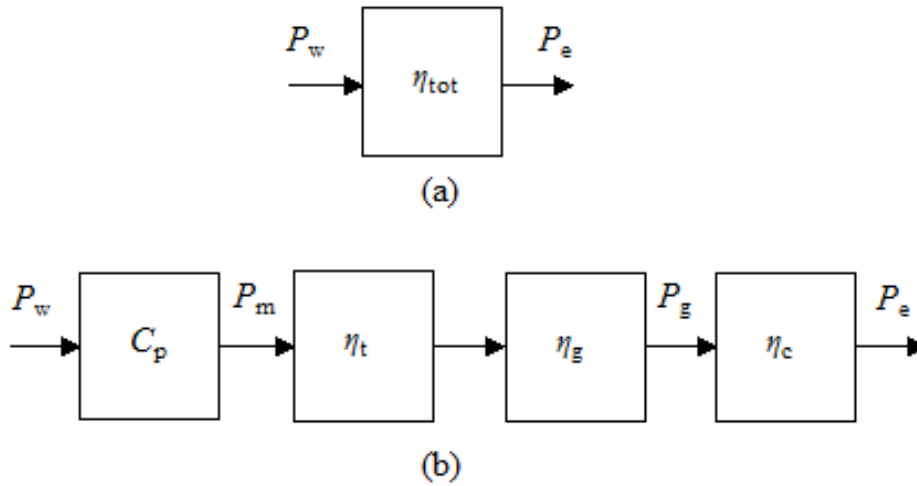
Figure 24.   Drive train including efficiency rates of a horizontal axis wind turbine, which is equipped with gearbox, PM generator and power converter. Overall efficiency is shown in (a), power coefficient, efficiency of transmission, efficiency of generator and efficiency of converter in (b).

The overall efficiency η_{tot} is one of the most important qualities of many electromechanical systems and also in wind power plants. η_{tot} is the product of power coefficient of the wind turbine C_p, efficiency of transmission η_t, efficiency of generator η_g, efficiency of converter η_c as follow

(44) $\eta_{tot} = C_p \eta_t \eta_g \eta_c.$

The efficiency of the generator depends on the loading factor. The efficiency of the transmission-generator combination is always low for low relative power but increases to approximately 90 % for 100 % relative power output.

The fraction of power extracted from the power in the wind by a practical wind turbine is usually given the symbol C_p. Using this notation and Eq. (9) the actual mechanical output power, P_m, can be written as

(45) $P_m = C_p \left(\frac{1}{2}\rho A U^3\right) = C_p P_w.$

The power coefficient is not a constant, but varies with the wind speed, the rotational speed of the turbine, and turbine blade parameters like angle of attack and pitch angle.

The air density ρ at sea level is 1.226 kg/m^3 at a temperature of 15°C. The air density is inversely temperature dependent. It decreases with about 0.006 kg/m^3 per °C. The air density decreases about 0.02 % per meter height above sea level.

The swept area may vary from less than one to several thousand square meters of greater horizontal axis wind turbine. At Høvsøre 8 MW windmills with rotor diameter of 120 m and a swept area of 11310 m^2 may be tested (International Starch Institute in Denmark 2012).

Although this equation seems simple, C_p is dependent on the ratio between the turbines angular speed and the wind speed. Tip speed ratio λ is given by

$$(46) \qquad \lambda = \frac{\Omega r_{max}}{U},$$

where r_{max} is the maximum radius of the rotating turbine in m and U is the undisturbed wind speed in m/s.

From Eq. (45), the power on the turbine axis for different turbines can be calculated. The power can vary from zero to few watts for a small one in the doldrums at light wind and again up to several megawatts for a big wind turbine at hard wind. Combining (45) and (46) for λ_{opt} we get the maximum power $P_{m,\,max}$ by

$$(47) \qquad P_{m,max} = \frac{C_{p,max}}{\lambda_{opt}^3} \frac{1}{2} \rho \pi r_{max}^5 \Omega^3.$$

(Patsios et al. 2008.)

Eq. (47) is valid currently in Maximum Peak Power Tracking context, when the model-based control (MBC) method is used. (Patsios et al. 2008.)

In this thesis the MPPT control method *Perturbation and Observation* (P&O) is used as in Patsios et al. 2008:1–2. This method uses only measured voltage and current output data and does not need any information about the power curve, the torque, the optimum tip speed ratio λ, the wind speed or angular velocity.

2.6.2   Vertical-axis wind turbines

Vertical-axis wind turbines are often wind turbines of variable speed. They are of three types, lift-based type like Darrieus turbine, drag-based types like cup anemometer and combined type. Windside turbine is a drag- and lift-based type. The vertical-axis turbines are typically smaller than 25 kW, but a 4 MW Darrieus turbine 100 m high and 60 m diameter has been built by a Canadian manufacturer. Table 4 shows manufacturers of turbines up to 50 kW and a promising design of 200 kW launched by Vertical Wind AB in Sweden 2010.

Table 4.   Manufacturers of vertical-axis wind turbines.

Company	Web Address	Country	Product
Fleximedica	http://www.reuk.co.uk	Italy	400 W–25kW
Ropatec	http://www.ropatec.com/	Italy	0.5–6 kW
Solwind Energy (UK) Ltd	http://www.solwindenergy.co.uk	United Kingdom	10–30 kW
Turby	http://windoption.com/2012/03/turby-urban-vawt/	Netherland	2 kW
Vertical Wind AB	http://www.verticalwind.se/SV/index.html	Sweden	200 kW
Wind Harvest	http://www.windharvest.com/	US	25 kW
Windside	http://www.windside.com/	Finland	20 W*–7.5kW
Zephyr Alternative Power Inc	http://www.zephyrpower.com/	Canada	50 kW

* 20 W can be achieved with a wind speed of 5 m/ s depending on the size of the turbine.

Vertical-axis turbines have several advantages over the typical horizontal axis turbines:

(i)   Generator can be on the ground for more easy access, rather than up in the air, or at least below the rotor

(ii)   Generally begin rotating at lower wind speeds

(iii)   Are quieter due to slow tip speed

(iv)   Lower susceptibility to cross-winds due to its structure.

There are also few disadvantages:

(i)   The maximum value of the power coefficient is clearly lower than for horizontal-axis wind turbines

(ii)   Darrieus wind turbine has not enough starting torque. A special machine is required to start a Darrieus rotor and it also requires wire ropes that hold the structure in place

(iii)   Small vertical-axis wind turbines of drag-based type and combined type becomes for reasons of cost, mounted on such a low altitude that they get poor wind conditions.

In a vertical-axis wind turbine there is stress on the bearings, if they are only in the lower end of the rotor shaft. This is because all weight of the rotor rests on these bearings and also the wind pressure on the rotor causes lateral forces in the bearings. To solve this problem, requires a massive structure which has a bearing in the upper end of the rotor. The massive structure may be a robust steel foundation or firmly attached steady wires.

Savonius-type wind turbine

Savonius-type wind turbine was invented by the Finnish sea captain S. J. Savonius in 1922. It is a vertical-axis wind turbine, used for converting power of wind into torque on a rotating shaft, and it is one of the simplest turbines. Aerodynamically, it is a drag and lift-type device, consisting of two scoops. The blades are overlapped with an overlapped distance, *e*, so the air may also flow through the rotor. Because of the curvature, the scoops experience less drag when moving against the wind than when moving with the wind. Differential drag and lift forces cause the Savonius turbine to spin. Savonius tested his invention even with several wings and with different wing shapes (Savonius 1925:13). Figure 25 shows a two-scoop Savonius-type wind turbine.

Savonius-type turbines are used whenever cost or reliability is much more important than efficiency. Larger Savonius-type turbines have been used to generate electric power on deep-water buoys, which need small amounts of power and need very little maintenance. Design is simplified because no yaw mechanism is required to allow for shifting wind direction, unlike horizontal axis turbines, and the turbine is self-starting. A larger electric generating wing rotor was sketched in 1925 (Savonius 1925).

The swept area of a wind turbine is one of the most important properties from power production point of view. The swept area of a Savonius type wind turbine is calculated by multiplying the maximum diameter with the height of the turbine.
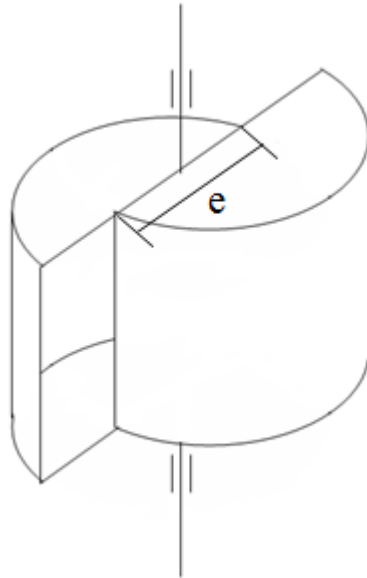
Figure 25.   Schematic drawing of a two-scoop Savonius-type wind turbine.

Small scale slow running vertical-axis wind turbines of Savonius type have been largely studied, for example in a wind turbine project in University of Northumbria in United Kingdom 2004.

"This project produces an investigational exploration of a Savonius rotor wind turbine adapted for household electricity generation. The innovative technology turbine collects wind energy and converts it into electricity, which in turn produces a 12 V output which is used to charge one heavy duty battery. In this study, a small electricity generator has been specifically designed for household installation. The generator is driven by a modified Savonius rotor. This type of rotor, which is of the vertical-axis variety, is chosen instead of a horizontal axis machine due to its simplicity and reliability." (Percival 2004.)

Savonius in a wind tunnel

The electric output power from a vertical-axis wind turbine of Savonius type, as is placed in a wind tunnel, can be explained by using the kinetic energy that passes the wind turbine. The explanation is fundamentally the same as for the horizontal axis wind turbine. As swept area, *A*, used the area facing the wind. However, only half of this surface gives drag force on the drag machine, as is described in Section 2.3.2.

Practically, when the turbine is placed in a wind tunnel with an inlet and an outlet the power that can be extracted from the wind is found by the following methodology.

The average of wind speed through the rotor area is given by

(48) $$U_{ave} = \frac{(U_1 + U_2)}{2},$$

where U_1 and U_2 are the inlet/outlet wind speeds in m/s. The mass of the airflows passing through the area, A, of the wind turbine per second in the stream tube is given by:

(49) $$m = \frac{\rho A(U_1 + U_2)}{2},$$

and according to the kinetic energy

(50) $$E_k = \frac{1}{2} m U^2.$$

Therefore the power extracted is

(51) $$P_m = \frac{1}{2} m (U_1^2 - U_2^2).$$

Substituting the mass of air into this equation, the power that the rotor can extract from the wind is

(52) $$P_m = \frac{1}{4} \rho A (U_1^2 - U_2^2)(U_1 + U_2),$$

when the swept area A is

(53) $$A = hD,$$

where h is the height of the turbine and D the diameter. (Percival 2004.)

The mechanical power at the turbine shaft is also

(54) $$P_m = T_m \Omega$$

where T_m is torque in Nm on the generator shaft.

The available power P_w from the wind is calculated by Eq. (9).

Then the power coefficient of the turbine is

(55) $C_p = \dfrac{P_m}{P_w}$,

$C_{p\,max}$ for the Savonius type wind turbine is close to 0.18 (Dobrev & Massouh 2012).

The helical vertical-axis turbine

When no transmission between turbine and generator is used, the coefficient of transmission, η_t, shown in Figure 24 falls off. The drive train efficiency of a direct driven vertical-axis wind turbine, with a three-phase PM generator, a rectifier bridge and a step up converter can be redrawn as shown in Figure 26. The overall efficiency η_{tot}, is the product of power coefficient of the turbine C_p, efficiency of generator η_g, efficiency of rectifier η_r and efficiency of converter η_c, as given below:

(57) $\eta_{tot} = C_p \eta_g \eta_r \eta_c$.

The coefficient of electric power after the generator is denoted by (C_{pg}) and it is

(58) $C_{pg} = C_p \eta_g$.

(a)

(b)
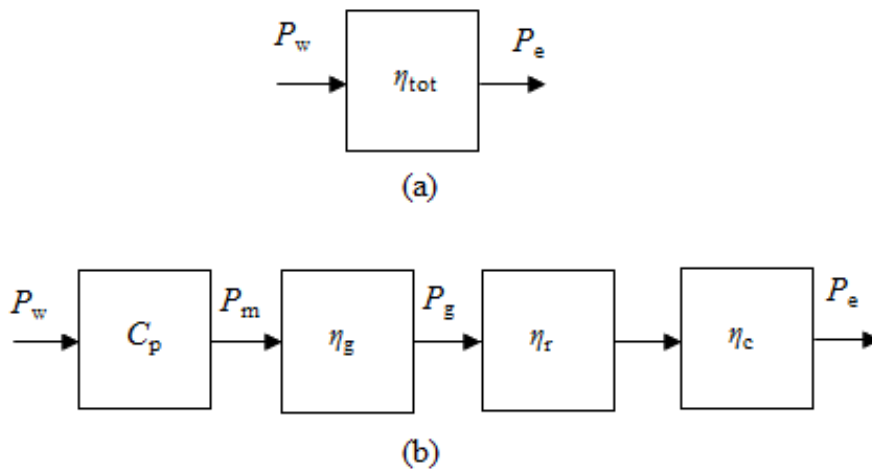
Figure 26.   Drive train including efficiency rates of a small helical vertical-axis wind turbine equipped with rectifier and step up converter. Total efficiency shows in (a), power coefficient, efficiency of generator, efficiency of rectifier and efficiency of converter in (b).

The output electric power, P_g from the three-phase generator is

(59) $P_g = \sqrt{3}VI\cos\varphi,$

where V is the line to line voltage, I the line current and $\cos\varphi$ is near 0.95 when rectifier is used, and 1.00 if a pure resistive load is used. Generator efficiency is

(60) $\eta_g = \dfrac{P_g}{P_m}.$

The efficiency of the studied small PM generator depends on generator connection. It was found that the efficiency of a sample PM generator about 30 % smaller than the WS-0.30B generator showed a best value of 0.90 with star connected generator and 0.95 with delta connected generator. The efficiency of used generators was not measured because of the mechanical construction of the wind turbines. The voltage drop was in this thesis used rectifiers 0.7 V per diode. The efficiency of rectifier is high, and it seldom discussed as a problem. The efficiency of a step up converter is in practice calculated by dividing output power with input power.

The efficiency of a step up converter depends on the operating conditions. The efficiency of a step up converter can vary from below 0.70 up to 0.94 (Texas Instruments 2014, Linear Technology 2014).

A study by Zhao et al. introduces a new type-helical Savonius rotor, applies computational fluid dynamics (CFD) to analyze and improve the performance of the rotor from aspects ratio, the value of the height divided by the value of the diameter (H/D), number of blades, overlap distance (e) and helical angle (θ). The results show the power coefficient of an optimum rotor reaches 0.2, when rotor has two blades and the value of the height divided by the value of the diameter is equal to 6, overlap distance is 0.3 m and helical angle is 180°. The starting torque is also found better than that of a conventional Savonius rotor. (Zhao et al. 2009.)

A two bladed Savonius rotor with endplates, semicircular and twisted blades was investigated by Saha et al. (2008:1367) and it was founded that this rotor has $C_{p, max}$ 0.18.

The Windside-type turbine can be considered as an improvement of Savonius-type turbine. It was invented and patented by Risto Joutsiniemi. The patent was registered in Finland 1985 (Joutsiniemi 1985). The turbine consists of two blades which are arranged as a helical turbine, which leads to smooth drag and reduced cogging. Some different types of Windside wind turbine are shown in Figure 27.

The blades are made of reinforced glass fiber. The studied small turbine, WS-0.30B, has a rotor diameter of 0.3 m and a height of 1 meter. The aspects ratio is then 3.3:1 which is lower than the optimum found by Zhao et al.
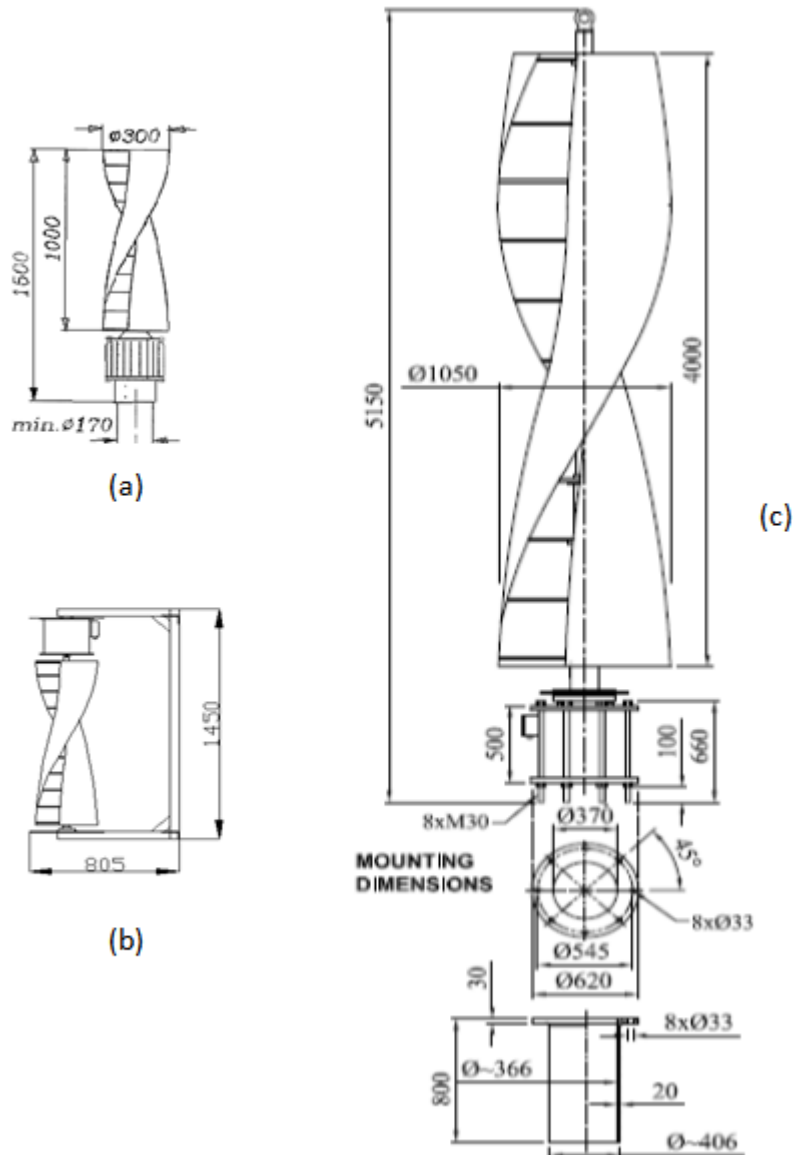
Figure 27.   Windside-type turbines. The type WS-0.30B (a), the type WS-0.30A (b) and the type WS-4B (c). (Oy Windside Production Ltd, home page 2012.). The dimensions are in millimetres.

A maximum roughness height R_{max} of 0.5 mm on the outer side of studied small Windside turbine was measured which is more than what (Ren & Ou 2009) suggested, as mentioned in Section 2.2.2. Measured roughness height of the blade reduces the lift force, while the drag force is increased due to surface friction, which is shown in a diagram in Ren & Ou 2009.

The design is direct driven, i.e. without gearbox. The studied wind turbine B has ball bearings only in the generator and is designed for a maximum wind speed of 30 m/s. WS-0.30A is fitted on a steel structure and has an upper bearing point. It is designed for a maximum wind speed of 40 m/s.

The studied WS-4 type is an up scaled wind turbine of a WS-0.30 but with the aspect ratio of the turbine close to 4:1. A wind turbine on the WS-4C type with solid shaft of 90 mm diameter was used at first but it had too low natural frequency so it must be changed out. The study of the larger wind turbine was then concentrated on the WS-4B type with a developed hollow shaft with an outer diameter of 120 mm and inner diameter 90 mm.

2.6.3 *Rotational dynamics of the wind turbines under study*

The rotational speed of variable speed wind turbines varies with wind speed and load. With gusty winds is the rotational speed of the studied wind turbines constantly either accelerating or decelerating. Rotating parts of the wind turbine has mass and therefore moment of inertia also called mass moment of inertia or rotational inertia, which counteracts a change in the rotational speed. The moment of inertia I_m of a hollow shaft is

(61) $$I_m = \frac{1}{2}m\left(\left(\frac{d}{2}\right)^2 + \left(\frac{D}{2}\right)^2\right),$$

where m is the mass in kg, d is the inner diameter and D the outer diameter both in m.

Moment of inertia should not be confused with area moment of inertia or second moment of inertia as is used in equations for the design of shafts and beams.

The angular acceleration phase demands a torque while the angular deceleration phase gives a torque back. The torque T_α due to desired angular acceleration of an unloaded frictionless rotating body with known moment of inertia is

(62) $$T_\alpha = I_m\alpha,$$

where I_m is the moment of inertia in kgm^2 and α is the angular acceleration in rad/s^2.

The kinetic energy E_k of a rotating body is

(63) $$E_k = \frac{1}{2}I_m\Omega^2.$$

2.6.4   *Power performance and annual energy yield*

Output power performance of the studied wind turbines in order to make comparisons between different connections of generators and battery configurations were needed and they were obtained from measured data by using the trend line function in Excel® software. Only polynomial trend lines are used. Cut in wind speed can be parameterized by setting a suitable intercept value when polynomial trend line is used. Equations of the trend lines are shown in the figures, in which the trend line has been used. Trend lines are regression lines to observed data points.

Regression analyses of obtained trend lines by data analysis tool in Excel® have been done. Regression statistics are presented in tables.

Multiple R is the correlation coefficient between the actual and the fitted values. R-squared (R^2) is the square of the correlation coefficient. Adjusted R-squared means adjusted for degrees of freedom. The standard error is the standard error of the regression. (Kling 2014.)

R-squared R^2 value measures how successful the fit is in explaining the variation of the data. The interpretation is:
  (i) R^2 values between 0.7–1.0 means good fit of function to data distribution
  (ii) R^2 values between 0.5–0.7 means moderate to poor fit and
  (iii) R^2 values below 0.5 means poor fit to data. (Taylor 2014.)

Annual energy yields on the AC side with different configurations of small wind turbine were calculated by the above mentioned software. Ten-minute average wind speed values from a randomly selected year were combined in intervals of 1 m/s from 0 to 30 m/s, as is shown in Figure 4. Annual energy yield of a wind speed interval was determined by multiplying the number of 10-minute values of the interval with output power estimated from the trend graph of each wind turbine performance at the average wind speed of the same wind speed interval and divide by 6000 so that the unit is converted to kWh. The total annual energy yield was given by the addition of energy yield values of intervals.

3   THE SYSTEMS UNDER STUDY

This chapter discusses the studied wind turbines and systems, including the equipment or parts that were developed during the study. Two different sizes of vertical-axis wind turbines were investigated (Section 1.5). The mechanics of the larger size was also improved partially. Peripheral devices were developed and tested. The turbines were mounted so that the systems could be studied in real conditions at the university.

For the smaller turbine two setups were used. The smaller turbines are mounted close together on the roof of Tritonia library building, while the larger turbine is mounted on the roof of Fabriikki building, all at the University of Vaasa.

3.1   WS-0.30B turbine system

The basic battery charging system with vertical-axis turbine, shown in Figure 28, has been manufactured and used in several years over the whole world without any peak power tracker or automatic star-delta switch. The system consists of the wind turbine with a direct coupled PM-generator and a charging controller with a function to avoid batteries from overloading. If needed, the charging controller connects an artificial dummy load to the batteries, and the artificial load dissipates the extra energy as heat. Wind powered battery charging system for voltage level from 12 V to 24 V described below have been manufactured and used. The basic system is robust without mechanical relays, but there is no feature to load energy to the battery bank in light winds when the rectified voltage is lower than the battery voltage.

The small basic wind turbine system on market consists of:
  (i)   A Windside wind turbine WS-0.30B with a swept area of 0.3 m^2
  (ii)   Basic equipment which are shown in Figure 29 and
  (iii) Two 12 volts deep cycle lead acid batteries, which could be connected in series or parallel.

The basic equipment includes a manual short circuit switch, a three-phase rectifier, a charging controller, a dummy load and a lubrication system.
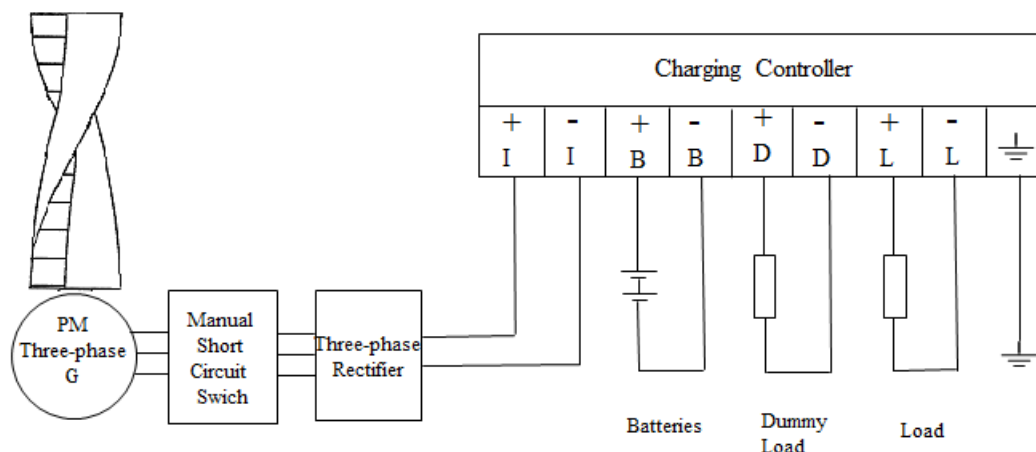
Figure 28. The basic WS-0.30B wind turbine system for 12 V or 24 V batteries.

Because this basic system has no automatic star-delta switch, it must be connected manually in star or delta. In order to have good charging characteristics in low wind speeds, star connection is often chosen. In strong winds this leads to operation in which the resistance and especially inductive reactance of the generator limits the output current as is described in Section 2.5.4.

3.2 The modified system with a WS-0.30B turbine

In the previous section described basic system was then supplemented with developed components to a modified system. The modified new system shown in Figure 29 was then studied carefully.

In the previous tests of a WS-0.30C wind turbine at site at University of Vaasa it was observed that it is impossible to accept the first natural resonance frequency because of a solid shaft with a diameter of 25 mm. Therefore, it was changed to the WS-0.30B wind turbine, which was equipped with solid shaft of diameter of 30 mm, and it was found that the vibrations from the first natural frequency were acceptable.

The modified wind turbine system for battery charging consists of the Windside turbine with a direct coupled Windside three-phase permanent magnet generator, a new developed automatic reversible star-delta switch, a breaker for short circuit of generator windings to stop the wind turbine, a three-phase rectifier bridge, a developed boost converter, measurement and control system, dummy load, loads, and a 12 V or a 24 V battery bank. Also, a fast mounted wind instrument for wind speed and wind direction measurement is available. Air temperature, humidity, and air pressure can also be measured.

The modified small wind turbine system consists of:

(i)   A Windside wind turbine WS-0.3 with a swept area of 0.3 m^2
(ii) Basic equipment which are shown in Figure 29
(iii) In this study developed peripheral equipment, which are the automatic and reversible star-delta switch and the boost converter. Both devices are shown in Figure 30 and
(iv) Two 12 volts deep cycle lead acid batteries, which could be connected in series or parallel.

Basic equipment includes of a manual short circuit switch, a three-phase rectifier, a charging regulator, a dummy load and a lubrication system. In this study, peripheral equipment as consisting of a DC-DC converter and the automatic reversible star-delta switch, which automatically switches the generator from star connection to delta connection and return to the star connection depending on the rotational speed of the generator was developed.
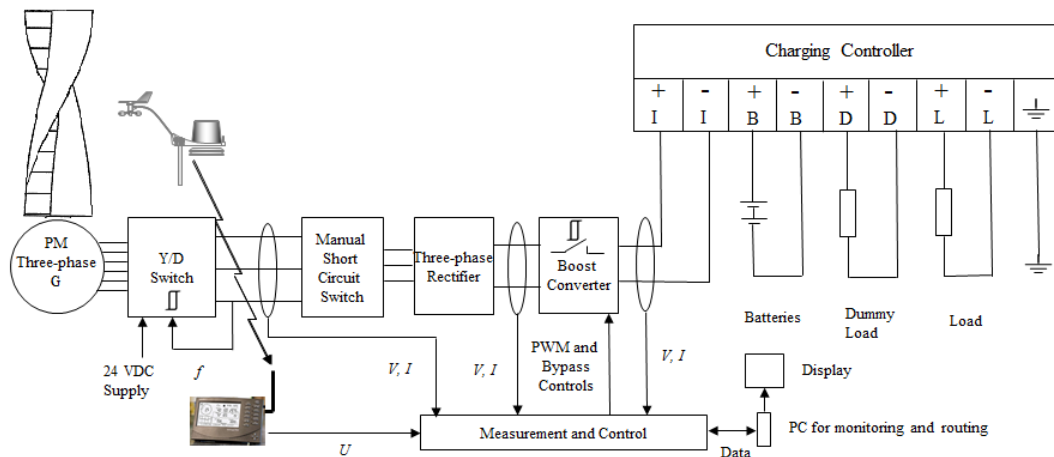
Figure 29.   The modified wind turbine system with a WS-0.30B wind turbine used with 24 V battery bank.

3.3   Methods to match the generator

Short circuit currents in small variable speed PM three-phase generators determine the boundaries for high output currents. The open circuit voltages of the generators are increased by higher rotational speed (Fig. 14 and Fig. A1.4). The increased frequency increases the internal inductive reactance and therefore the internal impedance. If the number of pole pairs can be held low, the frequency will be low. Because PM generators showed much higher impedance than batteries, especially at high speeds, the problem was on the generator side. However, a higher battery voltage results in lower charging current.

Series to parallel switching is possible if the phase windings are divided into several parts. Combining both, offers a sufficient speed increase for any application. Even the uses of combinations of series and parallel coils have been described. (Nipp 1999:54.)

A new generator type was introduced in Canada at the end of 2008, as described in the following text from a manufacturer's home pages in October 2008.

"Most wind turbines today use regular generators, which require a steady turning speed to effectively produce electricity. But wind blows at a wide variety of different speeds. As the shaft turns at different speeds based on the way the wind is blowing – and the blades are turning – the gearbox works to smooth out the large variation and deliver a steadier signal to the generator.

This new generator, called the Variable Input Electrical Generator, or VIEG, uses a series of coils, balanced with a series of different magnets that can operate independently, so only a few cells are turned on at low speeds and more cells are activated at higher speeds.

The generator eliminates the need for a gearbox, saving wind turbine developers money, and has almost no cogging torque or resistance to begin turning. The generator also can easily be modified to match different sites. For example, if a site has the wind resources to accommodate 1.6 megawatts of generation capacity, and the nearest convenient wind-turbine system is 1.5 megawatts, the generator can help add the additional capacity. (ExRo 2008.)"

Used method

The small wind turbines were tested for some time in the field with the basic generator connections of either star or delta. The advantages and disadvantages of the different generator connections were observed.

The classical star to delta switching has been used in numerous applications ever since three-phase machines were invented and it is also useful for three-phase PM machines. Motor application requires switching only from star to delta connection, not a reset back to the star connection.

Traditionally, in electrical drives star-delta switches are used to reduce starting current of three-phase motors. Since starting current after a few seconds has decreased, the switch can be switched either manually or automatically from star configuration to delta configuration. However, wide use of soft starters and frequency converters during the last twenty years has decreased the need for star-delta switches in motor drives.

To match the studied generators in different wind speed, the automatic reversible star-delta switch seems be a good solution. The automatic reversible star-delta switch has not previously been used in electrical systems for the studied wind turbines.

Since the target of this study was to use existing components as much as possible including generators, it became clear that it is a great advantage to develop an automatic reversible star-delta switch. WS-4 inverter or its settings were not changed within this work.

3.4 New automatic reversible star-delta switch

Use of a generator, which is star connected, gives poor charging characteristics at high rotational speed while a generator which is delta connected gives poor charging characteristics at low rotational speed. The automatic reversible star-delta switch is a simple but rational solution for this type of small wind power system with variable rotational speed and used for battery charging. It is connected between the generator and the short circuit switch shown in Fig. 29. The automatic reversible star-delta switch is used to increase the wind energy production in variable windspeeds, because the type of connection influences significantly on energy production. The characteristics of the generators were well known from tests conducted by the manufacturer and from own measurements made in the field. In light winds the generator is star-connected via NC (Normally Closed) contacts of the switch and in high wind speeds the switch automatically changes over to delta connection. When the wind speed decreases the switch returns to the star connection.

Two prototypes of the automatic reversible star-delta switch were constructed and tested. The first prototype of the automatic reversible star-delta switch was worked out with aid of the LabView® CompactRio equipment. To have galvanic isolation between the electronics and the contactor in the reversible star-delta switch box, an optical coupler with a phototransistor was constructed and tested.

Because the optical coupler with the phototransistor did not work well, an autonomous automatic reversible star-delta switch was developed.

The final version of the automatic reversible star-delta switch is an autonomous device, because its power supply is only from battery bank of the wind turbine and it has its control signal only, when it is controlling. The automatic reversible star-delta switch consisted finally of only three electrical or electronic parts, all mounted in the same box. The star-delta box was mounted on the roof of Tritonia

library building at a suitable height on the 7 m height wood pole of the studied vertical-axis wind turbine which worked continuously very well with the reversible star-delta switch during few years in many bad storms.

The final automatic reversible star-delta switch is shown in Fig. 30. The generator terminal is shown on the right side of the figure and the three phase lines are L_1, L_2 and L_3. The block f/V stands for the linear measurement converter that converts the frequency of the AC voltage from the generator to a DC voltage signal, Tr for the threshold relay and Cc for the coil of the contactor. The limit value for switching from star to delta or vice versa and its hysteresis can easily be changed on the threshold relay. Both the converter and the relay has 24 V DC power supply only from the battery bank of the wind turbine. Contactor makes the star-delta connection.
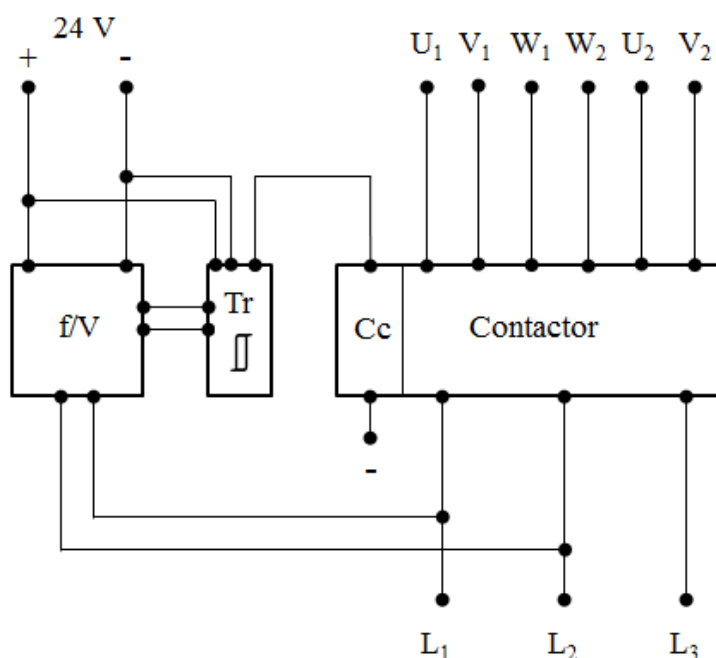
Figure 30.   The final version of the automatic reversible star-delta switch developed for WS-0.30B turbines.

The contactor is connected as in the simulated circuit shown in Fig. 19. The signal between the f/V-converter and the threshold relay is 0–10 V DC.

3.5   Rectifiers of studied wind turbines

Rectifiers used in this project are in three-phase six pulse bridge connection and they are mounted on heat sinks as black boxes. They are the basic parts of the

studied wind turbine systems. The rectifier bridge to the smaller wind turbine system has a rated current value of 20 A and to the larger wind turbine system a rated current value of 30 A. Frequency of the output voltage during operation of the studied small wind turbines is less than 70 Hz and of the larger wind turbine less than 30 Hz.

3.6   Maximum peak power tracker

Small stand-alone wind energy systems are an important alternative source of electrical energy, finding applications in locations where conventional generation is not practical. Most of these systems do not produce power at all wind speeds. Low wind speeds which are also low in output power are very common. To address this problem, the authors Knight & Peters have proposed a power electronic converter, designed for efficiency, simplicity and ruggedness. (Knight & Peters 2005:1.)

Unfortunately, there can be significant problems connecting a wind generator to a constant DC voltage. At low wind speeds, the induced voltage in the generator will not be high enough to overcome the reverse bias in the diode bridge. At high wind speeds, the frequency of electricity increases and the reactive impedance of the generator will be high, while the impedance of the battery load will be low. In the latter case, the poor impedance matching will limit power transfer to the DC system (Drouilhet, Muljadi & Holz 1995).

However, addition of a capacitor in series with the PM generator can also be used. This has the effect of lowering the generator's effective impedance at higher frequencies. The capacitor value is tuned so that it resonates with the inductor at a frequency at the upper end of the generator operating range. (Drouilhet, Muljadi & Holz 1995; Corbus et al. 1999:3)

To overcome the problem of too low generator voltage for battery charging in light winds in the lower range the system is completed with a DC-DC converter. The power generation from wind is given by the power equation (Eq. 9). The output power is very low in light winds, but it is increases rapidly with increase of wind speed. At low wind speeds, without some type of boost converter, the output voltage is up to a certain level lower than the battery voltage. Therefore, charging current level cannot be reached in this area. To avoid this problem, the studied vertical-axis wind turbine system is connected to a MPPT. In light winds, the MPPT is used to optimize the electrical output power to the battery. The developed MPPT consists mainly of a DC-DC converter. Two types of switched-mode

converters were designed, constructed and tested. In the first tests, a buck-boost-type converter was used, but in the tests that followed an ordinary boost converter produced better results.

Often in MPPT systems for wind generators, buck converters as in (Neammanee & Chatratana 2006), or buck-boost ones as in (Corbus et al. 1999:3) are used. Then the current in the generator in the system with MPPT is higher than in the uncompensated system at lower frequencies because it follows the maximum rotor power curve (De Broe et al. 1999). Lower frequencies produce lower impedances of generator, especially in the most common wind speeds in which the wind power plant is planned to operate. Because it was necessary to extract energy even from weak gusts, when the voltage is too low without a step up converter, it was decided to explore the MPPT solution with a boost converter.

3.6.1   Comparison of DC-DC converters

The output-input voltage ratios achieved by the three types of DC-DC converters are compared as a function of duty cycle in Figure 31. Notice that only the buck converter shows a linear relationship between the control (duty ratio) and output voltage. The buck-boost can reduce or increase the voltage ratio with unit gain at a duty ratio of 50 %. (Lindemann 2012.)

If is characteristic for Buck converter that

(64) $V_{\text{out}} = DV_{\text{in}},$

where V_{in} is input voltage, V_{out} output voltage and D duty ratio, and for

Boost converter that

(65) $V_{\text{out}} = \dfrac{1}{1-D} V_{\text{in}}$

whereas for Buck-Boost converter

(66) $V_{\text{out}} = \dfrac{D}{1-D} V_{\text{in}.}$
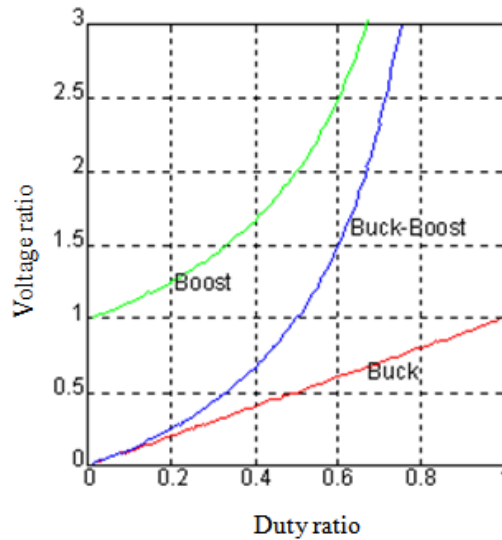
Figure 31. Comparative diagram of voltage ratio as a function of duty ratio for different type of DC-DC converters (Lindemann 2012).

As shown in Figure 31 the output voltage for an ideal boost converter is always higher than the input voltage. Hence, this converter was used in the battery charging system with smaller Windside turbine. A really good thing is that the switching transistor stays in the open position if it does not work, and if so, the system works as a system without MPPT. In practice, the inductor has resistive losses and the silicon diode has its characteristic voltage drop of about 0.7 V. The practical issues regarding the application of the step up converter are described in detail in the next section.

3.6.2 Step up converter

The unregulated DC output voltage from the rectifier bridge was used as input voltage V_{in} to the step up converter. The nominal voltage value of the battery bank was 24 V. The step up converter was calculated according to an Internet based calculation program (Schmidt-Walter et al. 2006). In the calculation, the following parameters were selected:

- (i) Minimum input voltage $V_{in\ min}$ = 10 V
- (ii) Maximum input voltage $V_{in\ max}$ = 30 V
- (iii) Output voltage V_{out} = 30 V
- (iv) Output current I_{out} = 6 A
- (v) Switching frequency f = 500 Hz and
- (vi) Inductor L = 200 mH
- (vii) Capacitor C_{in} = 2.2 µF (later added by 1500 µF)
- (viii) Capacitor C_{out} = 63 µF (later added by 1000 µF)

The above mentioned calculation program gave a value for the cross sectional area of the wire to be at least 6.14 mm². A core with cross sectional area 714 mm² was used.

The step up converter consisted of four switching transistors connected in parallel, a diode, an inductor and two capacitors. The switching transistors and the diode were mounted on heat sinks. The inductor coil was wound of two enameled isolated copper wires in parallel on a ferrite core. To avoid noise, the inductor was later potted in epoxy, because the used switching frequency is in the audible range. A capacitor of 1500 µF was in later tests and final use connected in parallel with the input side of the converter and another of 1000 µF in parallel to the output. The extra capacitor on the input side of the converter is used to smooth the rectified unregulated DC-voltage and the extra capacitor on output side to decrease the output voltage ripple and suppress high voltage peaks.

A circuit diagram of the step up converter is shown in Fig. 32. The battery bank is denoted by B, the internal resistance of the battery bank by R_b and the switch by S.
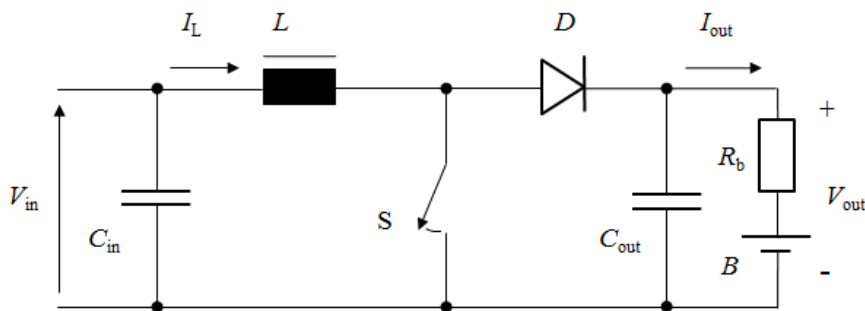
Figure 32.   A basic circuit diagram of the used step up converter.

Figure 33 shows the components of the step up converter.

Figure 33.   The components of the step up converter.

Figure 34 is from a situation when the boost converter was in tests in the electrical laboratory at the University of Vaasa.
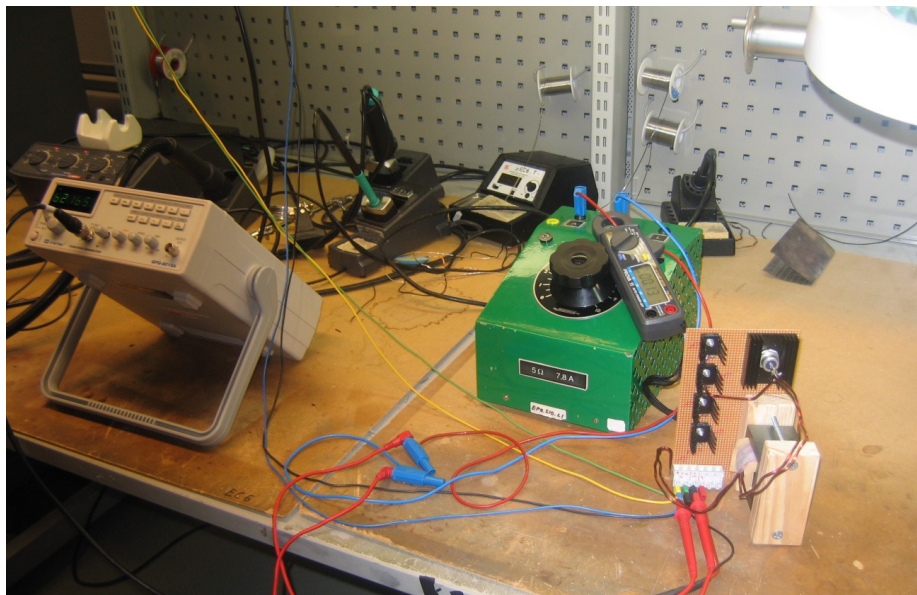
Figure 34.   The developed boost converter in laboratory tests.

The efficiency of boost coverter η_c is calculated by

$$(67) \qquad \eta_c = \frac{P_{in} - (P_{switch} + P_{inductor} + P_{diode})}{P_{in}},$$

where $P_{\text{in min}}$ is power input, P_{switch} is losses in the switch, P_{inductor} losses in the inductor and P_{diode} losses in the diode (Eichhorn 2008.)

The duty cycle D for the minimum input voltage is

$$(68) \qquad D = 1 - \frac{V_{\text{in min}}\eta_{\text{est}}}{V_{\text{out}}},$$

where $V_{\text{in min}}$ is minimum input voltage, V_{out} desired output voltage and η_{est} efficiency of the converter, e.g. estimated 80 % (Hauke 2014.)

The dc conduction losses in the switch become

$$(69) \qquad P_{\text{switch}} = DI_{\text{in}}R_{\text{switch on}},$$

where I_{in} is input current and $R_{\text{switch on}}$ is the on resistance of the svitch.

The inductor loss becomes

$$(70) \qquad P_{\text{inductor}} = I_{\text{in}}{}^{2}R_{\text{inductor}},$$

where R_{inductor} is the resistance in wire of the inductor.

The diode losses become

$$(71) \qquad P_{\text{diode}} = V_{\text{forward}}I_{\text{out}} + I_{\text{out}}{}^{2}R_{\text{diode}},$$

where V_{forward} is the forward voltage drop of the diode and R_{diode} is the forward slope resistance. (Eichhorn 2008.)

The parameter list above is supplemented with the following values:
  (i) $I_{\text{in}} = 8$ A
  (ii) $V_{\text{in}} = 25$ V
  (iii) $V_{\text{forward}} = 1.5$ V
  (iv) $R_{\text{switch on}} = 0.0675\ \Omega$ (4 pieces IRFP460 transistor coupled in parallell)
  (v) $R_{\text{inductor}} = 0.0074\ \Omega$ (self made)
  (vi) $R_{\text{diode}} = 0.0034\ \Omega$ (1 piece 60HFU460 diode)

$$(72) \qquad D = 1 - \frac{10 \cdot 0.8}{30} = 0.73$$

$$(73) \qquad P_{\text{switch}} = 0.73 \cdot 8 \cdot 0.0675 = 0.39 \text{ W}$$

$$(74) \qquad P_{\text{inductor}} = 8^2 \cdot 0.0074 = 0.47 \text{ W}$$

$$(75) \qquad P_{\text{diode}} = 1.5 \cdot 6 + 6^2 \cdot 0.0034 = 9.18 \text{ W}$$

$$(76) \qquad \eta_{\text{c}} = \frac{8 \cdot 25 - (0.39 + 0.47 + 9.18)}{8 \cdot 25} = 0.95$$

The control of MPPT converter was realized using LabView® on a PC. Input and output voltages and currents of the converter were measured by LabView®. The output power to the batteries where optimized by controlling duty cycle.

3.7 Batteries

The WS-0.30B systems studied included two Optima Yellow Top Absorbed Glass Mat (AGM) 55 Ah 12V batteries, coupled in series for 24 V use or parallel in for 12 V use. The internal resistance is 0.1 Ω.

The system with a WS-4B wind turbine included four of same type of batteries coupled in series and mounted in the inverter cabin.

The batteries play an important role and are central in the studied small wind power systems. The AGM type of batteries are one of the three types of lead-acid batteries which are nowadays used not only for wind power but also in many types of mobile applications such as electric vehicles. In this thesis other types of lead-acid batteries including Lithium batteries were not studied. Figure 35 shows the used battery type.

Figure 35.   The Optima yellow top SPIRALCELL® -type battery. (Optima batteries 2012).

The Optima yellow top SPIRALCELL® design AGM batteries are made especially for deep cycles, as often used in wind power systems with battery storage. (Optima batteries 2012.)

There are up to four phases of battery charging: bulk, absorption, equalization and float. The bulk stage is where the charger current is constant and the battery voltage increases. You can give the battery whatever current it will accept not to exceed 20 % of the ampere-hour rating and this will not cause overheating. The absorption phase is where the charger voltage is constant and current decreases until the battery is fully charged. This normally occurs when the charging current drops off to 1 % or less of the ampere-hour capacity of the battery. For example, the ending current for a 100 ampere-hour battery is 1.0 Amp or less. (Darden 2001.)

The optional equalizing phase is a controlled 5 % overcharge, which equalizes and balances the voltage (Darden 2001).

When charging the Optima yellow top SPIRALCELL® batteries recommended a maximum battery charging voltage of 15.0 V, the equalization phase should not be used. (Optima batteries 2012.) The equalization phase is shown in Figure 36 but this equalization phase was not used in the research of Windside turbines.

OPTIMA® REDTOP® can be rapid recharged by a maximum voltage of 15.6 V regulated. These batteries are designed for engine starting applications. They are not recommended or warranted for use in deep cycle applications. (Optima batteries 2012.)

The AGM battery manufacture Lifeline Batteries writes that equalizing phase of AGM battery should only be done when the battery is showing symptoms of capacity loss. If equalizing is necessary, first go through the normal charge cycle. (Lifeline batteries 2015.)

The optional float phase is where the charge voltage is reduced, held constant and used indefinitely to maintain a fully charged battery. Figure 36 shows a multi-stage charging algorithm from Deltran (Battery Tender) for a deep cycle AGM battery. (Darden 2001.)
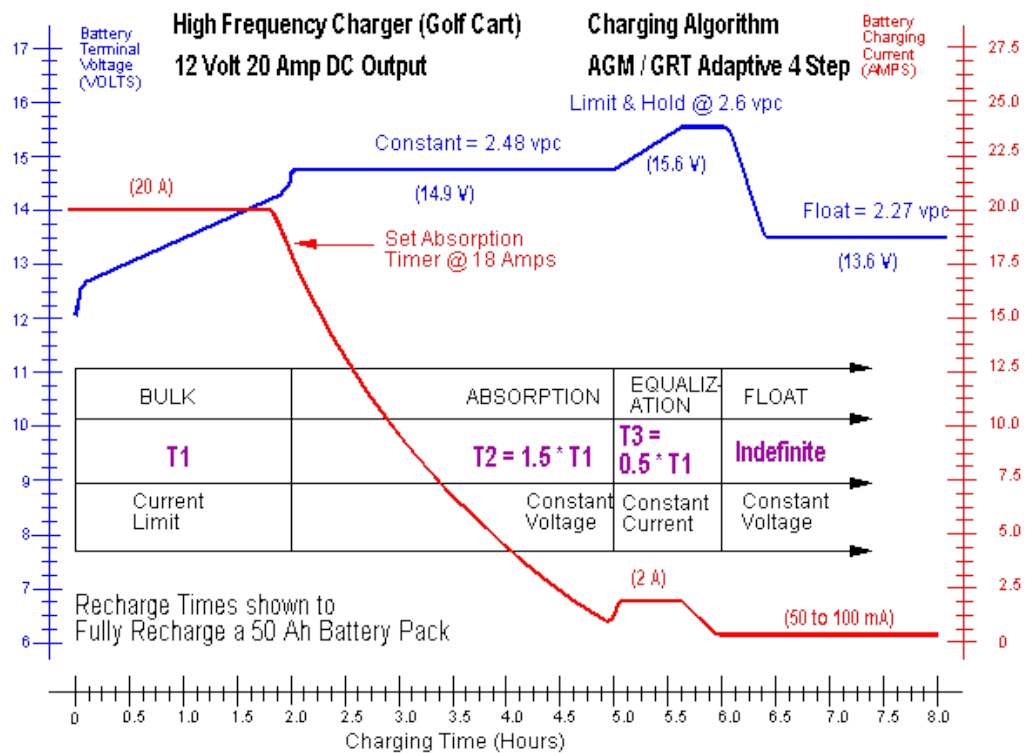
Figure 36. A multi-stage traditional charging algorithm a deep cycle AGM battery. (Darden 2001). The equalization phase is not recommended in charging of Optima yellow top SPIRALCELL® -type battery. (Optima batteries 2012).

The investigated wind turbine systems do not have these four charging phases described above, but only devices that prevent overcharging. This difference does not affect the analysis because the study focuses on detecting differences in energy transfer to the battery bank from similar systems in which only the charging voltage level varies. This is done by using the more efficient generator connection, according to the rotational speed of the generator or, in principle, according to the current wind speed using an automatically reversible star-delta switch and by increasing the charging voltage with a step up converter.

3.8 Suggested new control

The small wind turbines studied were used in stand-alone mode, connected only to a 12 V or 24 V battery bank. When the wind turbine is not connected to the grid there is no need for ordinary voltage and frequency control. However, the stand-alone system requires the batteries to store excess power generated for use when the wind is calm. Small wind power system for battery charging needs a charge controller to keep the batteries from overcharging. In a basic system with a

small Windside wind turbine a charge controller with dummy load is included. Even in the modified system with small turbine that is studied, a similar charge controller was used.

The common purpose of the study of the small wind turbines was to find ways to increase the output power, or to express it more precisely the yearly energy production. The wind is a natural phenomenon and the instant magnitude of the wind speed provides the power to the wind turbine shaft. The torque at the turbine shaft T_m is

(77) $$T_m = \frac{P_m}{\Omega},$$

where P_m is the mechanical power.

The turbine shaft power and torque, in the studied case, with variable speed is more complicated. However, fixed speed operation means that the maximum of power coefficient $C_{p,\ max}$ is available only at one particular wind speed. A lower power coefficient is observed for all other wind speeds, which reduces the energy output below that which might be expected from variable speed operation. That is, if the turbine speed could be adjusted in relation to the wind speed, a higher average power coefficient and a higher average output power could be achieved. The turbine torque T_m must be opposed by an equal and opposite load torque T_L for the turbine to operate at a steady rotational speed. If T_m is greater than T_L, the turbine will accelerate, while if T_m is less than T_L the turbine will decelerate. The mathematical relationship describing this is

(78) $$T_m = T_L + I_m \frac{d\Omega}{dt},$$

where I_m is the moment of inertia of the turbine, transmission, and generator, all referred to the turbine shaft.

One must notice that the moment of inertia effects on the dynamic performance of the wind turbine. If the moment of inertia of the turbine increases, the natural time constant of the rotating system also increases. This reduces energy production especially in gusty winds (Tang et al. 2008). Therefore, a wind turbine with low moment of inertia can produce more energy than a turbine with high moment of inertia. A wind turbine with high moment of inertia is more stable than a wind turbine with low moment of inertia. It can therefore be concluded that small wind turbines with low moment of inertia are suitable in low and gusty winds.

The torque produced by the turbine shaft rotates the direct driven generator. The resistive losses and the increase of impedance with high rotational speed, three times higher with star connected generator than with delta connection, limits the electric output power. This is a significant problem when using only star connected generator. The mechanical losses in bearings are small and practically independent of the rotating speed. The windage losses of the generators are small due to low rotational speeds.

The impedance of the generator increases with increased rotational speed, which prevents the output power to increase proportionally with increased rotational speed as is shown in Section 2.5.3. When using a three-phase generator, this can be partially prevented by using a reversible star-delta switch which has been tested in this work. Also, generators with series of coils can be used.

Control of WS-0.30B wind turbine

It was observed in laboratory and on site tests that there was a clear difference in maximum power output, if the generator was connected in star or in delta, and that especially in high rotational speed in the range of 700–1400 rpm with WS-0.30B wind turbines. At 1400 rpm, with the gust wind speed of about 30 m/s, the output power was increased by 60 % when the generator was connected in delta instead of star. This situation brought up the idea of having an automatic reversible star-delta switch and with hysteresis control to protect the contactor from chattering. If that can be done the energy output from the small wind turbine can be significantly increased in stormy winds. The control signal can be taken, either from wind speed or from rotational speed. It was found that a control signal taken from rotational speed is more stable than from wind speed due to moment of inertia of the wind turbine. Then the question arose as to how it can be realized and how a separate automatic reversible star-delta switch could be regulated without use of a computer. The control and test results of the separate automatic reversible, star-delta switch are described later in this section.

In light winds the torque at the turbine shaft is low and the rotational speed of the generator is therefore low. The output voltage from the generator is then low and if it is lower than the battery voltage (plus the voltage drops in the diodes) there will be no charging current to the battery bank. To avoid this problem a boost converter with a MPPT control was built and tested. The converter was successfully tested in the laboratory and field. The control of the boost converter is described in more detail in this section.

To avoid losses due to the converter in normal and high winds the main circuit was equipped with bypass switches. This solution was tested only by simulations

and not at the field. In the simulations the time was used as control signal, but in real situation some seconds average wind speed can be used.

Control of the boost converter

In this thesis, P&O MPPT system and P&O algorithm similar to that presented by Patsios, Claniotis & Kladas is used, except for the fact that here the duty cycle *D* optimizes output power from the MPPT converter instead of the input. The peak power tracking control algorithm was implemented in LabView® running on a PC. (De Broe, Drouilhet and Gevorgian 1999: 1–6; Koutroulis and Kalaitzakis 2006: 5–7; Patsios, Chaniotis & Kladas 2008: 1–2.)

The P&O MPPT control method used needs not any information about torque and rotational speed on the wind turbine (Patsios, Chaniotis & Kladas 2008: 1–2.)

In the developed boost converter with MPPT control only the outputs, i.e. voltage and current from the boost converter, are measured. The power is calculated and optimized by control of duty cycle on positive or negative steps until the maximal power point is reached. If the direction of the control step is wrong, so that the power decreases, making the logic to choose the other direction, thus it proceeds to the direction that makes the power to go to the maximum.

Wind turbine is loaded continuously with all that it can withstand in current wind conditions. If more power is to be drawn than that is available, the rotational speed reduces thus reducing the output voltage and output power.

If neither the turbine characteristics nor the wind speed are supposed to be known, an MPPT algorithm has to be implemented using an operational-seeking method based on the behavioral rules linked to power and speed variations (Mirecki & Roboam 2007:665.)

The boost converter used the duty cycle control and it was realized using Lab-View® software. The converter was first used in laboratory on a test bench, with a generator similar to those in the wind turbines in the field. The converter was completed with a P&O MPPT optimization. The test situation is shown in Figure 37.

Figure 37. The step up converter and the MPPT logic with the PM generator in a test bench.

The boost converter was later simulated with bypass switches in order to find a method to avoid the converter losses in wind speeds more than 5 m/s. In real tests of the boost converter it was found that this is a suitable threshold wind speed value to bypass the converter.

The constructed converter with the MPPT control was thus tested both in laboratory and in field tests. In the field test, two similar Windside WS-0.30B wind turbines at the same time were in use. Both were equipped with similar rectifier system, battery banks, measurement system and were mounted close to each other on a roof at 23 m height over ground level. Due to the fact that the wind turbines were mounted at only four meters distance to each other they operated in very similar wind conditions. Additionally, one was equipped with an automatic reversible star-delta switch and one with a boost converter with developed MPPT controller. The characteristic of the wind turbine with the automatic reversible star-delta switch were observed particularly in hard winds and the other in light winds. Winds, in the range from the cut-in wind speed 2.8 m/s to about 4.5 m/s, was observed many times. The wind turbine equipped with a boost converter with MPPT controller began to charge the battery bank at significantly lower wind speed than the wind turbine equipped only with an automatic reversible star-delta switch. In such low winds, the output power of the wind turbine with a boost converter was 1 to 2 W. This is because the wind turbine without a boost converter does not start to charge the battery bank if the output voltage after the rectifier bridge is lower than the voltage of the battery bank. However, in increasing wind speeds it was observed that the output power from the wind turbine without a boost converter in wind speeds above 5 m/s became higher than the output of the wind turbine with a boost converter, because of the relatively low

efficiency of the converter. Therefore, it is possible to get additional energy output if the converter is bypassed when the wind speed increases.

Control of the reversible star-delta switch

Since the measurement system of small wind turbines was realized in LabView®, it was possible to test the control of the prototype of the automatic reversible star-delta switch even in that software. From the field tests of the wind turbine suitable limit values and also the hysteresis value to the star-delta switch were found. The electrical connecting circuit of a conventional star-delta switch was known but the solution of the hysteresis in LabView® software was difficult to find.

The limits and the hysteresis values of the new autonomous automatic reversible star-delta switch are easily adjusted. The switch operates when the limits are exceeded. Suitable hysteresis band reduces the number of operations of the switch. The worked out reversible star-delta switch can be adjusted also to other manufacturer's small wind turbines.

The small wind turbine equipped with an automatic reversible star-delta switch connected to different battery banks was tested onsite. The turbine was first connected to a 12 V battery bank and later to a 24 V one. Figures 38–42 are from two storms at different times. In the measurements, a sampling frequency value of 1 Hz is used and the measurement is from 18452 to 32000 data points or observations. The measurement system was implemented using LabView® software.

Figure 38 shows the AC output power as a function of wind speed and Figure 39 the AC output power as a function of rotational speed, when the modified system shown in Figure 29 is connected to a 12 V battery bank. If the battery bank is fully charged, the excess power is redirected to a dummy load with a nominal value of 150 W. The two figures show that suitable upper and lower limits for control of the automatic reversible star-delta switch have been chosen. Figure 38 shows that the reversible star-delta switch has operated at wind speeds of 15 m/s. This is because of those observations by star connection is not found at wind speed from 17 m/s to 29 m/s. The upper limit was adjusted to 450 rpm and the hysteresis to 150 rpm as is shown in Figure 39. If the hysteresis is decreased the chatter of the contactor will increase and thus its life time decreases.

The equation of the power trend graphs in Figure 38 is used as AC electrical output power characteristics of the studied wind turbine when equipped with developed automatic reversible star-delta switch and is connected to a 12 V battery. The AC output power characteristic is here a polynomial function of $0.217U^2 + 1.7955U - 4$ in which U is wind speed.

The figure shows AC Power (W) on the y-axis versus Wind speed (m/s) on the x-axis, with the equation $P_{AC} = 0.217U^2 + 1.7955U - 4$ and $R^2 = 0.848$.
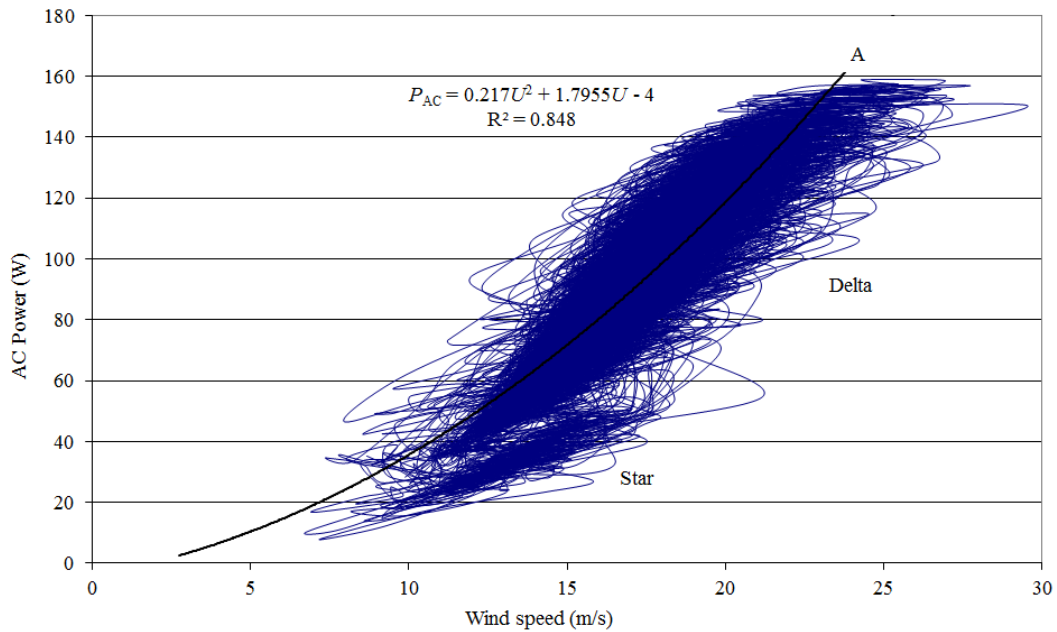
Figure 38.   The AC output power as a function of wind speed when a WS-0.30B is equipped with an automatic reversible star-delta switch and connected to a 12 V battery bank. Sampling frequency is 1 Hz and the measurement consists of 18452 data points.

In the top end of the trend graph is point A. Output power does not increase higher up than point A since the short circuit current of the delta connected generator connected to a 12 V battery charging configuration has been nearly reached.

The variation of output power value at a given wind speed value is due to the time constant of the wind turbine and is a normal phenomenon in wind power.

The main findings of regression analysis of the trend line of Figure 38 are shown in Table 5. The obtained R-squared value 0.848 means good fit of function to data distribution.

Table 5.   Results of regression analysis of the trend line of Figure 38.

Regression statistics	
Multiple R	0.921
R-squared	0.848
Adjusted R-squared	0.848
Standard Error	11.382
Observations	18452
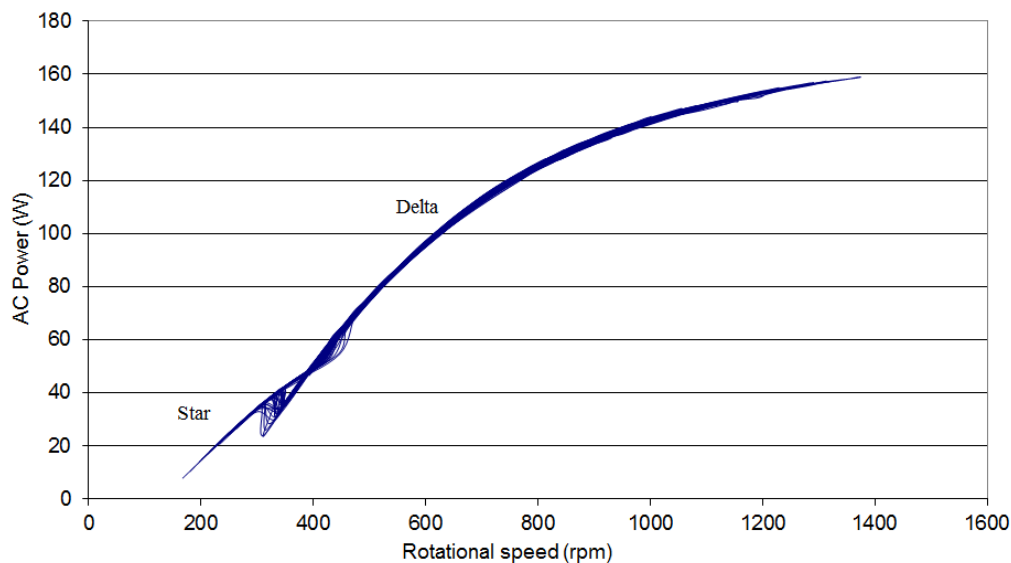
Figure 39. The AC output power as a function of rotational speed when a WS-0.30B is equipped with an automatic reversible star-delta switch and connected to a 12 V battery bank. Same measurement results as in Figure 38 are used. Sampling frequency is 1 Hz and the measurement consists of 18452 data points.

Figures 40 and 41 are from the measurement, when the small wind turbine with the modified system shown in Figure 29 is connected to a 24 V battery bank. If the battery bank is fully charged the excess power is redirected to a dummy load with a nominal value of 300 W. The output power increases to 270 W at a wind speed value of 27 m/s. Maximal output power 270W is close to twice the maximal power by 12V battery bank and nearly 300 W, which is the nominal power of this generator. In strong wind speeds, more than 20 m/s, the delta connection increases the output power significantly. Figure 40 is completed with a polynomial trend graph, which is later used in calculations of the energy production. The AC output power characteristic is a function $0.2677U^2 + 3.0829U - 12$ in which U is wind speed.
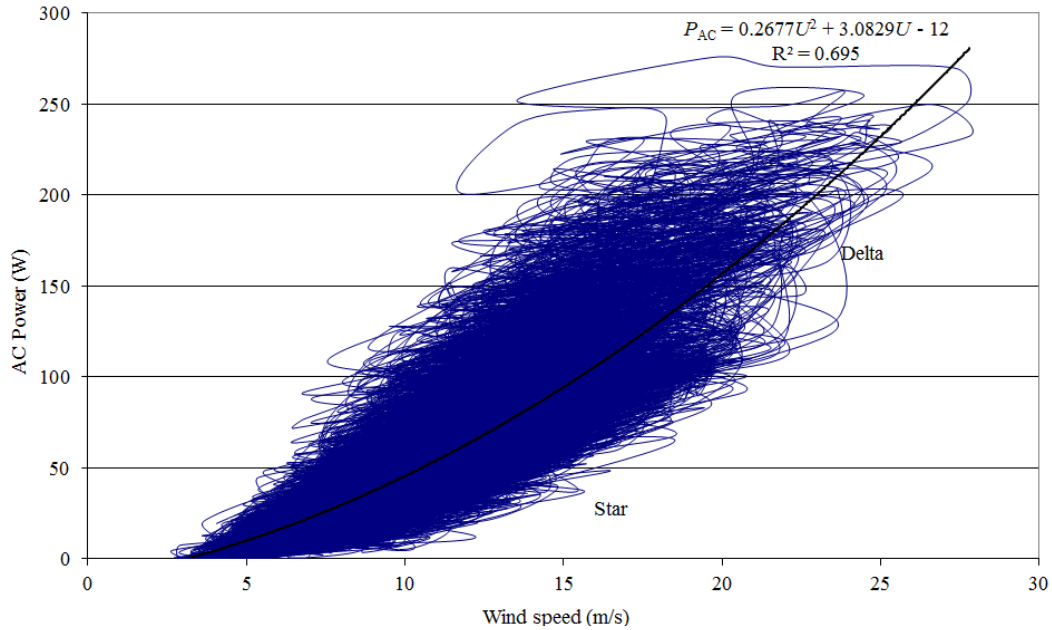
Figure 40. The AC output power as a function of wind speed when a WS-0.30B is equipped with a separate automatic reversible star-delta switch and connected to 24 V battery bank. Sampling frequency is 1 Hz and the measurement consists of 32000 data points.

The main findings of the regression analysis of the trend line of Figure 40 are shown in Table 6. The obtained R-squared value 0.695 means moderate but very near good fit of function to data distribution.

Table 6. Results of regression analysis of the trend line of Figure 40.

Regression statistics	
Multiple R	0.834
R-squared	0.695
Adjusted R-squared	0.695
Standard Error	21.016
Observations	32000

Figure 41 shows the AC output power as a function of rotational speed and from this figure we can see that upper limit to the star-delta switch is about 700 rpm and hysteresis near 200 rpm.
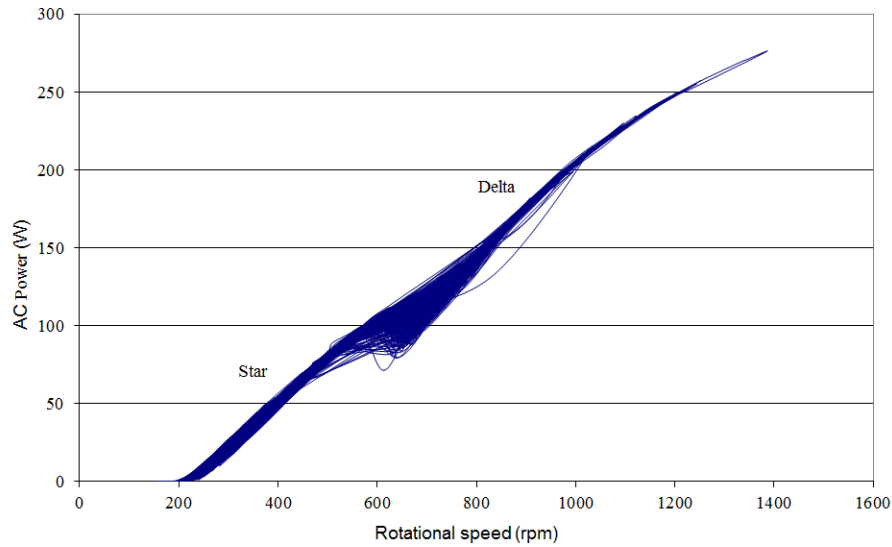
Figure 41. The AC output power as a function of rotational speed when a WS-0.30B is equipped with a separate automatic reversible star-delta switch and connected to 24 V battery bank. Here are used results from same measurement as in the figure above. Sampling frequency is 1 Hz and the measurement consists of 32000 data points.

The battery voltage during the above mentioned measurement process is shown in Figure 42. The battery voltage was increased from 21 V to 24 V during a time of 7 hours, which corresponds to the observation numbers 1–25200.
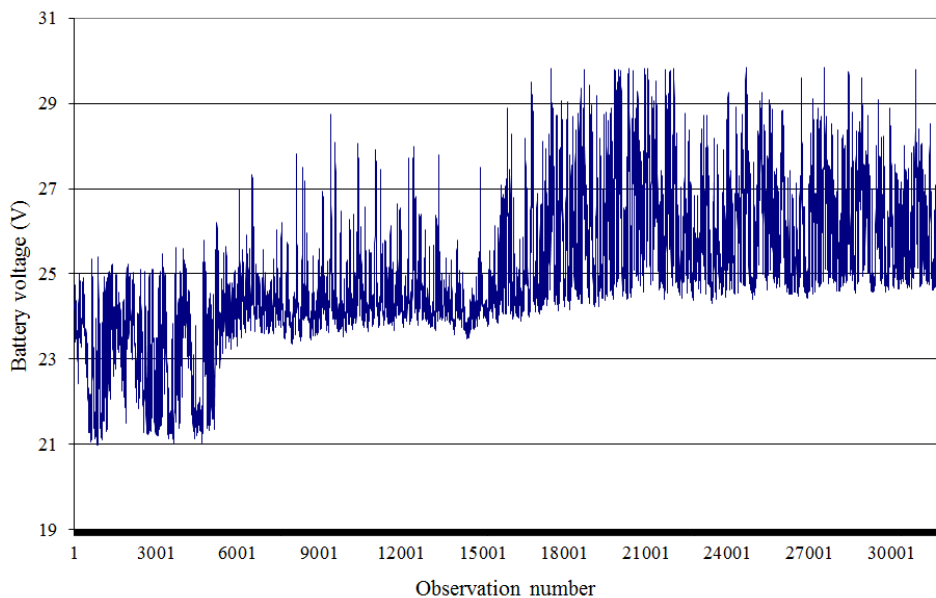
Figure 42. Battery voltage at the measurement when a WS.0.30B is equipped with star-delta switch and 24 V battery bank. Results are from same measurements as in the Figures 40 and 41.

The battery bank voltage is prevented from exceeding 30 V DC using the charging controller with connected dummy load shown in Figure 29.

The maximum output power value of 270 W in 24 V configurations is higher than in 12 V when the wind blows harder. The alternating output current by 24 V configurations follow the simulated graphs shown in Figure 22 and with 12 V configurations the simulated graphs of Figure 23. Because the battery voltage is two times higher with 24 V configurations than with 12 V configurations the output power is higher. However, 12 V configurations start charge the battery at lower wind speeds, due to lower battery voltage.

3.9   WS-4B turbine

The studied WS-4 wind turbine was equipped with a manual short circuit switch and a three-phase rectifier. This wind turbine was connected to an inverter which supplies the produced electricity to low voltage grid in the university campus. The battery bank is placed in same box as the inverter.

The larger wind turbine system studied consists of:
- (i)   A Windside wind turbine WS-4 with the swept area of 4 m^2
- (ii)   Basic equipment added by two pure resistors shown in Figure 43
- (iii)   A new developed hollow shaft to this wind turbine, and
- (iv)   Four 12 volts batteries, similar to that in the previous system, connected in series on the input side of an inverter, which was connected to internal low voltage AC network.

The basic equipment consists of a manual short circuit switch, a three-phase rectifier, a lubrication system while the developed peripheral equipment consists of the brake system. The new developed hollow shaft was needed to raise the natural frequency of the wind turbine, so that it became possible to examine the wind turbine in stronger wind conditions.

It was also possible to separately load the system, after the rectifier bridge, instead of the inverter, with pure resistors either 2.00 or 3.75 Ω by switching S in to position 1 or 2, as shown in Figure 43.
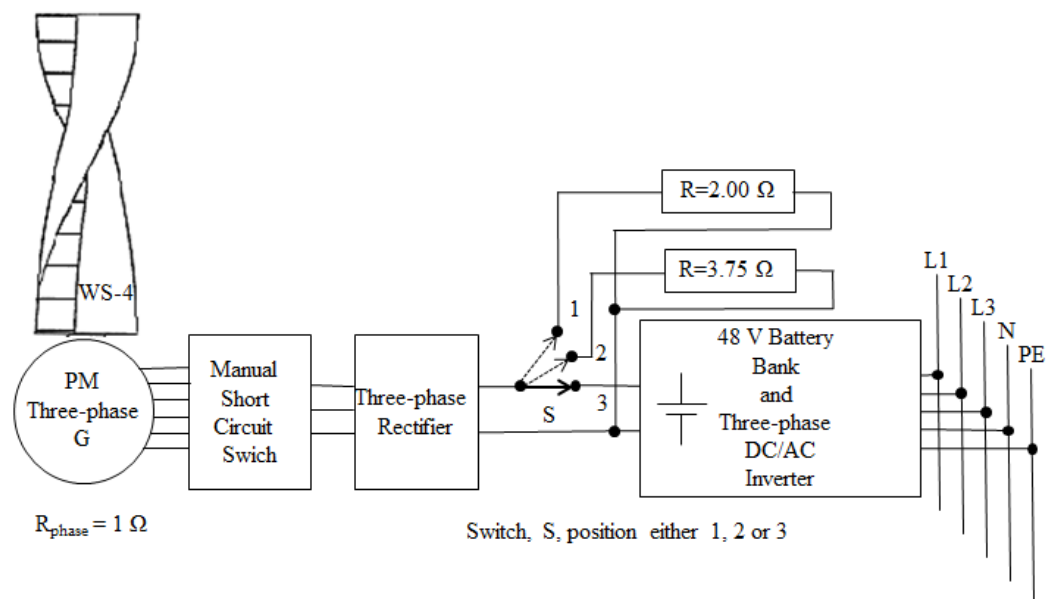
Figure 43.   The studied wind power system with a WS-4B turbine.

The maximum inverter output power of about 2 kW is obtained when the battery voltage is on the maximum value of 59.5 V; batteries are then discharged with about 50 A current. If battery voltage reaches 55.2 V level, low voltage blocking comes into effect, the device stops loading batteries until the battery voltage rises to its maximum of 59.5 V, after which the device again turns on and produces its maximum power to three-phase network.

The ability to load WS-4 wind turbine with pure resistors were arranged in the final stage of the investigation. The switch S can be in positions 1, 2 or 3. When the switch is in position 1 or 2, the battery bank and inverter are unused.

3.10   Mechanical aspects of the WS-4 turbine

During tests carried out on the WS-4C wind turbine it was observed that the first natural resonance frequency occurred during high winds. In view of this, work was carried out to develop a new WS-4B wind turbine with stiffer turbine shaft including also an automatic disc brake system.

Further, it proved impossible to accept the vibrations from WS-4C wind turbine with solid 90 mm shaft, without significantly limiting the rotational speed by using the brake system. However, a drastic limitation of the rotational speed would have limited the output power from the generator significantly.

From literature it was found the theory for vibrations using equations for cantile-vered beam and beam with fixed ends. Results from hammer shock testing, mod-al analysis and real tests of Windside wind turbines later shows that Eq. (79) gives us the right natural frequencies for fixed-free design both for solid and hol-low mixed shafts. The wind turbine shown in Figure 27b can be considered as a fixed-fixed design if the console is stable enough. The natural resonance frequen-cies of a fixed-free system is given by

$$(79) \qquad f = \frac{K}{2\pi l^2} \sqrt{\frac{E I_{am}}{m_l}},$$

where K for the modes 1 to 4 are 3.52, 22.0, 61.7 and 121, and l is the length of the shaft, E is the Young's modulus, I_{am} is the area moment of inertia and m_l is mass per unit length of turbine (Beardmore, R. 2012). Turbine mass consists of mass of free shaft, blades, consoles for blades, brake disc system and lifting eye.

Area moment of inertia or second moment of area is used in equations for the design of shafts and beams. Area moment of inertia should not be confused with moment of inertia or mass moment of inertia that is responsible for providing resistance against changing the rotational speed of a rotating body (Section 2.6.3).

Figure 44a shows a simplified wind turbine without an upper bearing and Figure 44b shows a simplified wind turbine with an upper bearing. The height of the turbine is denoted by l and the total mass of the turbine by m.

The area moment of inertia for a hollow shaft is given by

$$(80) \qquad I_{am} = \frac{\pi(D^4 - d^4)}{64},$$

where D is the outer diameter and d is the inner diameter. The shaft mass per unit length of a hollow shaft is given by

$$(81) \qquad m_l = \frac{\pi(D^2 - d^2)\rho_s l + m_b}{l},$$

where ρ_s is the density of the shaft material and m_b is the mass of the blades and consoles, brake disc system and lifting eye.
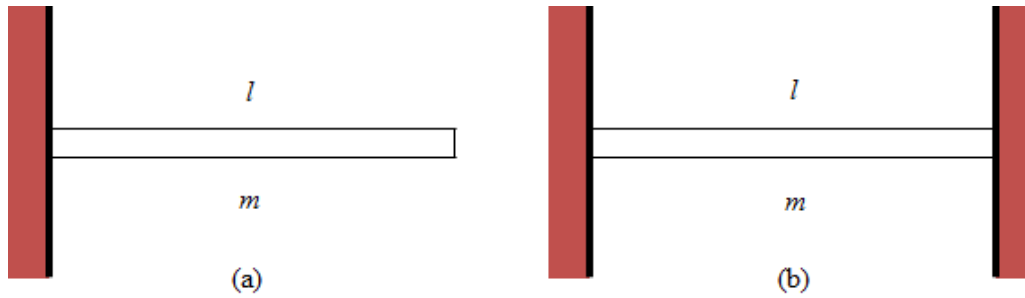
Figure 44.   A Fixed-free (a) and fixed-fixed (b) design.

The natural resonance frequencies of solid shaft as is in fixed-fixed system is also given by Eq. (79), where K of modes 1 to 4 are 22.4, 61.7, 121 and 200 respectively (Beardmore 2012).

The natural frequencies of a hollow shaft are expected to differ from the calculations of a solid shaft by changing the area moment of inertia and mass per unit length relative to the inner diameter of the shaft. The natural frequencies of a hollow shaft could also be calculated by Eq. (79). Optimal values for the natural frequencies are obtained when the most favorable inner diameter is chosen.

3.11   Development of a hollow shaft on the WS-4B wind turbine

Since it was found that a shaft of 90 mm diameter produced severe vibrations in high wind speeds, it was decided to develop a hollow shaft instead of using the brake system to reduce the maximum allowable rotational speed. The vibrations were transferred to both metal construction of wind turbine and building, and they were measured on the legs of the metal construction with a computer-based instrumentation system. With massive shaft with a diameter of 90 mm, the first natural frequency of 2.6 Hz was reached at a wind speed of 12 m/s when the shaft was 4 m long.

The manufacturer normally uses a solid shaft with a diameter of 120 mm for WS-4B wind turbine, but it was interesting to find the first natural frequency for a hollow shaft and how a hollow shaft works in real winds on site. If one could develop a stiffer shaft, there would be no need to limit the rotational speed in areas where the wind turbine effectively starts producing electricity.

In the design of a hollow shaft, which has bearings only at one end, the natural frequencies can be calculated by Eq. (79). Figure 45 shows that it is possible to find maximum values for the natural frequencies. In the design of a hollow shaft

made of steel, with a length of 4 m and outer diameter of 120 mm, the optimum values for the first natural frequency of 4.2 Hz, and the second natural frequency of 26.3 Hz were found when the inner diameter is chosen to be 70 mm.
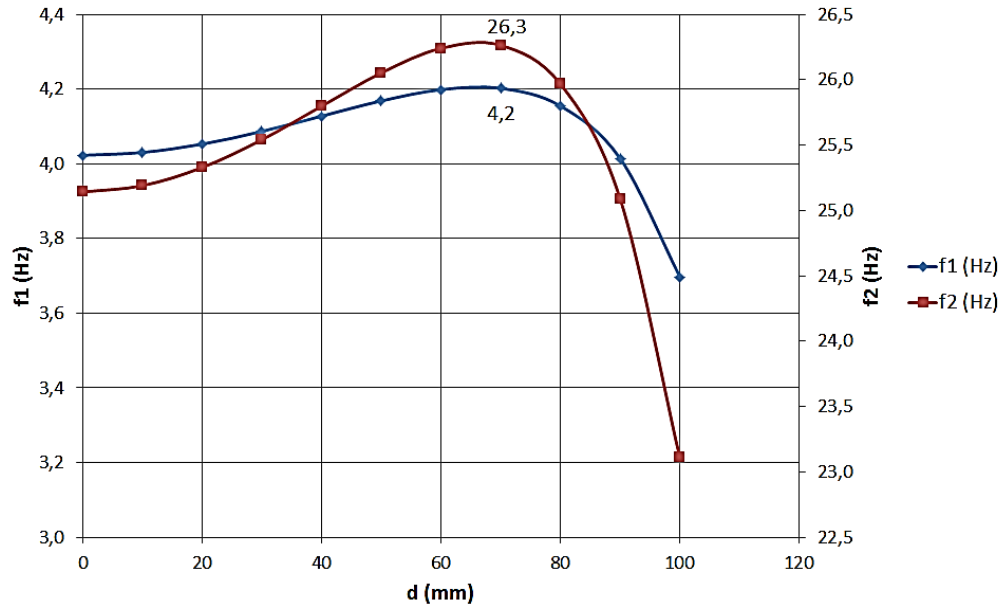
Figure 45. First and second natural frequencies as a function of the inner diameter. The diagram is calculated from fixed-free design of a hollow shaft, which is made of steel. The shaft has a length of 4 m and an outer diameter of 120 mm.

The first optimum natural frequency of 4.2 Hz corresponds to 252 rpm, which is equal to 4.2 multiplied by 60, and the second of 26.3 Hz corresponds to 1578 rpm. The first natural frequency of the new turbine shaft was measured both by hammer shock testing and modal analysis. Two different instruments were used in the two tests and both instruments registered the same values as the calculated value.

Finally, the inner diameter of 90 mm was chosen, because it was not possible to find a material with an inner diameter of 70 mm. Therefore, the first natural frequency has value of 4 Hz as shown in Figure 45 and it corresponds to 240 rpm of the hollow shaft used.

It can be seen from Figure 46 that the first natural frequency of the developed hollow shaft is 4 Hz, which is very close to the calculated value. This result is obtained by modal analysis. The measurements were made with aid of the software called 'Sound and Vibration Assistant' from National Instruments. The Sensor type was 603C01 from IMI Sensors.
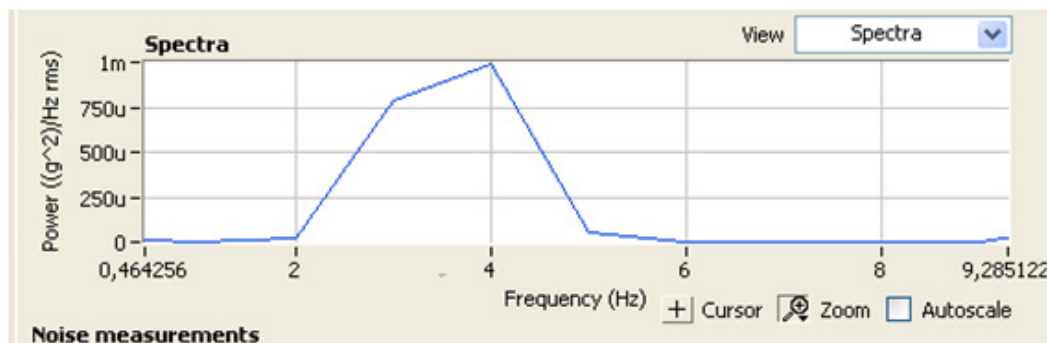
Figure 46.   Result from modal analysis measurement of the first natural frequen-cy of the developed hollow shaft, having an outer diameter of 120 mm and an inner diameter of 90 mm.

Also, in the design of a hollow shaft, which has bearings at both ends, the natural frequencies are calculated by Eq. (79), and in the same manner as above, the re-sults are displayed by graphs. Figure 47 shows fixed-fixed design of a hollow shaft, which is made of steel. The optimum natural frequencies f_1 and f_2 for a shaft having a length of 4 m and an outer diameter of 120 mm are 26.7 Hz and 73.7 Hz respectively, when an inner diameter of 70 mm is chosen.

The first optimum natural frequency of 26.7 Hz corresponds to 1602 rpm. The second optimum natural frequency became 73.7 Hz and corresponds to 4422 rpm. A rotational speed of 1602 rpm could be achieved if the wind speed reaches to about 105 m/s, which never has happened here. If a hollow shaft with dimensions as above is used in fixed-fixed construction, it is possible to achieve a very high safety margin to the first natural frequency.

The natural frequencies f_1 and f_2 for a shaft having a length of 4 m and an outer diameter of 120 mm are 25.5 Hz and 70.5 Hz respectively, when an inner diame-ter of 90 mm is chosen. The natural frequency of 25.5 Hz corresponds to 1530 rpm and 70.5 Hz to 4230 rpm. A rotational speed of 1530 rpm could be achieved if the wind speed reaches about 100 m/s, which is far more than our worst storms.
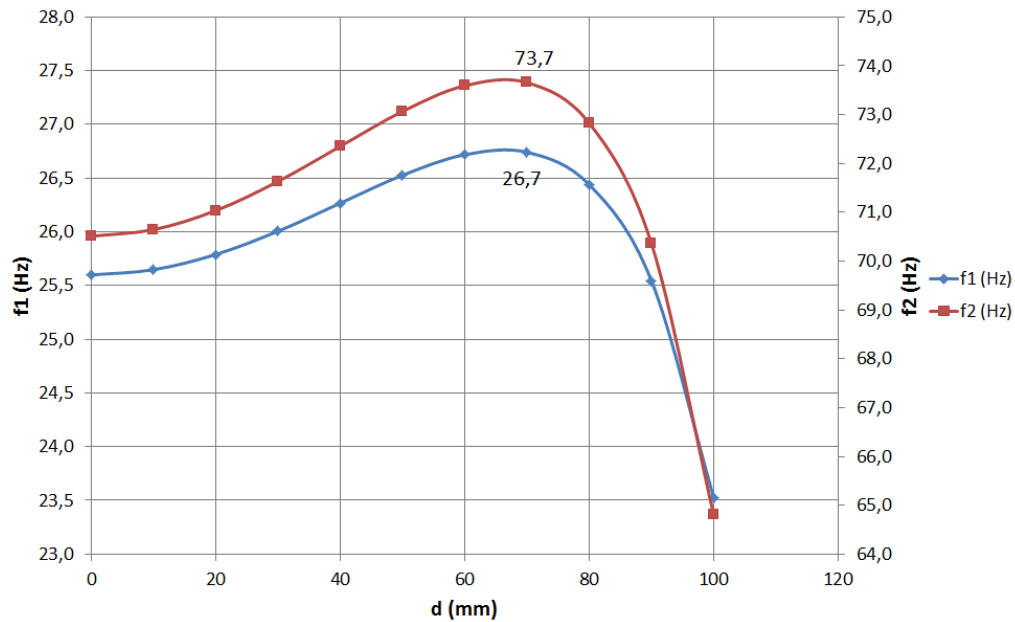
Figure 47.   First and second natural frequencies as a function of the inner diameter. The diagram is calculated from fixed-fixed design of a hollow shaft, which is made of steel. The shaft has a length of 4 m and an outer diameter of 120 mm.

If a WS-4B wind turbine is used in wind speeds above 17 m/s, there are three possible safe practices, and also a possibly hazardous method used to prevent the occurrence of the first natural frequency:

(i)   **Method 1:** A fixed-free configuration and a developed hollow shaft with an outer diameter of 120 mm and an inner diameter of 90 mm, but the wind turbine must be stopped if the wind speed exceeds 15 m/s. Compared to a wind turbine with solid shaft with a diameter of 120 mm, the area moment of inertia decreases by 32 % and the total mass with 31 %. If using solid shaft with a diameter of 90 mm, the wind turbine must be stopped approx. at 12 m/s but if using shaft with an outer diameter of 120 mm with the best inner diameter, as is 70 mm, the wind turbine can also safely produce energy at wind speeds of 15–16 m/s.

(ii)   **Method 2:** A fixed-free configuration and a hollow shaft with an outer diameter of 140 mm and an inner diameter of 80 mm, but the wind turbine must be stopped at speeds more than 20 m/s. Compared to a wind turbine with solid shaft with a diameter of 120 mm, the area moment of inertia increases by 65 % and the total mass decreases with 5 %. The wind turbine can also safely produce energy at wind speeds of 15-20 m/s.

(iii) **Method 3:** A fixed-fixed configuration and a solid shaft with a diameter of 90 mm and the first natural frequency occurs only at wind speeds above 65 m/s, but the output power should be limited to 2 kW at wind speeds above 20 m/s. Compared to a wind turbine with solid shaft with a diameter of 120 mm, the area moment of inertia decreases by 68 % and the total mass with 24 %. The mass of the metal structure of the upper bearing point will be added. The wind turbine can be safely used to produce energy also in wind speed of 12-30 m/s. This configuration is used by the manufacturer and was not studied in this study because it would have required extensive modifications to the steel structure for the power plant.

(iv) **Method 4:** This (the potentially dangerous, most probably unsafe) method uses a fixed-free configuration and a developed hollow shaft with an outer diameter of 120 mm and an inner diameter of 90 mm. By automatic switching between star and delta connection of the generator, at appropriate rotational speeds both in acceleration and deceleration, it should be possible to prevent the turbine to rotate at its first critical speed of rotation. The first critical speed of rotation can this way be skipped. The wind turbine can be used to produce energy also at wind speeds of 15-30 m/s. The output power should in this method also be limited to 2 kW at wind speeds above 20 m/s.

The first option causes loss of production of electricity at wind speeds above 15 m/s. In the second option there is loss of energy production at wind speeds more than 20 m/s. When using the third option, electricity is produced continuously. In the fixed-fixed design, the upper bearing must be stable enough so that its first natural frequency is preferably above 17 Hz. The last proposed method can be regarded as a more promising method than any of the safe ones in future development work. However, this method is not tested in practice.

The moment of inertia or mass moment of inertia of turbine shafts can be calculated by Eq. 61. The moment of inertia or mass moment of inertia decreases by 32 % for a developed hollow shaft with outer diameter of 120 mm and inner diameter of 90 mm compared with a solid shaft with a diameter of 120 mm.

Proposed control of a WS-4 wind turbine

The measurements taken on the WS-4B wind turbine showed that it was advantageous to switch over to delta when the wind speed exceeded about 9.3 m/s or the rotational speed exceeded about 100 rpm, but to return to the star connection in decreasing wind speeds when the rotational speed is around 160 rpm. To prevent disturbing mechanical vibrations in the steel construction of

the wind turbine and building, three safe methods are presented in this thesis, and there is one risky method to control this larger wind turbine from Oy Windside Production Ltd.

The WS-4 wind turbine can be controlled using conventional relay technology or with programmable logic. The first two methods require a braking system that can stop the turbine before first critical rotational speed is reached. The braking system may be controlled by a switch which is activated by wind speed. Such automatic braking system was used earlier when attempting to avoid unwanted vibrations at the facility for WS-4C. The third method uses a steel construction for the upper bearing and a current-limiting device to protect the generator against overload. The proposed fourth method has not been tested. Since a grid-connected inverter is used in the WS-4 system, no dummy loads were needed.

In this chapter we discussed the studied wind turbines and systems. Then developed devices or parts, including the use of them were described, finally tested and proposed control methods were also illustrated.

4 SIMULATIONS, MEASUREMENTS AND ANALYSIS

This chapter gives the results of measurements, and it includes discussions of the results obtained. Result from a simulation of bypass switches for the step up converter is also included. Two sizes of vertical-axis wind turbines from the same manufacturer were investigated. Technical data of studied Windside wind turbines is presented in Appendix 1. For all measurements, it was necessary to seek suitable measurement instruments and measurement systems. Initially, it was decided to examine only the smaller wind turbine, but during the process it became important to study also the similarities and differences between Windside wind turbine sizes.

Two stationary weather stations were used at the wind turbine installation sites. A special anemometer was used in the measurement of the characteristics of output power of WS-4B turbine. A wide logging system was built up at the mounting location for the study of WS-0.30B wind turbine. A power analyzer was used when WS-4B wind turbine was investigated. The mechanical vibrations were measured with three instruments. Before WS-4C wind turbine type was changed to the more wind-resistant WS-4B wind turbine with hollow shaft, an idea was to introduce a measurement system for continuous measurement of vibrations in the metal construction. It was planned to have automatic braking of the turbine, if there was unwanted vibration in the metal construction, but the automatic part of this system was not made because it was not needed after the change of turbine type. All measurement data was stored, transferred and analyzed digitally. Information on measurement systems and measurement devices used is given below.

Weather stations

Two Davis Vantage Pro™ 2 weather stations were mounted stationary on the turbine installation, sites at the roofs of Tritonia and Fabriikki buildings. (Davis Weather 2012.)

Voltage and current sensors

The electric quantities on the small wind turbines, i.e. voltage and current, were measured with sensors LV25-P respective LAH25-NP from Lem. (Lem 2012.)

LabView® measurement system

A system for measuring and recording data from WS-0.30B wind turbines was constructed using LabView® (which comes from Laboratory Virtual Instrumenta-

tion Engineering Workbench) software from National Instruments. LabView® is a platform and development environment for a visual programming language. Originally released for the Apple Macintosh in 1986, LabView® is commonly used for data acquisition, instrument control, and industrial automation on a variety of platforms including Microsoft Windows, Unix, Linux, and Mac OS (Operating System). (National Instruments 2012.)

CompactRio

In this thesis CompactRio was used when the star-delta control was worked out and it was the intention at that time to use this device to control the whole wind turbine. Later when the separate automatic reversible star-delta switch began to work, it was not necessary to use any separate control signal.

The CompactRio shown in Figure 48 is a small, rugged embedded control and data acquisition system. It is powered by National Instruments LabView® graphical programming tools for rapid development and features embedded real-time processor for reliable stand-alone or distributed operation. (National Instruments 2012.)

Figure 48. A CompactRio with Real-Time controller and 8 slots. (National Instruments 2012).

The CompactRio integrates an embedded FPGA chip that provides the flexibility, performance, and reliability of custom hardware and it includes hot-swappable industrial I/O modules with built-in signal conditioning for direct connection to a variety of sensors and actuators. (National Instruments 2012.)

Voltech PM6000 Power Analyzer

The Voltech PM6000 Power Analyzer was used in the output power as function of wind speed measurements on the WS-4B wind turbine. This power analyzer had truly appropriate ranges. Since the frequency was from 0 to 25 Hz, conventional energy measuring devices for 50 Hz could not be used. The PM6000 is an advanced digital sampling power analyzer that can be fitted with up to 6 meas-

urement channels. Each channel is a separate wattmeter with fully floating inputs for connection to the voltage and current of the power circuit to be measured. (Voltech 2012.)

Wind sensor

A cup anemometer P2546A manufactured by WindSensor was used for wind speed measurements of WS-4B wind turbine. (WindSensor 2012.)

4.1   WS-0.30B

The presented results are from field tests of two identical WS-0.30B wind turbines at University of Vaasa in Finland carried out over a period of four years (2006–2009). The results from the field test and the simulation of the developed boost converter are first described. The converter was used for approximately 6 months in 2007 and then the actual wind turbine system was connected to a 24 V battery bank. At the same time, long time tests of the star-delta switch were being done, together with another identical wind turbine, which also was connected to a similar 24 battery bank. Next a comparison of energy production between the use of 12 V and 24 V battery bank use is reported. Finally, the results when a 24 V battery bank was used are presented, without and with an automatic star-delta switch.

4.1.1   *Field test of the boost converter*

The results from the boost converter show how the converter works and the results support the use of a boost converter in battery charging in low wind speeds. In the field tests of the boost converter with the MPPT optimizing control, the interesting issue was the output current or output power to the battery bank. At the same time the output to another battery bank from another similar wind turbine, but without a boost converter was observed. The wind speed was observed from a wind speed instrument which was included in the arrangement for the measurements presented in Figures 40 and 41. The sampling frequency was 10 Hz. It was found that in wind speeds from 2.8 m/s to 4.5 m/s the one with converter produced an output current whereas the one without boost converter did not. The battery bank is 24 V.

Figure 49a shows the input and output voltages of the developed boost converter in an interval of 300 seconds. Figure 49b shows the input and output currents during the same interval.
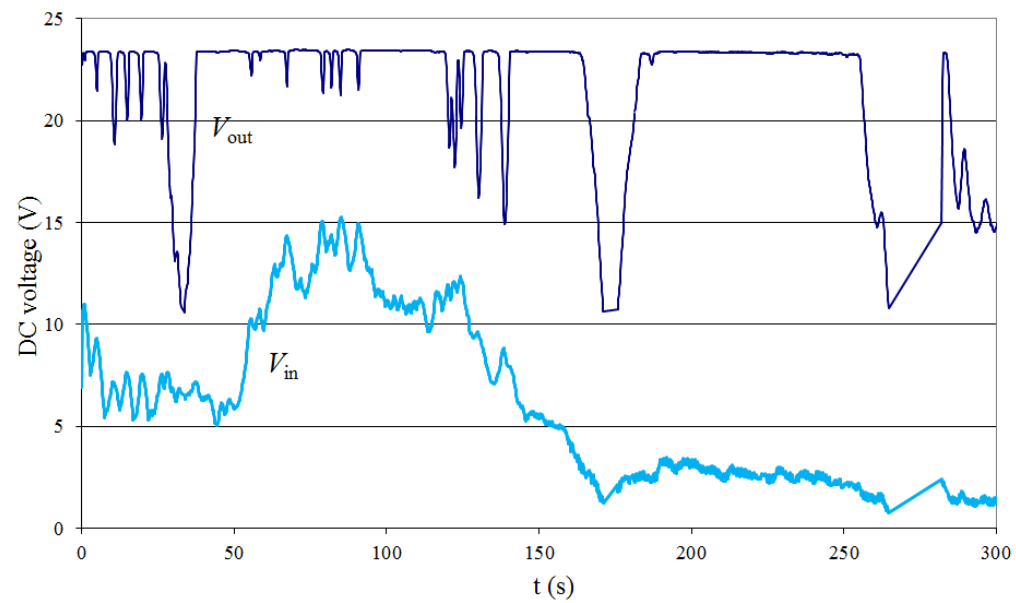
(a)
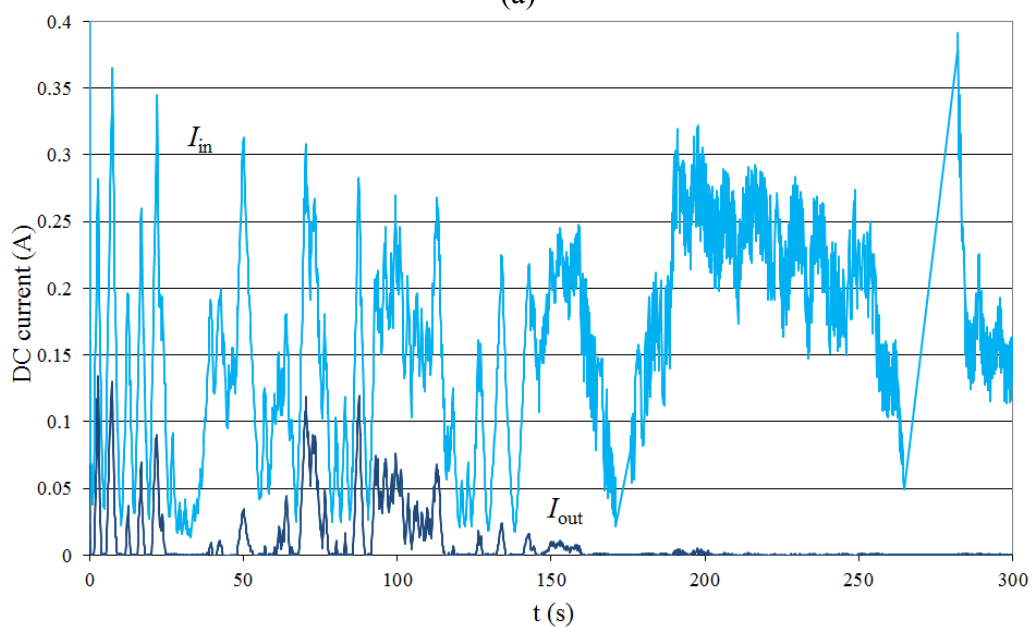
(b)

Figure 49. Inputs and outputs, voltages (a) and currents (b) of the boost con-
verter of WS-0.30B during a field test in Vaasa.

We calculate the efficiency from Figure 49 at time 80 seconds:

(82)
$$\eta_c = \frac{V_{out} \cdot I_{out}}{V_{in} \cdot I_{in}} = \frac{23 \cdot 0.06}{13 \cdot 0.13} = 0.82.$$

The boost converter was connected as shown in Figure 29, but the system used was without automatic reversible star-delta switch. The automatic reversible star-delta switch was used in another similar wind turbine system without a boost converter. The input to the charging controller was equipped with a diode and therefore the output from the boost converter can be lower than the voltage of the battery bank. The battery bank is 24 V. A minimum voltage of 11 V is used for V_{out} to save the PC's memory from unnecessary data.

It can be seen from Figure 49a that the output voltage collapses many times due to low wind speed, which was visually observed from a wind speed indicator. The input voltage to the converter is also very low. The output voltage collapsed significanly three times, at time instants of 35 s, 170 s and at 270 s due to the too low wind speed. The battery charging is stopped immediately when the output voltage decreases lower than the battery voltage.

It can be seen that when the output voltage collapses the output current is zero. It can also be seen that the output current is very low during the whole interval. It was found that there is no output power without the use of boost converter and therefore a converter is used in battery charging in light wind situations.

Figure 50 shows another interval with wind speeds at about 4.5 m/s. The wind speed was visually observed from same a wind speed indicator as above. The battery bank is also 24 V in Fig. 50. The sampling frequency of wind speed measurement was 1 Hz.

When the wind speed decreases significantly at time 100 seconds from start, the input voltage and the output current decrease markedly. The output voltage also decreases, but it remains higher than the battery voltage. When the input voltage decreases due to low wind speeds in intervals 1200 to 2000 seconds and 2500 to 3000 seconds the output voltage and output current remains high but the input current increases.

The wind speed drops temporarily below 4.5 m/s at times, 4200, 5000, 5800 s and after that a few times. Output voltage and output current also drop temporarily but they rise after the input voltage has risen. The wind speed in the other intervals is higher than 4.5 m/s and the output current varies only slightly.
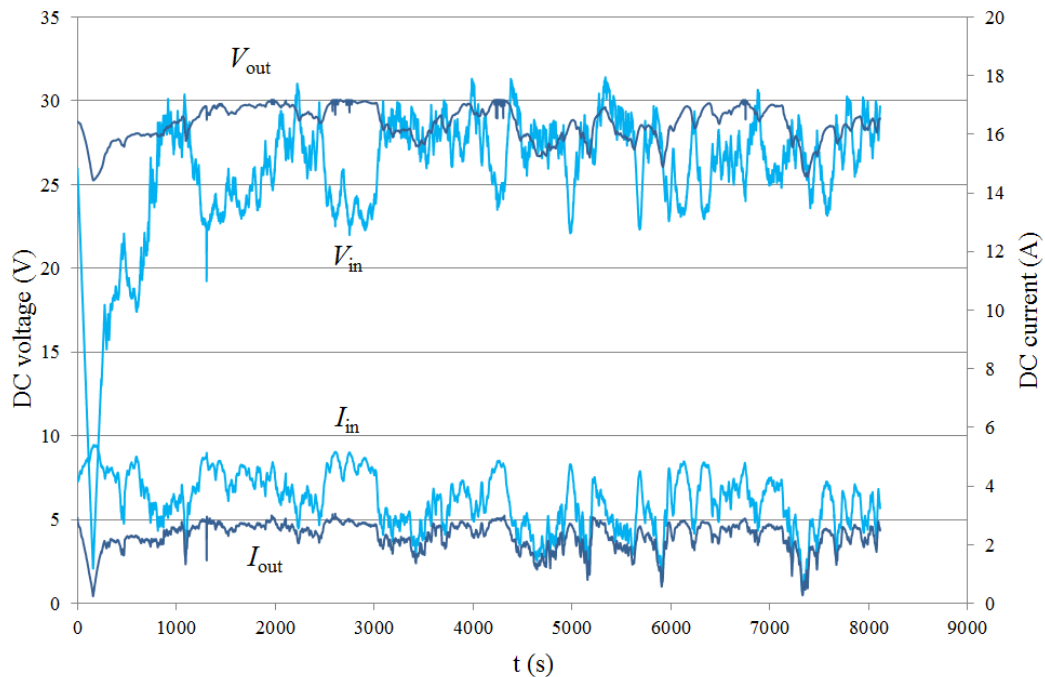
Figure 50. Field test of the boost converter in wind speeds over and below 4.5 m/s in Vaasa. The wind speed is below 4.5 m/s when the input voltage V_{in} drops below 24 V. A voltage scale is on the left hand side and a current scale on the right hand side.

We calculate the efficiency from Figure 50 at time 2800 seconds:

$$(83) \qquad \eta_c = \frac{V_{out} \cdot I_{out}}{V_{in} \cdot I_{in}} = \frac{30 \cdot 4.8}{23 \cdot 8} = 0.78.$$

Theoretical calculation of efficiency of developed step-up converter (Page 71) gave a value of 0.95 (Eq. 76) with biggest losses in the diode (Eq. 75). However, the efficiency of the tested converter is here calculated to 0.78 in a used point. The fact that the maximum efficiency of the developed boost converter was not higher than that is probably due to a hand-wound coil, split core and losses in the lines.

4.1.2 Result from simulations of the boost converter

Due to the low efficiency (around 0.8) of the developed boost converter, it is not recommended to be used in the middle range and in strong wind speeds. The boost converter can then be bypassed with a signal from a suitable value of wind speed. Such a boost converter was simulated using Simplorer® simulation software. The simulated boost converter is shown in Figure 51. To bypass the con-

verter in wind speeds over 4.5 m/s three switches are used. However, in the simulation in Figure 51, the time is used as control signal. The simulated generator is shown on left side. The switches S2, S3 and S4 changes modes at the time 200 ms and the boost converter is then bypassed.

R_4 corresponds to the resistance of inductor L_4, R_5 is the leakage resistance of C_2 and R_6 is the internal resistance of battery bank.
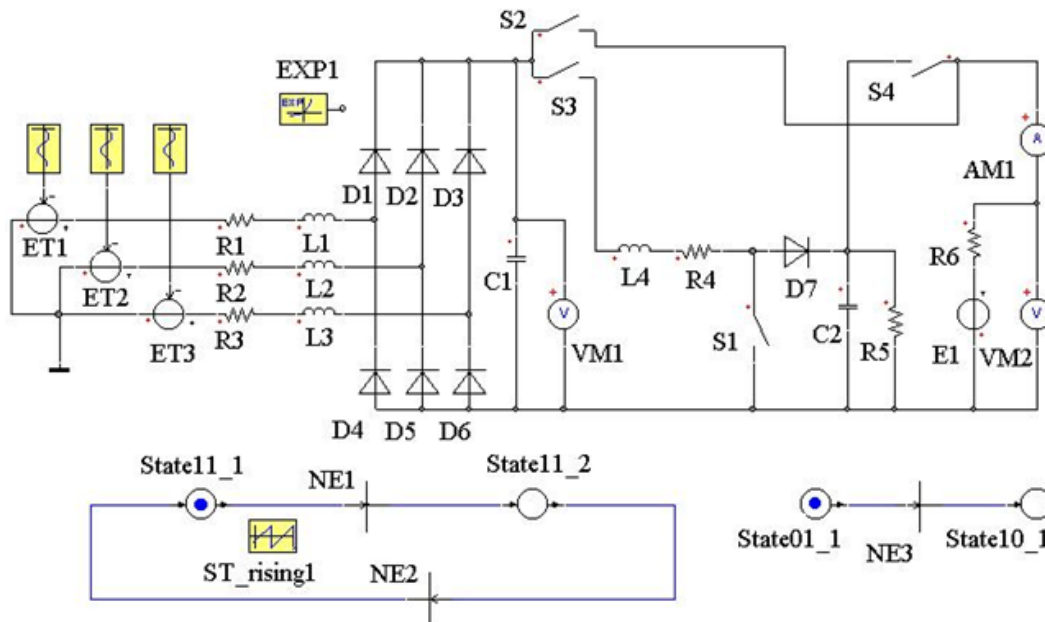
$R_1 = 3.6\ \Omega$	$R_5 = 600\ \Omega$	$L_3 = 37$ mH
$R_2 = 3.6\ \Omega$	$R_6 = 0.2\ \Omega$	$L_4 = 200$ mH
$R_3 = 3.6\ \Omega$	$L_1 = 37$ mH	$C_1 = 1502\ \mu$F
$R_4 = 0.05\ \Omega$	$L_2 = 37$ mH	$C_1 = 1063\ \mu$F

Figure 51.　The simulated circuit of the boost converter with the bypass switches S2, S3 and S4. The battery bank is 24 V and denoted by E1.

The simulated results of the boost converter at the time of bypass are shown in Figures 52 and 53. Figure 52 shows a situation when the rotational speed is 300 rpm which corresponds to a wind speed of 4.4 m/s. Current as indicated by AM1 goes to the battery bank before the bypass. After the bypass, the voltage VM2 decreases to the battery voltage and AM1 tends to zero, which clearly shows that no battery charging can occur by too low rotational speed or too low wind speed without a boost converter.
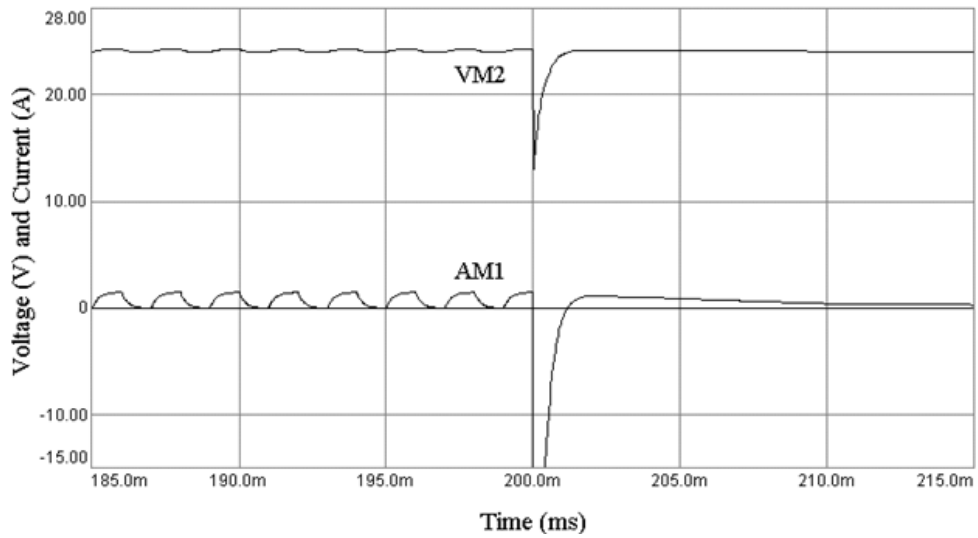
Figure 52. Bypass of the boost converter at time instant of 200 ms, when the rectifier output voltage is lower than the battery voltage. The curves are based on simulations. The simulated rotational speed is 300 rpm and duty cycle 50 %.

Figure 53 shows a simulated case, where the output voltage of the rectifier is greater than the battery voltage. After the bypass moment, VM2 voltage remains higher than the battery voltage and the battery bank is charged better than through the boost converter.
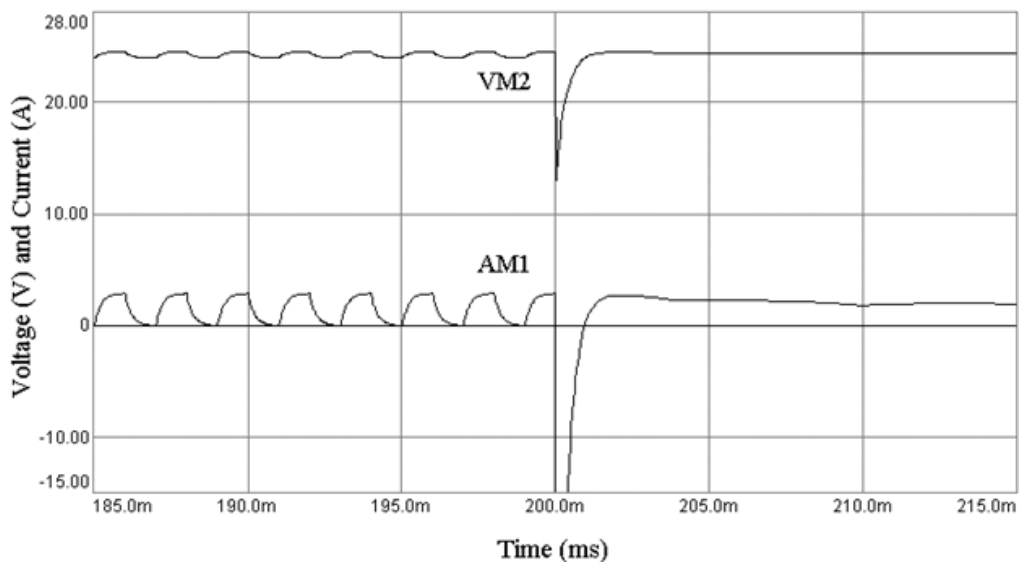
Figure 53. Bypass of the boost converter at time instant of 200 ms, when output voltage of the rectifier is greater than the battery voltage. The curves are based on simulations. The simulated rotational speed is 500 rpm and duty cycle 50 %.

In the simulation mode, the output voltage to the battery bank can be increased by changing the duty cycle but increased output voltage means that the input voltage VM1 decreases. This is because the AC current increases and the voltage drops across the resistances R_1–R_3 increases. In a real situation, the load on the turbine increases so that the rotational speed decreases rapidly and therefore reduces the output voltage and current, or in other words the output power from the wind turbine. This phenomenon was observed many times in the field tests of the boost converter. For example in Fig. 49a after time 200 s the input voltage to the step up converter is so low so the output current tend go to zero shown in Fig. 49b.

4.1.3   Comparison of battery bank of 12 V and 24 V

When using the new star-delta switch, a comparison of energy produced to two 12 V, 55 Ah batteries connected in series (24 V) and in parallel (12V), can be made. In the comparison, the distribution of wind speed from measurements in field tests carried out for year 2006 shown in Figure 5 at the University of Vaasa is used. The distributed wind speed used is shown in form of number of 10-min average values in Figures 54 and 55. The produced electric energy has been calculated using Excel® software. The procedure is described in Section 2.6.4. The result shows that energy production is considerably higher with 24 V configurations than with 12 V configurations. Figure 54 shows the produced energy and distribution of wind speed in one year when 12 V battery bank is used and Figure 55 when 24 V battery bank is used. The same wind data and the same wind turbine were used in this comparison of different voltages. The output performance, or in other words trend lines of output power from Figures 38 and 40 were used in the calculations.

Let us give an example of calculation of energy by 12 V battery bank in wind speed interval 4–5 m/s. In this interval are 6010 pieces of 10 minutes average values shown in Figure 54. The output power in the interval is calculated by the equation $0.217 * 4.5^2 + 1.7955 * 4.5 - 4$ from page 79 to 8.474 W. Then the energy W in the interval is 6010 multiplied by 8.474 and divided by 6000 or 8.48 kWh, which means integer value of 8 kWh, as is shown in Figure 54.

The annual energy production by a 12 V and a 24 V battery bank has been calculated using Excel® program and by using equations for the trend graphs, which were shown in Figures 38 and 40. The annual energy productions which are calculated by this method using integers are 76 kWh for a 12 V battery bank and 81 kWh for a 24 V battery bank. Annual energy yield from the small wind turbine increases by about 7 % when a 24 V battery bank is used instead of a 12 V.
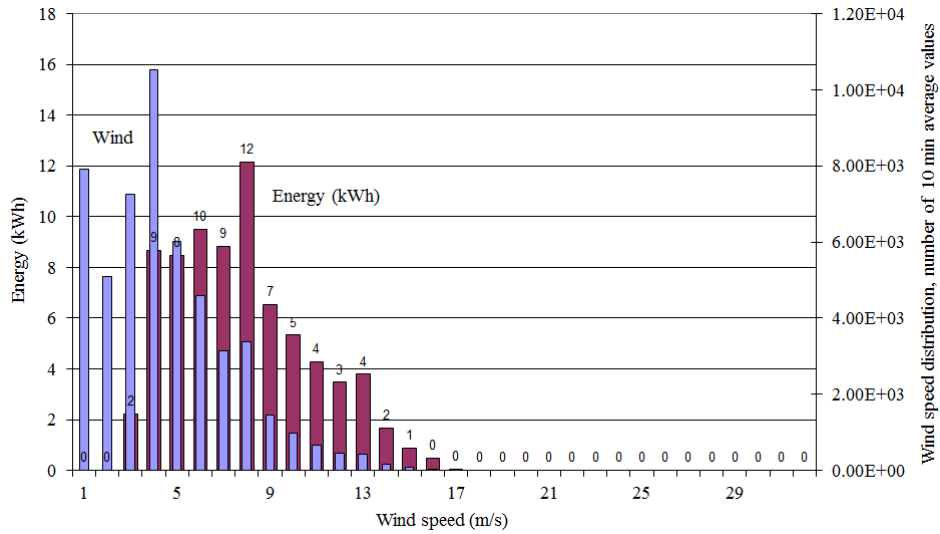
Figure 54.   Calculated energy production (red columns) and distribution of wind speed (blue columns) in wind speed intervals for one year when a WS-0.30B wind turbine with 12 V batteries is used. Energy is shown by integers.

Comparison of Figures 54 and 55 shows, that the sum of the annual energy production is significantly higher when the 24 V battery bank is used.
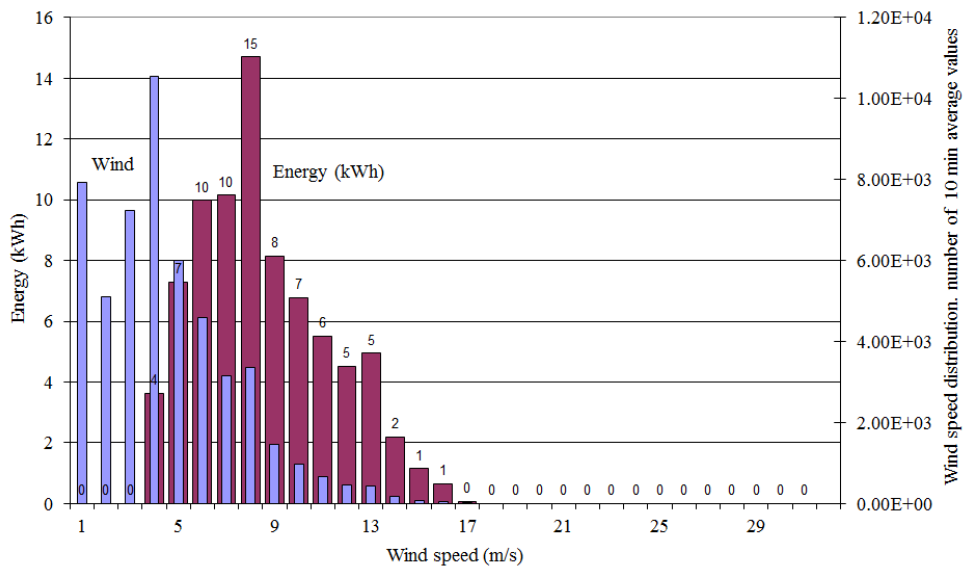
Figure 55.   Calculated energy production (red columns) and distribution of wind speed (blue columns) in wind speed intervals for one year when a WS-0.30B wind turbine with 24 V batteries is used. Energy is shown by integers.

The used method for calculation of annual energy is similar to the method in (IEC 61400-12 2014). KWh metering was not used because appropriate meter for function in systems with low frequency could not be found.

If a 12 V configuration instead of a 24 V system with increasing wind speeds is used, the currents in the system that have similar values as is shown in Figure 23, but because the battery voltage is lower, the output power is also lower.

Since it was found that the wind turbine produces more power to a 24 volt battery bank, only this was used in the development of an automatic reversible star-delta switch.

4.1.4   *Energy production to 24 V battery bank without and with the new star-delta switch*

Let us first look at measurements based on pure star connected generator. Figure 56 shows the AC output power as a function of wind speed from a test of a WS-0.30B wind turbine with only star connected generator. Output power does not exceed 160 W, even though the wind speed reaches 27 m/s. Trend line for the output power and the equation $0.0912U^2 + 3.7288U - 10$ for the trend line are shown in Figure 56. The distributed energy production for star connected generator can be calculated using the equation for this trend graph. By star-delta connection the output power at this wind speed of 27 m/s was 270 W shown in Figure 40. The output power at this wind speed was so increased by more than 60 %!

The distributed energy production for star-delta connected generator can be calculated by using the equation $0.2677U^2 + 3.0829U - 12$ of Figure 40. Figure 57 shows a comparison between distributed energy productions with the two generator configurations.

The annual energy yield by different generator connection is shown in Figure 57. The annual energy yield by star configuration is calculated to be 74 kWh and by star-delta configuration was earlier given to be 81 kWh. Therefore, the annual energy yield from the small wind turbine increases by more than 9 % when an automatic reversible star-delta switch is used instead of star connection.
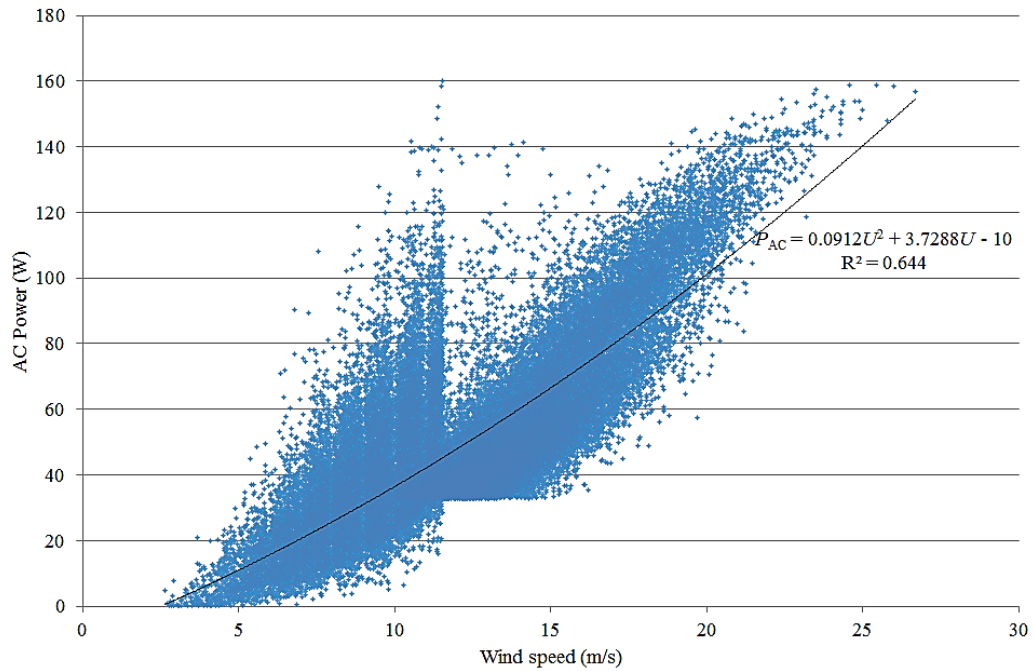
Figure 56. The AC output power as a function of wind speed from a test of the WS-0.30B wind turbine when the generator was star connected. Sampling frequency is 1 Hz. The measurement consists of 51025 observations and is composed of same low wind speed data as Figure 40 and new high wind speed data.

The combined wind data does not coincide completely in wind speed area 10–15 m/s in Figure 56, but the number of observations is so numerous that the trend line becomes true. The main findings of the regression analysis of the polynomial trend line of Figure 56 are shown in Table 7. The R-square value of 0.644 means moderate fit of the function to data distribution.

Table 7.   Results of regression analysis of the trend line of Figure 56.

Regression statistics	
Multiple R	0.802
R-squared	0.644
Adjusted R-squared	0.644
Standard Error	14.889
Observations	51025

In the comparison shown in Figure 57, the same wind speed distribution as in the previous section is used, but wind speed distribution is not shown.
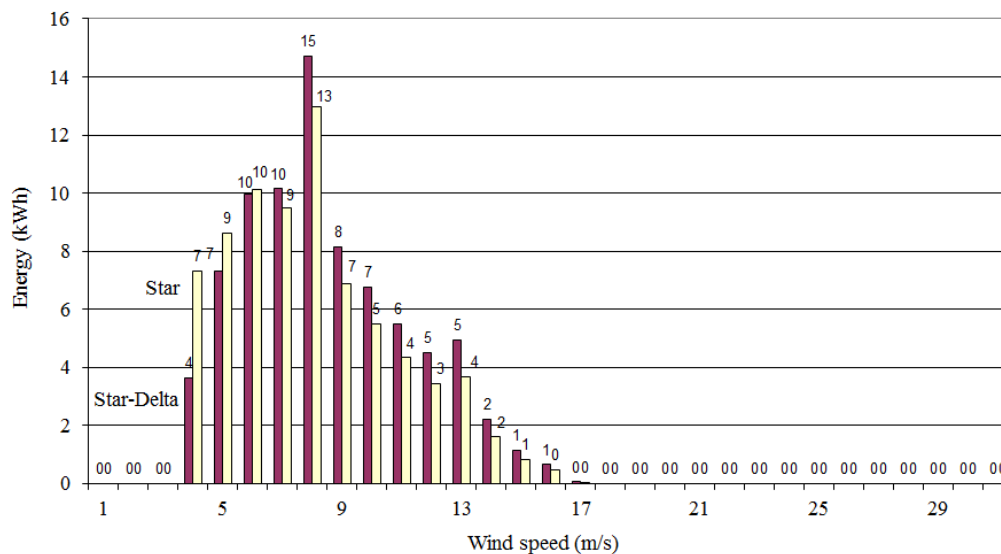
Figure 57. Comparison of energy production of WS-0.30B in wind speed inter-
vals using automatic reversible star-delta (column left) or star (col-
umn right) configuration and 24 V batteries.

4.2   Discussion of the results from study of WS-0.30B

If the studied wind turbine is installed on a windy site, or is exposed to high wind
speeds, the energy production will be considerably higher with an automatic re-
versible star-delta switch rather than without it. The developed boost converter
was tested on site. The measured results are logical with respect to the operation
of the boost converter in low wind speeds. However, the converter is bypassed in
higher wind speeds to avoid power loss. The use of a 24 V battery bank instead of
12 V produces more electrical energy especially at high wind speeds. This is due
to those short circuit currents with 12 V configurations by the different generator
connections limiting the actual output current to near the same value as by 24 V
configurations.

4.3   WS-4B

The larger wind turbine mounted on the roof of Fabriikki building is shown in
Figure 58. Development work of a hollow shaft for the WS-4 wind turbine was
started be-cause the use of a solid shaft with a diameter of 90 mm produced
strong vibrations at wind speeds above 12 m/s. The characteristics of the output
power and rotational speed for the wind turbine, with the two different ways of
connecting the generator were not known when development work began.

Figure 58. WS-4B wind turbine at field site at University of Vaasa, Finland.

A LabView®-based measuring system for measuring the vibrations was pur-chased and tested. As the energy could not be measured with a conventional kWh meter because of low frequency in generator voltage, an electronic power meter was used. The sig-nal from the anemometer was converted to a DC signal by means of an f/U con-verter, which solved the problem of synchronization. The initial measurements of the output power from the wind turbine showed cut-in wind speeds for charging batteries with star and delta connected generator to be 4 m/s and 7 m/s. Therefore, measurements were also done when pure resistors were used as electrical load.

A WS-4B turbine, with a developed hollow shaft, was mounted on the roof of a 23 meter high building called Fabriikki at the University of Vaasa situated near the shore of the Gulf of Bothnia in Vaasa. The turbine is connected as is shown in Figure 33. The generator can be manually connected either in star or delta. The AC output power was measured after the generator and before the six-pulse recti-fier bridge. The load consisted of a grid connected inverter or a pure resistor of either 2 Ω or 3.72 Ω. The anemometer was mounted at half height of the turbine blades and in relation to the current wind direction at approximately 1 m perpen-dicular to the turbine. Measurements were taken at wind speeds from zero to 17 m/s. The measurements were analyzed by XY charts and by trend graphs.

4.3.1   Measuring equipment and measurement circuit

The output power was measured by a Voltech PM6000 6 channel power analyzer and wind speed by a cup anemometer P2546A manufactured by WindSensor. A frequency to voltage (f/U) converter was used to convert the signal from the anemometer to a measurable voltage signal in the power analyzer. Despite the fact that the frequency at the output of the generator is low it was possible to measure the frequency, voltages, currents and output power using the power analyzer. The sampling frequency was 3 Hz.

The measuring equipment was placed in a cabinet in the field and the power analyzer was connected to intranet for downloading of measurement data. The rectified DC power was lead to a 48 V battery bank in the cabinet for the inverter. The battery bank consisted of four 12 V batteries connected in series. A boost converter stage steps up the DC voltage to the inverter. DC input voltage to the boost converter is set so that it can vary from 55.5 to 59.5 V. Necessary measurements were made with resistive loads instead of the inverter to ascertain whether this affects the properties of AC output power. The inverter was connected to the three-phase internal grid of 400 Volts.

4.3.2   Characteristic of the output power

The investigated WS-4B wind turbine starts to charge a 48 V battery bank at a wind speed of 4 m/s when the generator is star connected and at a wind speed of 7 m/s when the generator is delta connected. The output power from the wind turbine is greater at wind speeds above 9.3 m/s when the generator is delta connected instead of star connected, and the rated power is reached at wind speeds near 19 m/s. The output power of WS-4B wind turbine measured when the generator is star connected and a characteristic polynomial trend line with the equation $6.6592U^2 - 49.981U + 90.558$ is shown in Figure 59.
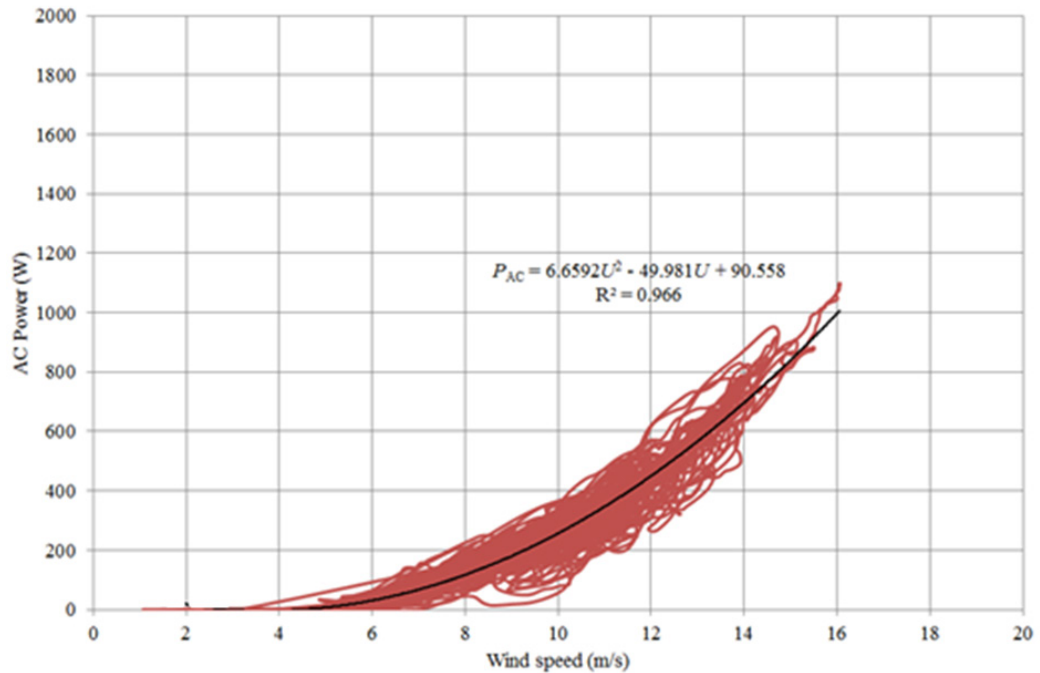
Figure 59. The output power, measured at the terminals of generator, as a func-
tion of wind speed with WS-4B wind turbine when the generator is
connected in star. Sampling frequency is 3 Hz and number of obser-
vations 12978.

The main findings of the regression analysis of the polynomial trend line of Fig-
ure 59 are shown in Table 8. The R-squared value of 0.966 means good fit of the
function to data distribution.

Table 8. Results of regression analysis of the trend line of Figure 59.

Regression statistics	
Multiple R	0.983
R-squared	0.966
Adjusted R-squared	0.966
Standard Error	35.740
Observations	12978

The measured output power of WS-4B wind turbine when the generator is delta
connected and a characteristic polynomial trend line with the equation
$9.4417U^2 - 65.017U - 10$ is shown in Figure 60. Cut-in wind speed with delta
connected generator was 7 m/s.

The equation shown on the figure:

$$P_{AC} = 9.4417U^2 - 65.017U - 10$$
$$R^2 = 0.934$$
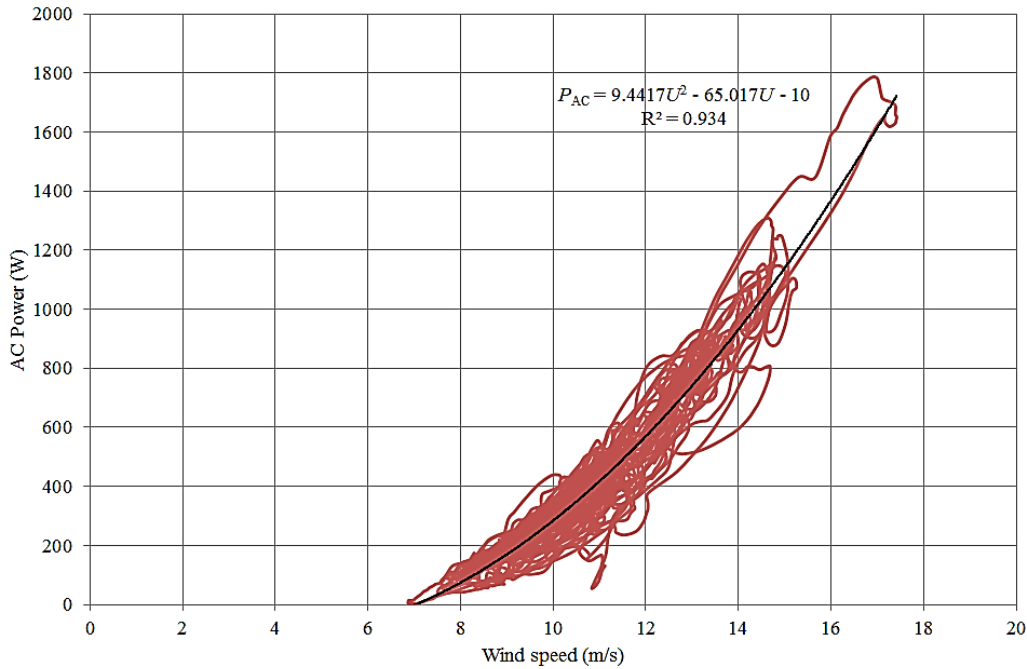
Figure 60.   The output power, measured at the terminals of generator, as a function of wind speed with WS-4B wind turbine when the generator is connected in delta. Sampling frequency is 3 Hz and number of observations 4106.

The main findings of regression analysis of the polynomial trend line of Figure 60 are shown in Table 9. The R-square value of 0.934 means good fit of the function to data distribution.

Table 9.   Results of regression analysis of the trend line of Figure 60.

Regression statistics	
Multiple R	0.967
R-squared	0.934
Adjusted R-squared	0.934
Standard Error	70.474
Observations	4105

The intersection of the trend lines of Figures 59 and 60 is calculated with a quadratic equation at an AC output power value of 202 W with a wind speed value of 9.3 m/s. Star connected generator provides higher output power than delta connected below this point, but delta connected generator above the point.

The first natural frequency of the rotor shaft as was used was calculated from Figure 45. The first natural frequency occurs when a rotational speed of 240 rpm

is reached. The Figure 61 shows that when the generator is delta connected, the first natural frequency occurs already at point D, when output power reaches 1300 W, which affected proposals for the control of the investigated turbine.

Let us next look more at Figure 61. It shows the construction of the initial method proposed to use in the investigated wind turbine with a developed hollow shaft having an outer diameter of 120 mm and an inner diameter of 90 mm. The shaft is a fixed-free design, and the rotational speed affects two limits which control the automatic reversible star-delta switch.

The rotational speed of this turbine is higher by delta connected generator than with star connected. The rotational speed of the turbine varies with the wind speed. At low rotational speed below value rpm_1, the generator is always star connected. The wind turbine starts charging batteries at point A.
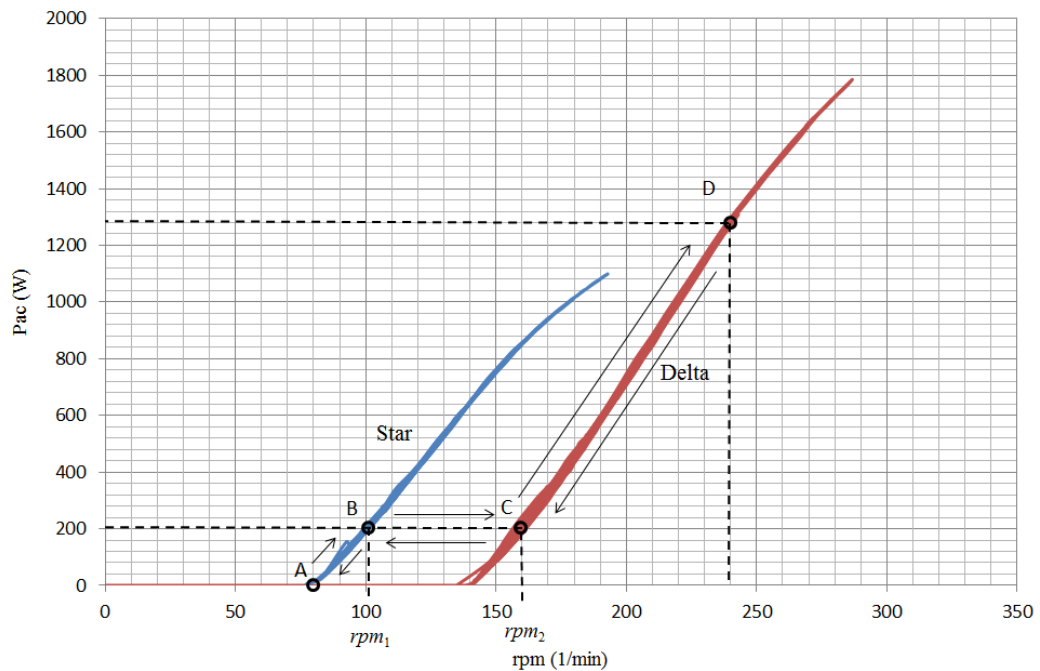
Figure 61. The measured output power of WS-4B turbine as function of rotational speed when the generator is connected in star or delta. Results from Figures 59 and 60 are used.

If the rotational speed increases to point B (wind speed of 9.3 m/s) and the rotational speed limit value rpm_1 is reached, then the generator switches to delta connection. Then, the generator is unloaded and if the wind speed increases, the rotational speed increases further between points B and C, and in point C when the rotational speed limit value rpm_2 is reached, the star-delta switch keeps the gener-

ator in delta connection. Rotational speed range from 100 rpm to 160 rpm is thus not used for energy production.

If the rotational speed increases beyond point C, and point D is reached, the automatic breaking system stops the turbine to avoid vibration of the turbine shaft due to the first natural frequency.

If the rotational speed decreases between points C and D, and at point C the rotational speed limit value rpm_2 is reached, the star-delta switch links the generator back to star connection. If the rotational speed decreases further between points C and B, and in point B the rotational speed limit value rpm_1 is reached, the star-delta switch keeps the generator in star connection.

If the change in rotational speed reverses between the limit positions rpm_1 and rpm_2 and reaches a previously passed limit position, the generator is switched back to previous connection. In other words, if the increasing rotational speed passes the limit position rpm_1; but then reaches the limit rpm_1 again with decreasing rotational speed, the generator is switched back to the star connection. If the rotational speed is decreasing and passes the limit position rpm_2; but then reaches the limit rpm_2 again with increasing rotational speed, the generator is switched back to the delta connection.

The reversible star-delta switch can be made with conventional contactors and the control by using a logic module. The disadvantage of the first control method proposed from Section 3.11 is that it is not able to use the wind speeds above 15 m/s; but the advantage is that it is a safe method, and when used, there are no vibrations from the natural frequencies of the turbine shaft.

Figure 62 shows, that with star-connected generator using the developed shaft with an outer diameter of 120 mm and an inner diameter of 90 mm, the first natural frequency occurs at a wind speed of about 19 m/s. With delta-connected generator the first natural frequency occurs at a wind speed of about 15 m/s.

The fourth proposed method prevents the occurrence of the first natural frequency by taking a step over it and the method can be discussed on the basis of Figure 62. The figure shows the rotational speeds as functions of wind speed with the generator star and delta connected.
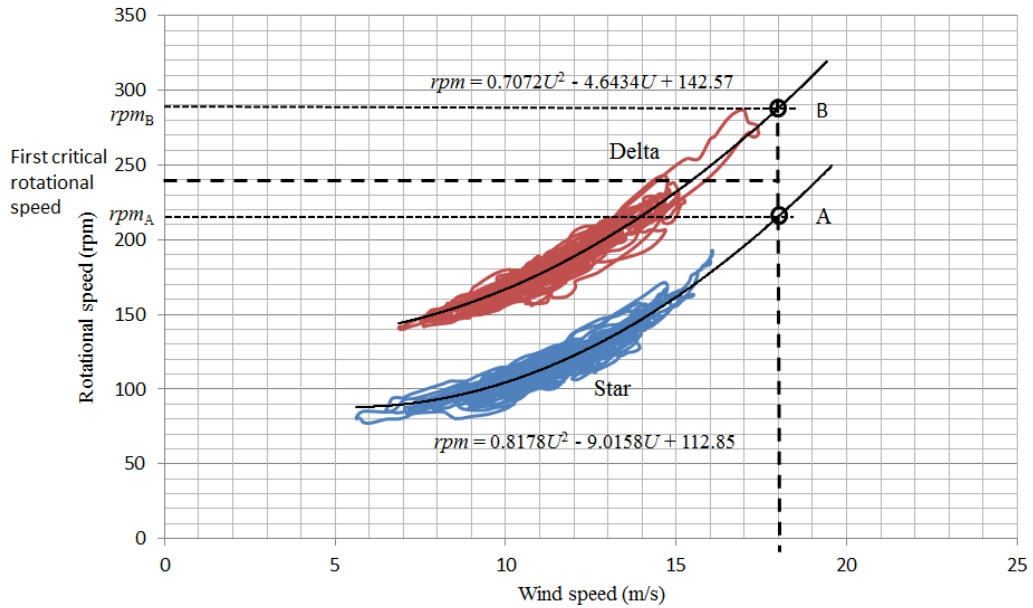
Figure 62. The measured rotational speed of WS-4B wind turbine as a function of wind speed when the generator is star or delta connected. Results from Figures 59 and 60 are used.

The rotational speed of the turbine increases with increasing wind speed. Two different cases are explained in the following paragraphs.

The first critical speed is skipped by changing the generator connection from star to delta with increasing wind speeds over 18 m/s at point A. Rotational speed at point A is 215 rpm. The rotational speed will increase with the time constant of the wind turbine to 288 rpm, which is the second rotational speed limit at point B. In further increasing wind speeds, delta connection could be used.

With decreasing rotational speed from high rotational speed above 288 rpm the connection of the generator is changed from delta to star at point B. The rotational speed is reduced to 215 rpm, and the first critical rotational speed is skipped again.

If the rotational speed reverses between the limit positions rpm_A and rpm_B and reaches a previously passed limit position, the generator is switched back to previous connection.

With the fourth method described in Section 3.11, the second natural frequency would be reached at a wind speed of 98 m/s. The wind turbine can nevertheless be stopped at wind speed of 30 m/s. The output power of the turbine must be limited to 2 kW so that the generator and rectifier bridge are not overloaded. Further-more, the generator should be equipped with an over-temperature protection. The

open voltage can rise to 473 V with Y-connector, which requires adequate isolation of the generator windings. The drawback with the fourth method proposed is that the higher output power of a delta-connected generator in wind speeds between 10 m/s and 18 m/s is not being used. The advantage is that the wind turbine can be used in wind speeds between 18 m/s and 30 m/s, and even at higher wind speeds if necessary. If the rotational speed of the turbine, switches quickly from the first limit value to the other and vice versa, there will be no significant problems due to the first natural frequency. However, this method has not been tested. Such a WS-4 wind turbine, which also has an upper bearing, should have no problems from the natural frequencies of the recorded wind speeds. In that case, the automation of the star-delta switch can be optimized to maximize the output power from the wind turbine.

Figure 63 is produced to show the values at low wind speeds as well. This is achieved by combining two separate measurements. Figure 63 gives results from measurements of both star and delta connection and shows in principle the output power with star-delta combination.
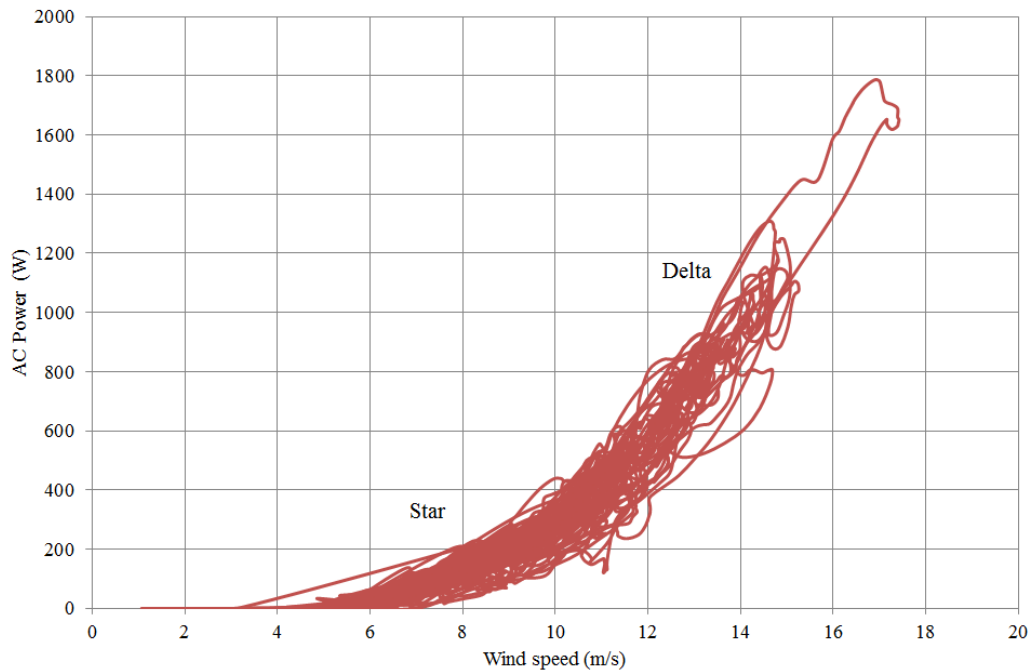
Figure 63.   The output power of WS-4B wind turbine, measured at the terminals of generator, as a function of wind speed with a star-delta combination. Results from Figure 59 and 60 are used.

Figure 64 shows measured coefficient of electric power C_{pg}, at the generator output terminals as a function of rotational speed by star and by delta connection.

The coefficient of electric power is obtained by dividing electric power output with calculated power in the wind according to Eq. 9. Drag coefficient C_d and lift coefficient C_l of Windside rotor were not measured because they were not targets for this work. The maximal C_{pg} in battery charging with star connection is concentrated around 0.15 and with delta 0.17.

The efficiency of generator η_g was not determined (Section 1.5), and therefore it is only to state that maximum values of power coefficients $C_{p, max}$ are at least 0.15 by star connected generator and 0.17 by delta connected because η_g is less than 1 and is in the denominator when $C_{p, max}$ is calculated by Eq. 58 on Page 54. The values 0.15 and 0.17 are near the same as other researchers have found from other similar wind turbines in Section 2.6.2.

The Windside rotor has at least double value for $C_{p, max}$ value than that of the drag machine described on pages 29 and 30. Half of the drag machine rotor is shielded from the wind. The Windside rotor has semicircular blades with overlap and moving air can blow through the gap into the back of the opposite blade.
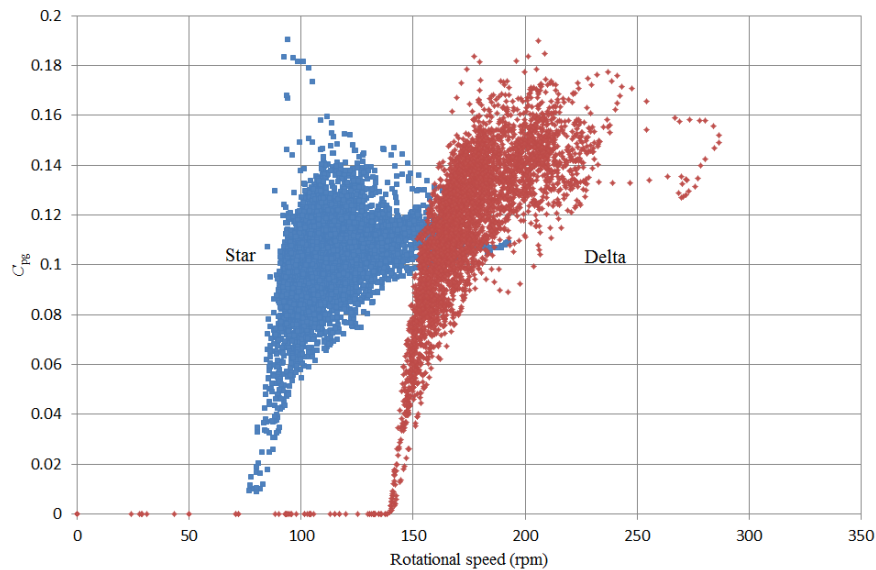
Figure 64.   The C_{pg} of WS-4B wind turbine as a function of rpm in star and delta connection. Results from Figures 59 and 60 are used.

Figure 65 shows C_{pg}, also measured at the output terminals of generator, as a function of wind speed in star and in delta connection.
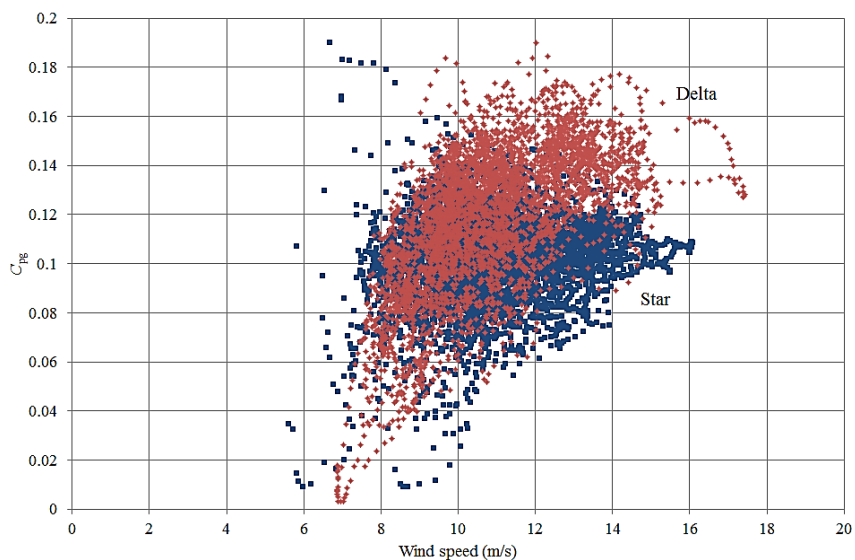
Figure 65. The C_{pg} of WS-4B wind turbine as a function of wind speed in star and delta connection. Results from Figures 59 and 60 are used.

Figure 66 shows the tip speed ratio λ in Eq. (46) as a function of wind speed in star and delta connection. Figure 66 shows that the turbine rotates faster when the generator is delta connected compared to star connected, which depends on the number of winding turns between phase terminals. The number of winding turns between phase terminals determines the open circuit voltage of the generator. The lambda is greater than 1 in the low loaded state due to low output voltage when the turbine is connected in delta. This indicates that the wind turbine really is aerodynamically a combined type.
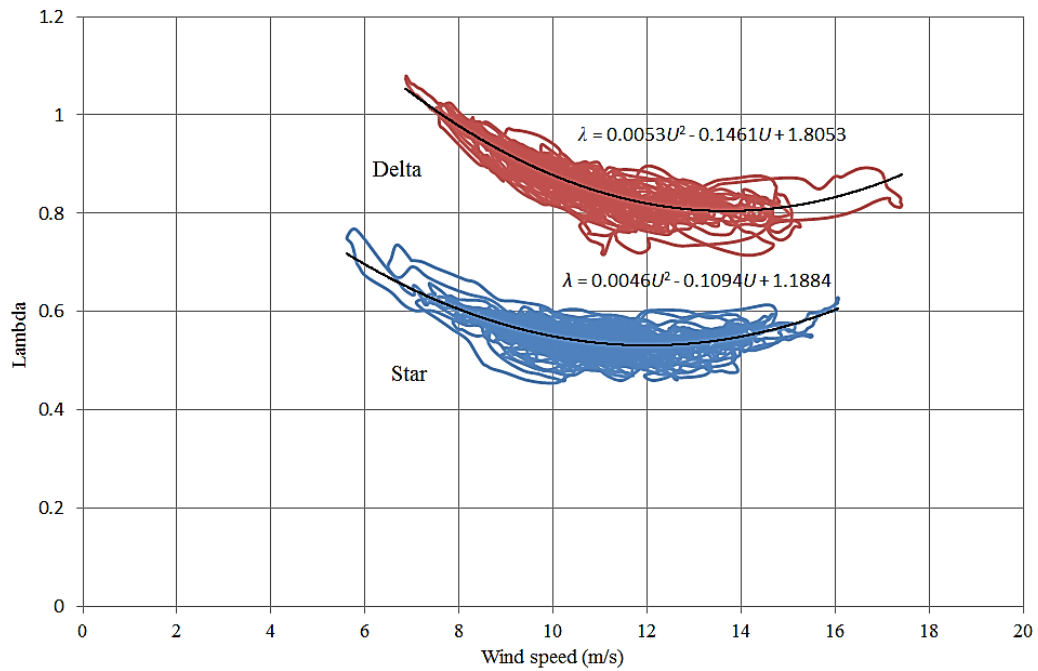
Figure 66. Lambda in star and delta connection as functions of wind speed. Star appears in lower curve and delta connection of the upper curve. Results from Figures 59 and 60 are used.

In order to verify the measurements of the output power to batteries, measurements were taken of the output power to pure resistors as shown in Figure 43. The inverter and battery bank are described in Section 3.9. Two resistors, 2.00 Ω and 3.75 Ω, were used separately as the load instead of the 48 V battery bank and the inverter. The generator was star connected. Figure 66 shows the AC power output as a function of wind speed of the WS-4B wind turbine when a resistor of 3.75 Ω was used as load.

It was visually observed that the rotational speed decreases when the load is a small pure resistor in comparison with the battery bank as load. When Figures 67 and 68 is compared some other differences can be seen. At very low and high wind speeds the wind turbine supplies more output power to the resistor than to the battery bank.
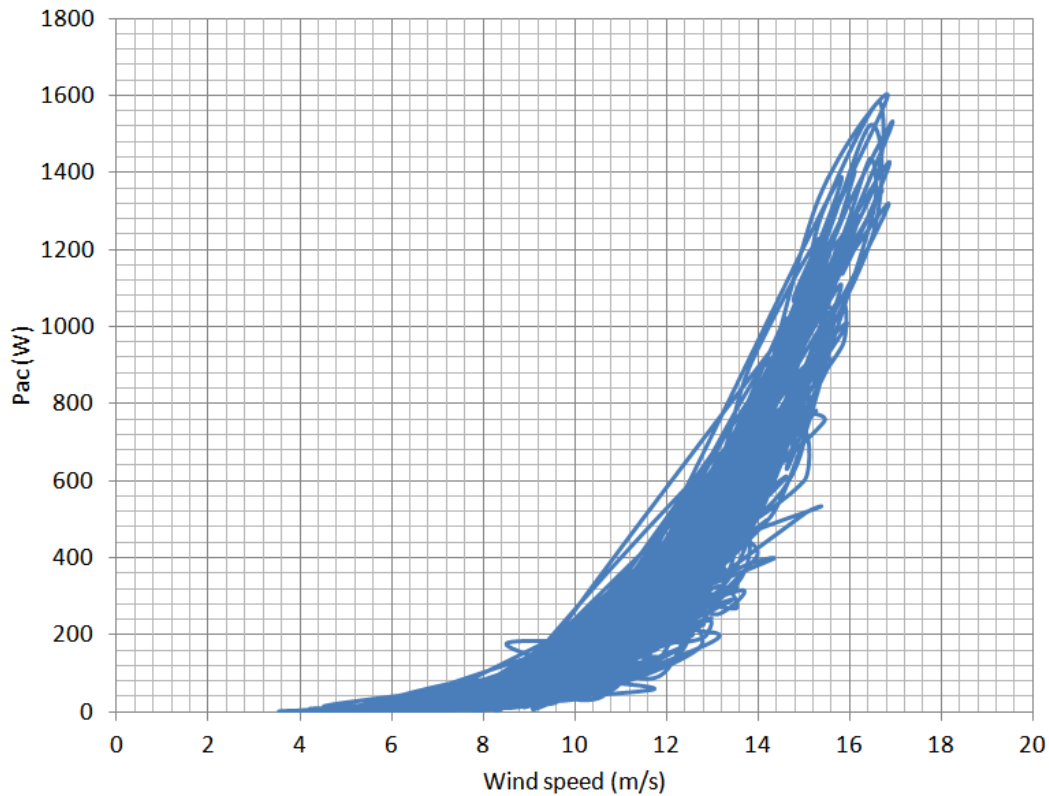
Figure 67. The output power of the WS-4B measured at the generator terminals as a function of wind speed when the generator is star connected. The load is a pure resistor of 3.75 Ω and it is connected after a bridge rectifier. Sampling frequency is 3 Hz.

The wind turbine supplied 200 W more output power to a 3.75 Ω resistance than to the 48 V battery bank with wind speed 16 m/s. The control of inverter held the battery voltage between 55.5 V and 59.5 V. At wind speeds from 8 m/s to 12 m/s, the wind turbine supplied more power to the battery bank than to the resistor.
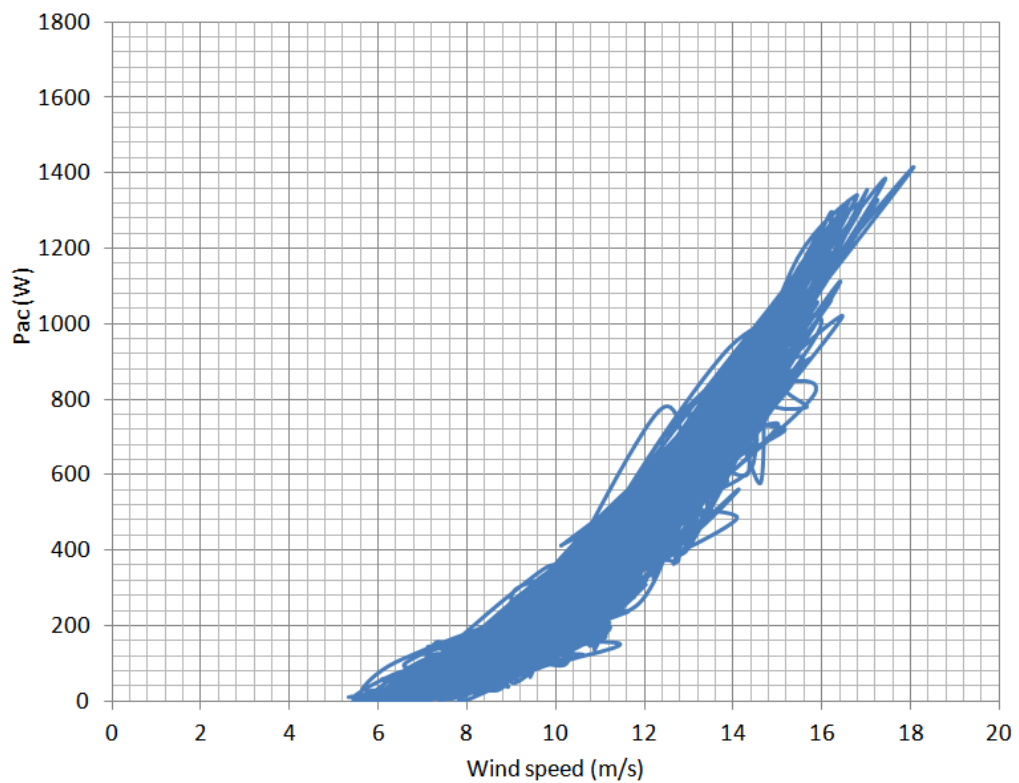
Figure 68. The output power of WS-4B, measured at the generator terminals, as a function of wind speed when the generator is star connected. The load is a battery bank of 48 V and the inverter. Also here is a bridge rectifier connected between the generator and the load. The inverter supplies power to low voltage AC grid. Sampling frequency is 3 Hz.

4.3.3   Energy production

The energy production was measured at terminals of the generator, which was connected in star. The alternating current is rectified and fed to the battery bank provided in the cabinet for the inverter. The electrical energy flows through the boost device further to the inverter and then to low voltage grid. Energy measurement is done with a Voltech PM6000 power analyzer. The energy was measured for almost two and a half months. Wind data is taken from the stationary Davis weather station at the mounting site of the WS-4B wind turbine. Figure 69 shows the wind speeds recorded during the measurement period. The average wind speed of 10 min intervals during the measurement period was 3.25 m/s.
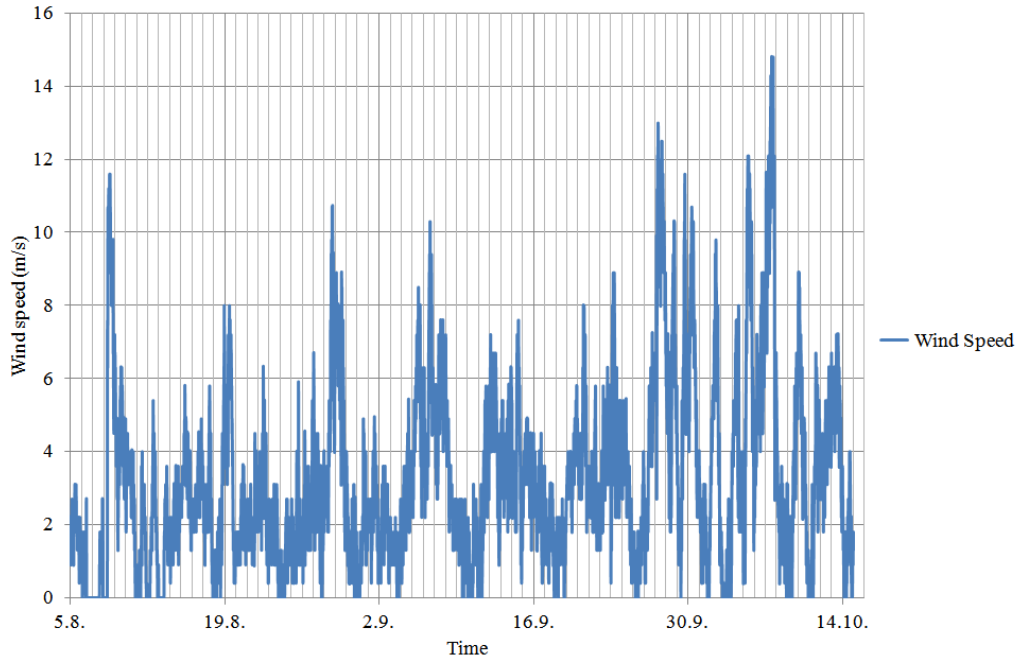
Figure 69.   The wind speed of 10 min intervals at installation site of WS-4B including the period in which energy is measured in year 2011.

Figure 70 shows the energy production of the WS-4B wind turbine during the same period of two months and ten days. The best energy production of 5 kWh was measured during days 27th to 28th September 2011. It can be seen from Fig. 69 that the wind speeds then were much higher than the average value during the measurement period.
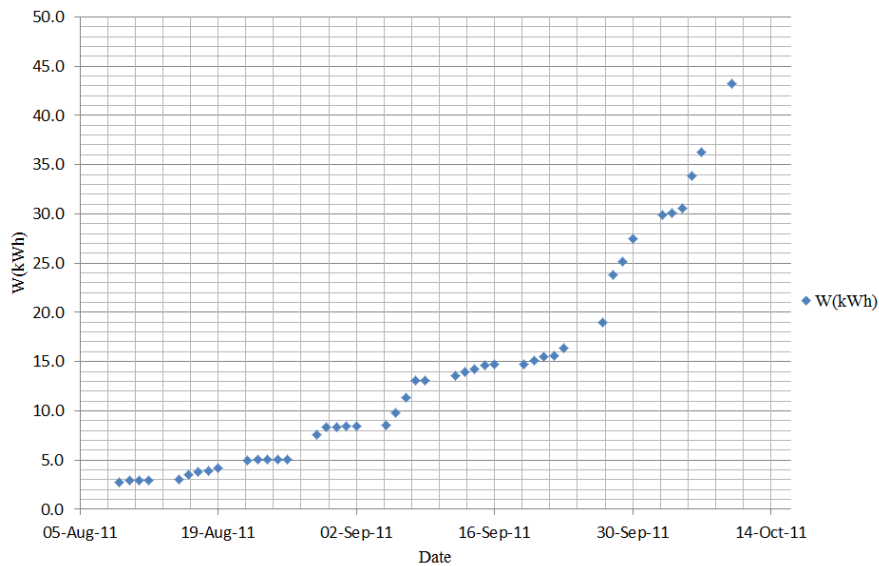
Figure 70.   Cumulative energy production of WS-4B during the measured period.

5 CONLUSIONS

This chapter gives conclusions and answers to the research questions. The aim of this thesis was to increase the energy production of the investigated vertical-axis wind turbine for battery charging by peripheral equipment and control. The intention at the beginning was to use only the basic components, such as the generator and turbine without planning and building new ones. The development work of a new shaft for the larger wind turbine was necessary as there was too much vibration in the shaft with a diameter of 90 mm. Early experiments were conducted to increase the output power in low and high wind speeds. During initial tests in low wind speeds it was observed that the charging voltage is too low compared to the battery voltage. If star connection is used in high wind speeds, the charging current is limited due to the higher impedances of the generator.

The small wind turbines and the Tritonia weather station were installed first. The small wind turbines are on the roof of Tritonia library building located at the university campus. A temporary control room is on the sixth floor in a room planned to be used for the ventilation plant for the building. A measurement system for measuring the electrical magnitudes of the wind turbines of the smaller wind turbine was built. Five personal computers were utilized in the study of the wind turbine with a vertical-axis.

At the beginning of this work, it was decided to have a centralized optimized control system for the study of the smaller turbine. Later, when the autonomous automatic reversible star-delta switch started working, the need for a centralized control system was reduced.

The measurements on the larger wind turbine started after appropriate measuring instruments were acquired. These measurement results support well the measurement results of the smaller wind turbine.

5.1 Main findings from this study

The results of this thesis show that small vertical-axis wind turbines can achieve higher overall efficiency by using well-tried electronic and electrical components in new ways. However, every component increases the total losses and consideration must be taken in each case.

All energy measurements in this research have been done in natural conditions, as the intention is, to find out how well the turbine works in a variety of natural wind

conditions. The wind conditions at the installation sites of the wind turbines were measured.

The extent to which the results of this research provide answers to the questions posed at the beginning of the thesis is discussed below. The research questions RQ 1 and RQ 2 are considered in the research of a small wind turbine, a Windside WS-030B, while the *RQ 3* and *RQ 4* issues are based on research of the small and the large wind turbine, Windside WS-4B. The research question *RQ 5* is a recurring theme throughout the research.

> *RQ 1:   What is the effect of the voltage level used on the production of electricity?*

The result of measurements shows that it is advantageous to use 24 V battery configurations instead of 12 V. In a 12 V battery configuration compared with a 24 V configuration, the battery voltage is only half, while with different generator connections the short circuit currents and the highest charging current are same, so the output power becomes only half. It was found that cut-in speed is lower with 12 V battery configurations than with 24 V battery configurations due to the lower voltage on the battery bank. The cut-in speed is the wind speed where the wind turbine begins producing electricity. However, it was found that the annual energy yield to be near 7 % higher with 24 V battery configuration than with 12 V battery configuration (Section 4.1.4).The result is dependent on the open voltage of the generator and wind conditions observed during the year.

> *RQ 2:   How to increase the produced electric energy in low wind speeds?*

The method chosen was to charge batteries even in very weak wind gusts by raising the rectified DC voltage across the battery terminals. A direct current (DC-DC) step up converter with MPPT logic was developed and tested. Tests performed in low wind speeds show that the output power is one or two watts, with the developed device. However, it was also observed that the advantage with this developed device was quite modest due to its low efficiency and a low output power of the turbine at low wind speeds. It is still possible to improve the converter efficiency, but a low output power of the turbine in low wind speeds cannot be improved with peripherals. In order to have good efficiency with increasing wind speeds, the converter is supplemented with an automatic bypass.

RQ 3:   *How the studied wind turbines would give excellent charge characteristics in the entire operating range, especially at high wind speeds?*

The selected solution method was to construct a separate automatic reversible star-delta switch as an added feature to the wind generator. This was successful and the results are the most important part of this research. The annual energy production is increased by more than 9 % when an automatic reversible star-delta switch is used instead of using only star connection (Section 4.1.4). The output power was significantly increased in high wind speeds by the aid of an automatic reversible star-delta switch.

Test results show that the developed automatic reversible star-delta switch worked properly and reliably. It is possible to change the set point for the wind speed in order to change the generator coupling. The star-delta switch for the larger wind turbine can have two set points. The measured output power characteristics of the Windside turbine shows that it works well in high wind speeds. However, during the study natural frequencies were observed in turbine shafts, which limited the use in genuine high wind speeds.

RQ 4:   *How to overcome the problems of natural frequencies?*

The answer to RQ 4 is to avoid the natural frequencies by limiting the rotational speed or by skipping the first natural frequency by switching connection of the generator. Investigated turbines were of the types that have no upper bearing point. Through hammer shock testing and modal analysis it was found that the wind turbines under study have the same natural frequency as a boom which is attached only at one end. Such a construction is called fixed-free construction. Using a fixed-fixed configuration produces a design with less vibration problems. The choice of a coarser shaft to the smaller turbine, and the development of a coarser hollow shaft for the larger wind turbine meant that the turbines could be used in higher winds without impeding vibrations. It is preferable to avoid natural frequencies in the design of a wind turbine; otherwise it will be damaged sooner or later. The hollow shaft of the larger wind turbine provides lower mass moment of inertia and therefore it will be better able to take energy from wind gusts.

RQ 5:   *How to implement the developed devices so that their function is automatic and can be applicable to real wind power system?*

The small wind turbine was supplemented with automatic light and strong wind systems. Light wind system consisted of a step up converter that had bypass and

MPPT logic. It is possible to automate a step up converter in low wind speeds without impairing the overall efficiency. The strong wind system consisted of a separate automatic reversible star-delta switch. Also, the developed reversible star-delta switch for the smaller wind turbine is fully automatic and works well.

The investigation also provides answers on C_{pg} value, output power as a function of the wind speed, for the larger wind turbine. The energy production of the turbines was measured and presented. The energy production is closely related to swept area of the turbine. One difference is that with the larger wind turbine, electricity production begins at slightly higher wind speed.

The larger wind turbine produced enhanced performance in high wind speeds. The wind turbine was supplemented with an automatic braking system for operation in hazardous winds, a hollow shaft was developed and proposals for control of a reversible star-delta switch given. A vibration measurement system was procured, which could have been used for controlling the braking system; but this was not realized.

The investigated wind turbine systems were already equipped with automatic lubrication systems by the manufacturer. They were also equipped with automatic charging regulation systems, which protected the batteries against overcharging.

In this work, several measurement instruments and multiple data-logging systems were used. All the measurements of this thesis were done by the author.

Presented solutions to the research questions provide answers to characteristics of Windside vertical-axis wind turbine, and the opportunities to improve them so that the turbine can produce more electricity. Wind energy of gusts is taken into account by using 1 Hz sampling frequency in power measurements. Very central are solutions to mechanical issues, the difference between energy supply for charging either batteries or only resistors and good performance in strong winds. Presented solution is not ideal or optimal, but clear and effective solution context of limitations as seen in Section 1.5. Investigations of other vertical-axis wind turbines can be made in a similar way and then the results can be compared easily.

5.2   Contributions from this thesis

The most outstanding contribution of this study is the new simple and automatically reversible star-delta switch that was developed for small vertical-axis wind turbines. The power supply to the switch can be from the battery bank of the con-

trolled wind turbine. Therefore, it is possible to use the switch in wind turbines installed standalone from the grid. If it fails, it stays in the star mode. The developed switch showed no disadvantages. The output energy of the investigated wind turbines showed a substantial increase. The lifetime of the investigated wind turbines appear to be over 10 years which means that there will be many storms with increased energy production.

Another useful contribution is the outcome of the investigations on the natural frequencies of the small vertical-axis wind turbines. Although the mechanical design of the wind turbines differs slightly from a straight beam type, it was found that the equations used for determining the natural frequency of the wind turbines under study were appropriate. In this context, it was found that a hollow shaft has the best optimum value of the inner diameter. It was also found that the energy production of the wind turbine can be greatly improved with stiffer turbine shaft. The moment of inertia decreases by hollow shaft and this improves the function of the turbine in gusty winds. About 200 kg raw material per large wind turbine is saved.

The final contribution is the knowledge of output power characteristics with different generator connections in various real wind conditions of the investigated wind turbines. Similar measuring instruments, measuring principles and results of treatments may be used in any other equivalent examination. Any of the measurements taken may also be repeated.

5.3   Further studies

The output mechanical torque from the wind turbines studied in real wind conditions could be measured. To measure the torque, it is necessary to do mechanical work on the wind turbine for applying torque measuring equipment, as the current design does not have a suitable connection point for such equipment. A study of small wind turbines in tough real wind conditions of more than 30 m/s in hurricanes is also possible. The rotor and shaft of the wind turbine could wholly or partly be made of other materials such as carbon fiber, aramid fiber or other similar new material. Furthermore, the electrical systems can now definitely be supplemented with developed and proposed components. The systems can then be further studied. Also, evaluation of the efficiency for large generator, power electronics and turbine under partial loads can be done. Gust measurements at university can also be done. Also, C_p of the rotors as a function of wind speed could be studied. Testing of the proposed methods with star-delta logic for the large wind turbine can be performed.

References

Akwa, J. V., Vielmo, H. A. & Petry, A. P. (2012). A review on the performance of Savonius wind turbines. *Renewable and Sustainable Energy Reviews Volume 16, Issue 5*. 3054–3064.

Alam, J. & Iqbal, M.T. (2009). Design and development of hybrid vertical-axis turbine. *Electrical and Computer Engineering, 2009. CCECE '09. Canadian Conference on Digital.* 10.1109/CCECE.2009.5090311. 1178–1183.

American Wind Energy Association (AWEA). (2012). [Cited 16.04.2012]. Available at: http://archive.awea.org/faq/basicwr.html

Ani, S.O., Polinder, H. & Ferreira, J.A. (2011). Energy Yield of Small Wind Turbines In Low Wind Speed Areas. *Adaptive Science and Technology (ICAST), 2011 3rd IEEE International Conference.* 10.1109/ICASTech.2011.6145160. 93–98.

Ansys Simplorer. (2014). An intuitive, multi-domain, multi-technology simulation program. Homepage available at: http://www.ansys.com/Products/Simulation+Technology/Electronics/Electromechanical/ANSYS+Simplorer

Aura, L. & Tonteri, A. (1996). *Sähkökoneet ja tehoelektroniikan perusteet.* A book of electrical machines and principles of power electronics (in Finnish). WSOY 1996, 544 p.

Beardmore, R. (2012) Natural Freq's beams/shafts. [Cited 18.07.2012]. Available at: http://www.roymech.co.uk/Useful_Tables/Vibrations/Natural_Vibrations.html

Ceyhan, Ö. (2012). Towards 20MW Wind Turbine: High Reynolds Number Effects on Rotor Design. *50th AIAA Aerospace Sciences Meeting including the New Horizons Forum and Aerospace Exposition* 09–12, 2012, 1–14.

Chow, F. K., De Wekker, S. F.J. & Snyder, B. J. (2012). *Mountain Weather Research and Forecasting Recent Progress and Current Challenges.*Series: Springer Atmospheric Sciences 2012, XIII, 750 p.

Clague, P. & Qi, T. Z. (2008). A novel design of Savonius wind turbine water heating in residential settings. *15th International conference on Mechatronics and Machine Vision in Practice (M2VIP08), 2–4 Dec 2008, Auckland, New-Zealand.* 2008 ISBN: 978-0-473-13532-4. Digital Object Identifier: 10.1109/MMVIP.2008.4749543. 259–262.

Climate Prediction.net. (2007). [13.04.2012]. Available at: http://www.climate prediction.net/taxonomy/term/4?page=1

Corbus, D., Baring-Gould, I., Drouilhet, S., Gervorgian, V., Jimenez, T., New-comb, C. & Flowers, L. (1999). Small Wind Turbine Testing and Applications Development, *Windpower '99 Burlington, Vermont* June 20–23, 1999, p.6. Available: National Technical Information Service (NTIS), U.S. Department of Commerce, 5285 Port Royal Road, Springfield, VA 22161, 703-605-6000 or 800-553-6847.

Danish Wind Industry Association. (2001). [Cited 24.09.2010]. Available at: http://www.windpower.org/en/tour/wtrb/drag.htm

Darden Bill. (2001). Deep cycle battery frequently asked questions. [Cited 24.05.2012]. Available at: https://www.pacificpowerbatteries.com/aboutbatts/ Deep%20Cycle%20Battery%20FAQ/dcfaq6.html.

Davis Weather Instruments. (2008). [Cited 20.08.2008]. Available at: http://www.davisweathergadgets.com/

De Almeida, B. R. & Oliveira Jr., D. S. (2011). Control system for vertical-axis wind energy conversion system. *Power Electronics Conference (COBEP), 2011 Brazilian*. 10.1109/COBEP.2011.6085273, 825–830.

De Broe, A. M., Drouilhet, S. & Gevorgian, V. (1999). A peak power tracker for small wind turbines in battery charging. *IEEE Transactions on Energy Conversion*, Vol. 14, No. 4, December 1999, 1630–1635.

Deb, B., Gupta, R. & Misra, R. D. (2013). Performance analysis of a helical Savonius rotor without shaft at 45° twist angle using CFD. *Journal of Urban and Environmental Engineering (JUEE)* 2013 v.7, n.1, [Cited 20.08.2013], 126–133.

Dobrev, I & Massouh, F. (2012). Exploring the Flow around a Savonius Wind Turbine. *16th Int Symp on Applications of Laser Techniques to Fluid Mechanics. Lisbon, Portugal*, 09–12 July, 2012.

Drouilhet, S., Muljadi, E. & Holz, R. (1995). Optimizing Small Wind Turbine Performance in Battery Charging Applications. *NRELRP-441-7808 UC Category 12 13 DE950092 1 1.* Available: National Technical Information Service (NTIS), U.S. Department of Commerce, 5285 Port Royal Road Springfield, VA 22161 (703) 487–4650, 1995, 1–13.

Eggleston, E. and AWEA Staff. (1998). *What Are Vertical-Axis Wind Turbines (VAWTs*)? [Cited 30.08.2012].   Available at: http://www.soetownsville.org/ external_atmosphere/verticle_wind_axis.html

Eichhorn, T. (2008). Boost Converter Efficiency through Accurate Calculations. [Cited 12.4.2015]. Available at: http://powerelectronics.com/power-management/boost-converter-efficiency-through-accurate-calculations.

Eid, A, M., Abdel-Salam, M. & Abdel-Rahman, M. T. (2006). Vertical-axis wind turbine modeling and performance with axial-flux permanent manget synchronous magnet generator for battery charging applications. *Power Systems Conference, MEPCON, Eleventh International Middle East v 1, 2006*, 162–166.

Eldridge, F. R. (1980). *Wind Machines*, 2nd ed., Van Nostrand Reinhold, New York, 1980. Energy research Center of the Netherlands (ECN), 1755LE, Petten, the Netherlands.

Enercon. (2014). Enercon wind energy converters. [Cited 11.6.2014]. Available at: http://www.enercon.de/p/downloads/EN_Eng_TandS_0710.pdf

ExRo Looks to Wind to Generate Profit. (2008). [Cited 12.10.2010]. Available at: http://www.greentechmedia.com/articles/read/exro-looks-to-wind-to-generate-profit-5087/

Finnish wind atlas. (2012). [Citeted 20.04.2012]. Available at: http://www.tuuliatlas.fi/en/index.html.

Gipe, P. (2004). Wind Power: Renewable Energy for Home, Farm, and Business, 2nd Edition. Chelsea Green Publishing Company. 498 p.

Global wind systems. (2007). [Cited 12.10.2009]. Available at: http://earthguide.ucsd.edu/virtualmuseum/climatechange1/08_2.shtml.

Hauke, B. (2014). Basic Calculation of a Boost Converter's Power Stage. [Cited 12.4.2015]. Available at: http://www.ti.com/lit/an/slva372c/slva372c.pdf

IEC 61400-1. (2013). [Cited 15.09.2013]. Available at: http://webstore.iec.ch/preview/info_iec61400-1%7Bed3.0%7Den.pdf

IEC 61400-2. (2013). [Cited 16.09.2013]. Available at http://webstore.iec.ch/preview/info_iec61400-2%7Bed2.0%7Den_d.pdf.

IEC 61400-12. (2014). [Cited 19.06.2014]. Available at: http://www.eeechina.cn/upload/fck/2011-08-19/634493393600341043.pdf

International Starch Institute in Denmark. (2012). [Cited 20.09.2012]. Available at: http://www.starch.dk/isi/energy/wind.htm.

Johnson, G. L. (2001). *Wind Energy Systems*. Kansas State University, Englewood Cliffs, NJ: Prentice Hall. 419 p.

Joutsiniemi, R. (1985). Tuuliroottorirakenteen roottorirakenne. Available at: http://worldwide.espacenet.com/publicationDetails/originalDocument?FT=D&date=19850228&DB=EPODOC&locale=fi_FI&CC=FI&NR=67919B&KC=B&ND=4

Kamoji, M.A., Kedare, S.B. & Prabhu, S.V. (2009*). Performance tests on helical Savonius rotors.* Renewable Energy [Web document] 2009: 34, [Cited 19.08.2013], 521–529. Available at: http://www.sciencedirect.com/science/article/pii/S0960148108002486.

Kling, A. (2014). Regression in Microsoft Excel. [Cited 10.07.2014]. Available at: http://arnoldkling.com/apstats/regression2.html

Knight, A. M. & Peters, G. E. (2005). Simple Wind Energy Controller for an Expanded Operating Range. *IEEE Transaction on Energy Conversion*, Vpl. 20, No. 2, JUNE 2005.

Koutroulis, E. & Kalaitzakis, K. (2006). Design of a Maximum Power TrackingSystem for Wind-Energy-Conversion Applications. *IEEE Transactions on Industrial Electronics*, Vol. 53, No. 2. APRIL 2006, 486–494.

Kragten, A. (2009). *Windmills using aerodynamic drag as propelling force; a hopeless concept*. KD 416. [Cited 22.08.2013], 2009, 1–8. Available at: http://www.bidnetwork.org/en/member/adriaankragten

Laitone, E. V. (1997). *Wind tunnel tests of wings at Reynolds numbers below 70 000. Experiments in Fluids* 23. 405–409. (Springer-Verlag 1997).

LEM. (2012). [Cited 20.052012]. Available at: http://www.lem.com

Lifeline Batteries. (2015). [Cited 18.04.2012]. Available at: http://www.lifelinebatteries.com/manual.php

Library on Human Powered Flight. (2012). [Cited 18.04.2012]. Available from World Wide Web: http://library.propdesigner.co.uk/index.html

Lindemann, P. A. (2012). [Cited 02.05.2012]. Available at: http://www.basaap.com/peter/H%20Diving/pr/converter.shtm.htm

Linear Technology. (2014). [Cited 23.06.2014]. Available at: http://www.linear.com/product/LTC3862

Manwell, J. F., McGowan J. G. & Rogers A. L. (2009). *Wind Energy Explained: Theory, Design and Application*. 2nd ed. United Kingdom: John Wiley & Sons Ltd. 689 p.

Miley, S. J. (1982). A catalog of low Reynolds number airfoil data for wind turbine applications. Springfield, *VA: National Technical Information Service, U.S. Dept. of Commerce*, 1982.

Mirecki, A, Roboam, X. & Richardeau, F. (2004). Comparative Study of Maximum Power Strategy in Wind Turbines. Industrial Electronics, *2004 IEEE International Symposium on Volume*: 2. 10.1109/ISIE.2004.1571949, 2004, 993–998.

Mirecki, A. & Roboam, X. (2007). Architecture Complexity and Energy Efficiency of Small Wind Turbines. *IEEE Transaction on Industrial Electronics*, vol. 54, No. 1., [Cited 27.08.2013], February 2007, 660–670.

Mohan, N., Underland, T. M. & Robbins, W. P. (2003). *Power Electronics*. JohnWiley & Sons, Inc. 802 p.

National Instruments. (2012). [Cited 01.05.2012]. Available at: http://finland.ni.com/

Neammanee, B. & Chatratana, S. (2006). Maximum Peak Power Tracking Control for the new Small Twisted H-Rotor Wind Turbine. *Energy for Sustainable Development*, March 2006, p. 6. [Cited 24.06.2008]. Available at: http://www.aseanenergy.info/view.asp?ResID=8152

Nipp, E. (1999). *Permanent Magnet Motor Drives with Switched Stator Windings*, KTH, ISSN-1102-0172, 1999, p. 315.

Optima batteries. (2012). [Cited 15.05.2012]. Available at: http://www.optimabatteries.com/optima_products/yellowtop/index.php

Oy Windside Production Ltd, home page. (2012). [Cited 24.05.2012]. Available at: http://www2.windside.com/accessories.html

Patsios, Ch., Chaniotis, A. & Kladas, A. (2008). A hybrid maximum power pointtracking system for grid-connected variable speed wind-generators. *IEEE Power Electronics Specialists Conference* (2008), 1749–1754.

Percival, M. C., Leung, P. S. & Datta, P. K. (2004). The development of a vertical turbine for domestic electricity generation, *European Wind Energy Conference*, published on CD Rom only, UK (2004).

Pure Energy Systems Wiki. (2012). [Cited 13.04.2012]. Available from World Wide Web: http://peswiki.com/index.php/Directory:Vertical_Axis_Wind_Turbines#Companies.

Ren, N. & Ou, J. (2009). Numerical Simulation of Surface Roughness Effects on Wind Turbine Thick Airfoils. *Asia Pacific Power and Energy Engineering Conference* (2009). p. 4. Available: 978-1-4244-2487-0/09/ ©2009 IEEE.

Saha, U.K. & Rajkumar, M. J. (2005). On the performance analysis of Savonius rotor with twisted blades. *Renewable Energy* [Web document] 2006: 31, [Cited 20.08.2013], 1776–1788. Available at: http://www.victordanilochkin. org/research/turbine/papers/On%20the%20performance%20analysis%20of%20Savonius%20rotor%20with%20twisted%20blades.pdf.

Saha, U.K., Thotla, S. & Maity, D. Optimum design configuration of Savonius rotor through wind tunnel experiment. J. Wind. Eng. Ind. Aerod. 96, 1359–1375, (2008)

Sargolzaei, J. (2007). Prediction of the power ratio in wind turbine Savonius rotors using artificial neural networks. *International Journal of Energy and Environment*, Issue 2, Volume 1, 2007.

Savonius, S. J. (1925). *The wing rotor in theory and practice.* Available at: http://www.prh.fi/stc/attachments/innogalleria/savonius_kirja.pdf

Schmidt-Walter, H., Wenzel, H, Zänker, T., Morgan, R & Kegan, J. (2006). *Design of Switch Mode Power Supplies.* [Cited 02.09.2007]. Available at: http://schmidt-walter.eit.h-da.de/smps_e/smps_e.html

Swamy, M. M. (2002). 4.2 Uncontrolled and Controlled Rectifiers in The Power Electronics Handbook / edited by Skvarenina, T. L. ISBN 0.8493-7336-0. 664 p.

Tammelin, B. 1991. *Meteorologista taustatietoa tuulienergiakartoitukselle* (in Finnish). Finnish Meteorological Institute, Helsinki. 332 p.

Tang, C., Pathmanathan, M., Soong, W. L., & Ertugrul, N. (2008). Effects of Inertia on Dynamic Performance of Wind Turbines. *Australasian Universities Power Engineering Conference,* 2008, p. 6.

Tavner, P. J. (2012). *Offshore Wind Turbines- Reliability, Availability & Maintenance*. Institution of Engineering and Technology. ISSN/ISBN: 978-1-84919-229–3, 269 p. 245–246.

Taylor, S. (2014). [Cited 16.07.2014]. Available from Word Wide Web: https://www.wou.edu/las/physci/taylor/g302/graphing_techniques.pdf

Tempel, J. van der & Molenaar, D.-P. (2002). Wind Turbine Structural Dynamics −A Review of the Principles for Modern Power Generation, Onshore and Offshore. *Wind engineering volume* 26, No. 4, 2002, pp 2011–220. [Cited 2.10.2013]. Available at: http://www.lr.tudelft.nl/fileadmin/Faculteit/LR/Organisatie/Afdelingen_en_Leerstolen/Afdeling_AEWE/Wind_Energy/Research/Publications/Publications_2002/doc/Tempel_Windturbine_structural_WT_structural_dynamics.pdf

Texas Instruments. (2014). [Cited 23.06.2014]. Available at: http://www.ti.com/lit/ds/symlink/tps61220.pdf

Vestas. (2014). [Cited 09.06.2014]. Available at: http://control-design.de/home_eng/Applications/Windenergy/body_windenergy.html

Voltech. (2012). [Cited 02.05.2012]. Available at: http://www.voltech.com/products/poweranalyzers/PM6000.aspx

Walker, J. F. and Jenkins, N. (1997). Wind Energy Technology. John Wiley & Sons Canada, Limited, 161 p.

Weather stations at University of Vaasa. (2010). Home page of two weather stations at University of Vaasa. Available at: http://lipas.uwasa.fi/~tuulisaa/

Wilson, D. (2014). [Cited 10.06.2014]. Understanding Hybrid Energy Solutions in the OSP. Available at: http://www.ospmag.com/issue/article/Understanding-Hybrid-Energy-Solutions-in-the-OSP

Wind Power: An interactive presentation. (2010). [Cited 12.04.2010]. Available at: http://pclab.et.teiath.gr/hermes/Aerodynamics2_en.php

Windsensor. (2012). [Cited 20.05.2012]. Available at: http://www.windsensor. com/technical/P2546A%20Data%20Sheet.pdf

Zhao, Z., Zheng, Y., Xu, X., Liu, W. & Hu., G. (2009). Research on the Improvement of the Performance of Savonius Rotor Based on Numerical Study. *Sustainable Power Generation and Supply, 2009 SUPERGEN '09 International Conference on*. Available : 10.1109/SUPERGEN.2009.5348197 IEEE.

APPENDICES

Appendix 1. Technical data of investigated wind turbines

Fig. A1.1. Technical Data of Windside wind turbine WS-0.30B. The dimensions are in mm.

WS4B—dte08

WINDSIDE   WS-4B dimensions and technical info

Windside WS-4B technical info:
- Weight: 800 kg
- Swept area: 4 m²
- Generator: 36A in delta, 21A in star connection
- Voltage: 12V battery charging mode 15V
          24V battery charging mode 30V
          48V battery charging mode 60V
          - For direct resistance load, voltage
            depends on use
- Fastening of the turbine with 8 pc of M30 bolts
- Wind load, side force to the middle point of the vane,
  Calculated 2,1 m up from the generator:1000 kg
- The weight of the base depends on
  the height of the mast - in other words
  on the length of the torque arm.
- WS-4B-model Max 800 rpm
- WS-4B Guaranteed at constant wind speed of 40 m/s

Materials:
- Vanes: fibre glass
- Fastenings: marine grade aluminium
- Shaft: Ø120&Ø90 mm crome coated steel
- Generator and Generator End Plates: dip galvanized steel
  or marine grade aluminium
- All bolts stainless steel or dip galvanized (A4, A2 or Zn)

Assets of Windside wind turbines:
- No need to stop or secure during storms
- Produces max. amount of energy in storms
- No need to be turned to the wind direction
- Soundless; 0 dB, measured in 2 meters distance
  from the vane
- Stands snow, frost, heat and humidity
- Long lifespan
- Minimum need of maintenance, only lubrication
- Safe to people, animals and nature

windside
OY WINDSIDE PRODUCTION Ltd

E-mail and internet: Tel.:   +358-208-350 700   The Manufacturer reserves
finland@windside.com   Fax: +358-208-350 701   all rights to all modifications
www.windside.com   Mobile: +358-400-315 037   without further notice.

Ø1050 4000 5150

500 100 660

8xM30 Ø370 4.5°

MOUNTING DIMENSIONS

8xØ33

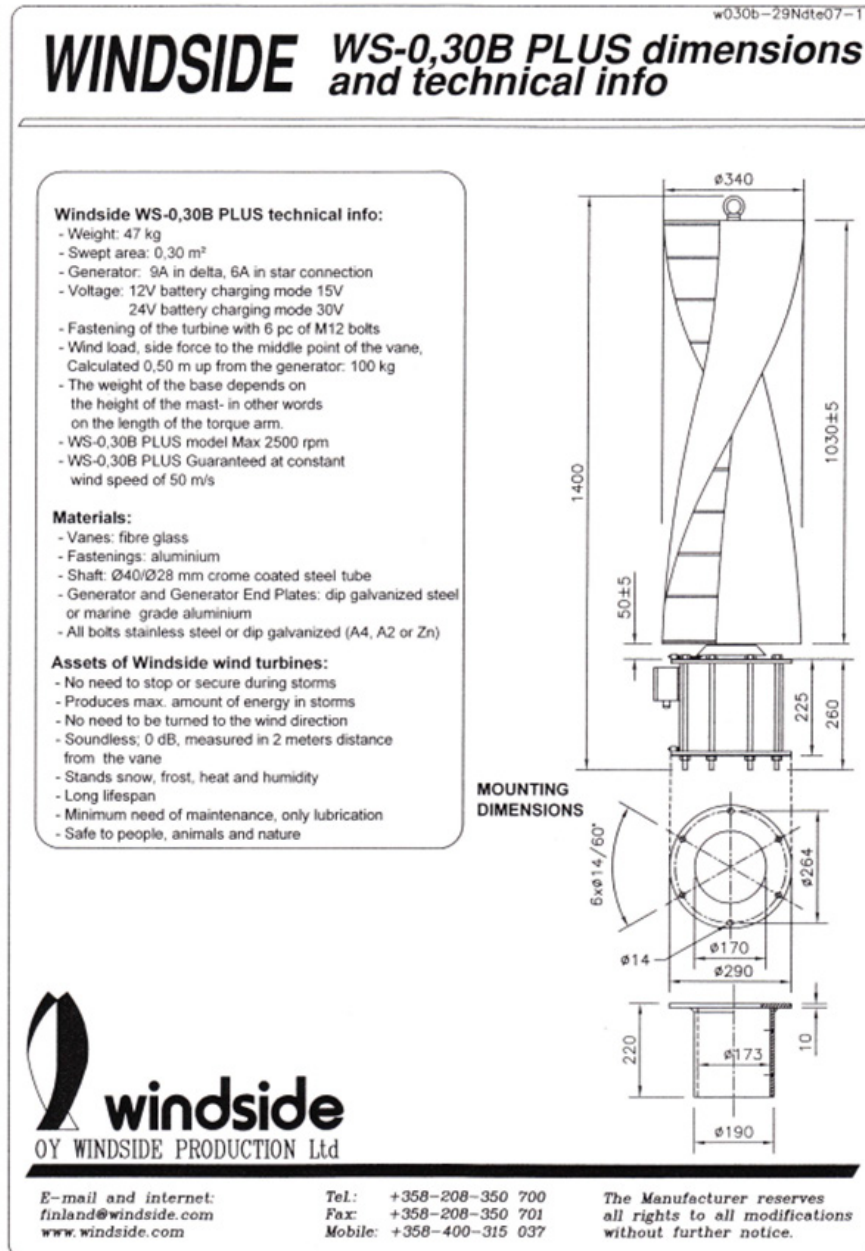Ø545 Ø620

30

8xØ33

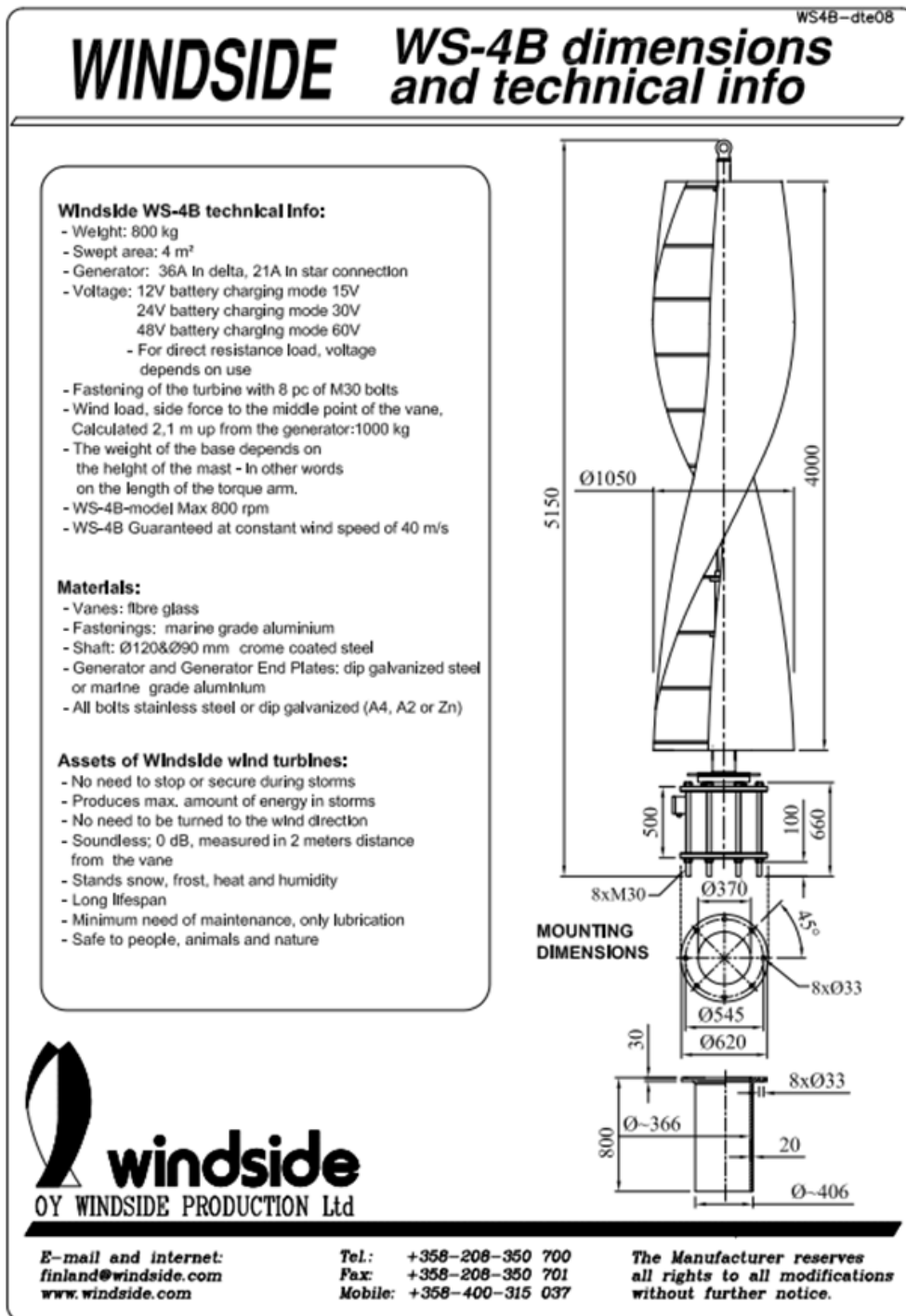800 Ø~366 20

Ø~406

Fig. A1.2.   Technical Data of Windside wind turbine WS-4B. The dimensions
              are in mm.

Windside has made measurements specially on the generators only by rotating them mechanically. The open circuit voltage is measured on DC side after the six-pulse rectifier and the measured currents are direct currents to the batteries. Fig. A1.3-5 shows characteristic of the used PM generator of WS-4B wind turbine.
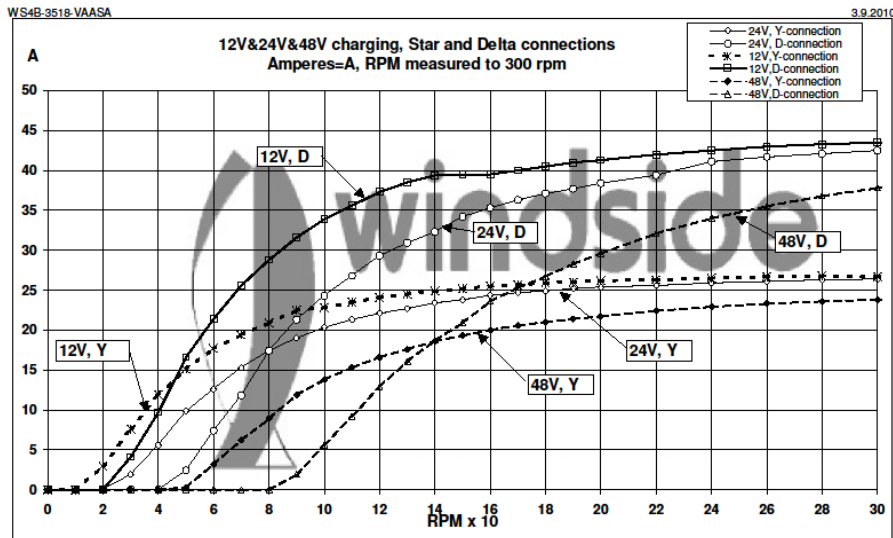
(Oy Windside Production Ltd 2012).

Fig. A1.3.   The characteristic of the WS-4B wind generator in star or in delta charging at different voltage.
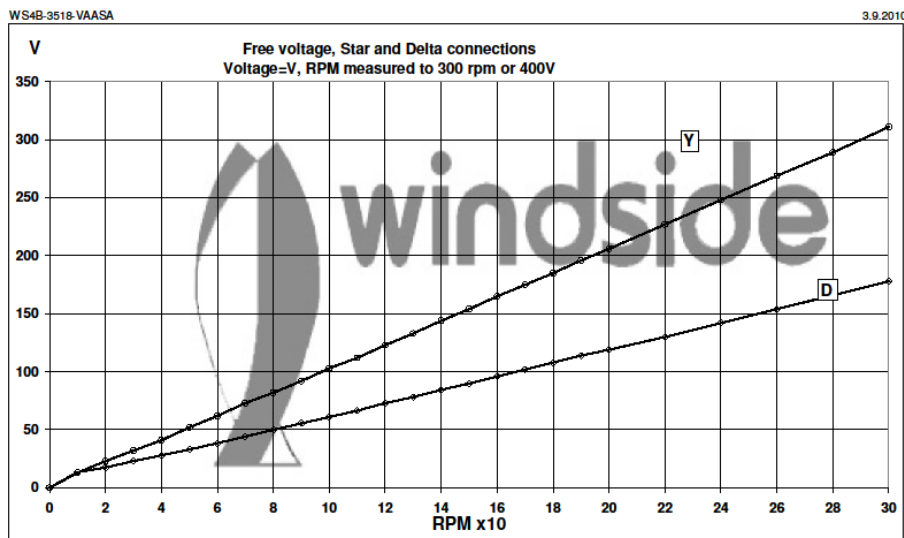
(Oy Windside Production Ltd 2012).

Fig. A1.4.   The open circuit voltage of the studied wind generator WS-4B.

(Oy Windside Production Ltd 2012).
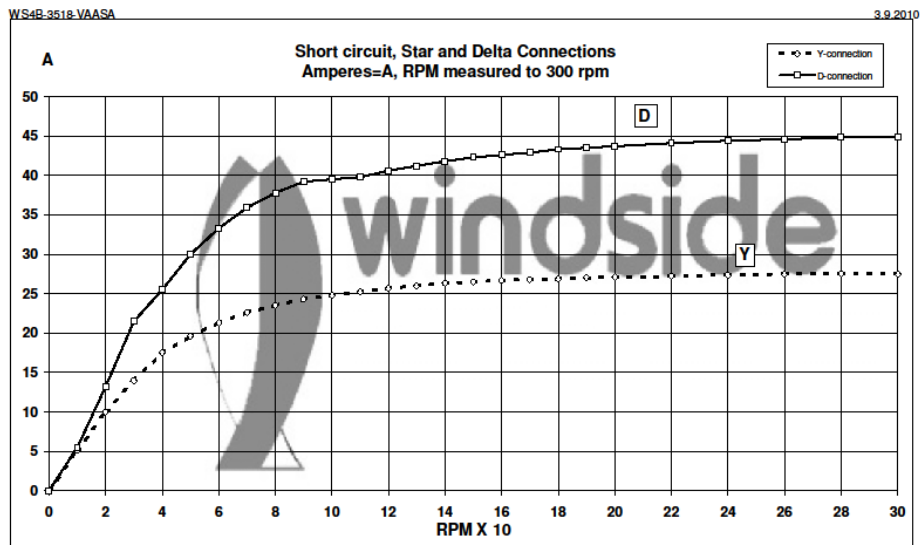
Fig. A1.5.   The short circuit characteristic of the studied wind generator WS-4B.

Appendix 2. Calibration certificates

Svend Ole Hansen ApS

SCT. JØRGENS ALLÉ 5 · DK-1615 KØBENHAVN V · DENMARK
TEL: (+45) 33 25 38 38 · FAX: (+45) 33 25 38 39 · WWW.SOHANSEN.DK

WIND
ENGINEERING
FLUID
DYNAMICS

CERTIFICATE FOR CALIBRATION OF CUP ANEMOMETER

Certificate number: 07.02.2073   **Date of issue:** September 12, 2007

Type: WindSensor P2546A Cup Anemometer   **Serial number:** 4050

Manufacturer: WindSensor, Søkrogen 9, 4000 Roskilde, Denmark

Client: University of Vaasa - Electrical engineering, Wulffintie 34, 65101 VAASA, Finland

Anemometer received: August 16, 2007   **Anemometer calibrated:** September 9, 2007

Calibrated by: tmh   **Calibration procedure:** MEASNET

Certificate prepared by: soh   **Approved by:** soh

Calibration equation obtained: v [m/s] = 0.62044 · f [Hz] + 0.20421

Standard uncertainty, slope: 0.00073   **Standard uncertainty, offset:** 0.03837

**Covariance:** -0.0000033 (m/s)²/Hz   **Coefficient of correlation:** ρ = 0.999997

Absolute maximum deviation: -0.019 m/s at 13.175 m/s

Barometric pressure: 1012.1 hPa   **Relative humidity:** 33.7%

Succession	Velocity pressure, q. [Pa]	Temperature in wind tunnel [°C]	Temperature in control room [°C]	Wind velocity, v. [m/s]	Frequency, f. [Hz]	Deviation, d. [m/s]	Uncertainty u_c (k=2) [m/s]
2	9.90	27.6	22.0	4.120	6.3211	-0.007	0.042
4	15.32	27.5	21.9	5.122	7.9290	-0.002	0.041
6	21.84	27.4	21.9	6.115	9.5227	0.003	0.043
8	29.46	27.3	21.9	7.101	11.1125	0.003	0.047
10	38.18	27.2	21.9	8.084	12.6963	0.002	0.051
12	48.49	27.2	21.9	9.109	14.3490	0.002	0.057
13-last	60.18	27.1	21.9	10.148	16.0070	0.012	0.062
11	73.57	27.2	21.9	11.220	17.7787	-0.014	0.068
9	87.15	27.2	21.9	12.214	19.3316	0.015	0.074
7	101.39	27.3	21.9	13.175	20.9366	-0.019	0.080
5	118.85	27.4	21.9	14.266	22.6643	0.000	0.086
3	136.43	27.5	22.0	15.287	24.2957	0.009	0.092
1-first	155.04	27.6	22.0	16.300	25.9482	-0.004	0.098
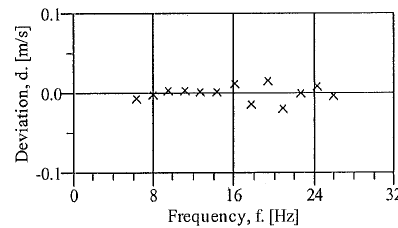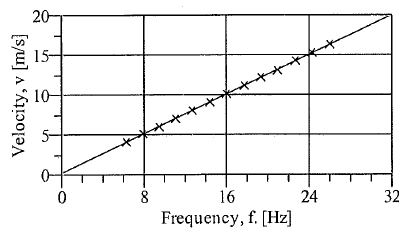
DANAK
Reg. nr. 452

Page 1 of 2

Fig. A2.1.   Certificate of WindSensor P2546A cup anemometer.

Voltech Instruments Ltd
148 Sixth Street Harwell International Business Centre
Didcot Oxon OX11 0RA UK

www.voltech.com

ISO 9001
REGISTERED COMPANY

Sales & applications support telephone: **+44 (0)1235 834555**

Sales & applications support facsimile: **+44 (0)1235 835016**

Operations, accounts & service telephone: **+44 (0)1235 861173**

Operations, accounts & service facsimile: **+44 (0)1235 861174**

E-mail: **sales@voltech.co.uk**

VOLTECH INSTRUMENTS
148 Sixth St, Harwell International Business Centre, Harwell, Oxon, OX11ORA

Certificate of Conformance

PM6000 Universal Power Analyzer

PM6000 Serial No: 200006700253

Voltech Instruments certifies that the above product has been manufactured
to the highest quality standard of workmanship. It conforms to the
manufacturers published specification.

See enclosed documents and CD for Calibration Certificates and data

Quality Engineer: _____ Date: 6. JVL. 2009

Page 1 of 1   VPN 96-036/1

Fig. A2.2.   Certificate of PM6000 universal power analyzer.

Metek GmbH • Fritz-Straßmann-Str. 4 • 25337 Elmshorn

University of Vaasa
Bertil Brännbacka
Puuvillakuja 3

65200 Vaasa
Finland

Your ref.	Our ref.	Elmshorn,
	Lü/Mi	01. December 2009

Project No. 3850
Repairing of Ultrasonic Anemometer USA-1

Packing List No.   1201 - 01   Customer No. 11969

After repairing we deliver:

pos.	description of goods	quantity
1	Ultrasonic Anemometer USA-1 H4 Serial-No. 2004 11007/01 **- repairing -**	1

number and kind of packages	weight, kg	measures
1 x carton	6,5 kg	80 x 41 x 37 cm

M E T E K
Meteorologische Messtechnik GmbH
Fritz-Strassmann-Str. 4
D - 25337 Elmshorn
Tel.: +49 4121 / 43 59-0
Fax: +49 4121 / 43 59-20

Delivery accept:

N. Miketta
....
Place, Date, Sign
METEK GmbH

....
Place, Date, Sign

Fig. A2.3.   Calibration of Anemometer USA-1 H4.

ME|EK
Meteorologische Messtechnik GmbH

This system was sent back after

inspection and/or repair.

Check always the correct setting of the

system parameter and output variables.

Datum	*30.11.09*	Serial number	*2004.11007/01*		
AD = 0	/	M1 =	/	P1 =	*1756*
AI = 1	/	M2 =	/	P2 =	*1757*
AO = 0	/	M3 =	/	P3 =	*1756*
AT = 10	*1*	MD = 20	*20*		
AV = 1	*10*	NO = 28	*31*		
AZ = 0	*0*	OA = 0	*0*	TC =	*29330*
BR = 9600	*9600*	OD = 1	*1*		
D1 = 0	/	OI = 0	/		
D2 = 0	/	PR = 0	*0*	O1 =	*2205*
D3 = 0	/	SA = 0	*0*	O2 =	*2203*
D4 = 0	/	SF = 10000	*10000*	O3 =	*2215*
D5 = 0	/	SY = 0	*0*	O4 =	*2223*
D6 = 0	/	TR = 4000	*4000*	O5 =	*2224*
D7 = 0	/	TV = 100	*0*	O6 =	*2223*
D8 = 0	/	TZ = 0	/		
DC = 0	/	US = 1	/	Version	*2.33*
FR = 0	*0*	VR = 6000	*6000*		
HC =	*1*	ZR = 100	*100*		
HT = 0	*2*				
LD = 0	/	N1, N2, N3	*repcall*		

VD_Rücksendung_USA-1_eng.doc

Fig. A2.4.   Calibration and repair of Anemometer USA-1 H4.

Appendix 3. Map of wind turbine installation sites

Figure A4.1 shows a map of wind turbine installation sites at the university campus in Vaasa.

Fig. A3.1. Wind turbine installation sites.